INTERNATIONAL ENERGY AGENCY

Programme of R, D & D on Advanced Fuel Cells

Annex II : Modelling & Evaluation of Advanced SOFC

Final report on SOFC Data

FACTS & FIGURES

Prepared by Ulf G. Bossel

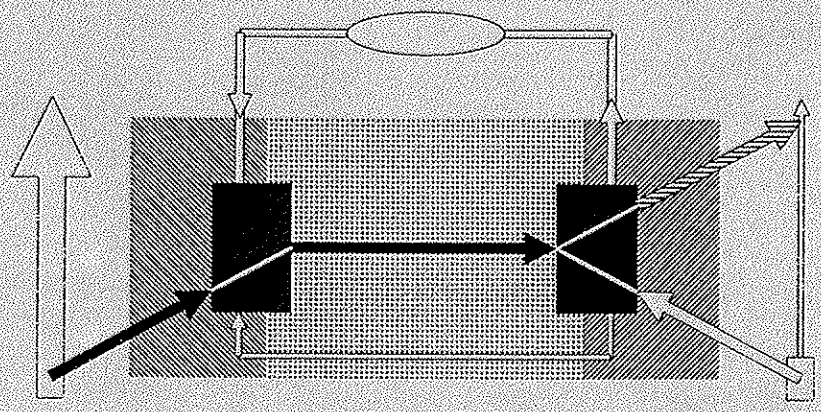

Swiss Federal Office of Energy, Operating Agent Task II

Berne, April 1992

Editor : Léo Dubal, Swiss Federal Office of Energy, CH - 3003 Berne (Switzerland)

PREFACE :

THE IEA PROGRAMME OF R, D & D ON ADVANCED FUEL CELLS

International Energy Agency

The International Energy Agency was formed in November 1974 to establish cooperation among a number of industrialized countries in the vital area of energy policy. It is an autonomous body within the framework of the Organization of Economic Cooperation and Development (OECD). Twenty-two countries are presently members, with the Commission of the European Communities also participating in the work of the IEA under a special arrangement.

Programme of R,D&D on Advanced Fuel Cells

The IEA Implementing Agreement for a Programme of R,D&D on Advanced Fuel Cells was established in April 1990 and comprised initially two annexes. One dealt with the analysis of the Balance-of-Plant of Molten Carbonate Fuel Cells and the other with the Modelling and Evaluation of Advanced Solid Oxide Fuel Cells. Five new annexes are in preparation. There are now ten signatories to the agreement: Denmark (DEA), Germany (KFA-Jülich on behalf of BMFT), Italy (ENEA), Japan (NEDO), the Netherlands (NOVEM), Norway (NCSIR), Spain (Hidroeléctrica Espanola), Sweden (NEA), Switzerland (OFEN), United Kingdom (DOE).

Annex II: Modelling and Evaluation of Advanced Solid Oxide Fuel Cells

The collaborative effort was scheduled for an initial two year term of Annex II, with Switzerland acting as Operating Agent. The targeted objective was to advance natural gas-fuelled solid oxide fuel cells technologies through:

i) the numerical modelling of innovative concepts which have the potential for low-cost mass production and higher conversion efficiency; the establishment of the necessary experimental data base and the model validation;

ii) the elaboration of recommended practices for SOFC products evaluation and their application to available SOFCs in order to assist the development taking place in industry, strengthen confidence and prevent confusion in the market.

The original signatories were Italy, Japan, the Netherlands, Norway, and Switzerland. They have been joined by the United Kingdom, Denmark and Germany.

The task-sharing work has been divided into seven *activities*, each with an appointed *activity leader*:

i) Stack Design Tool (Norway)
ii) Micromodelling (Switzerland)
iii) SOFC Data (Denmark)
iv) Recommended Practices for Electrochemical Evaluation (United Kingdom)
v) Recommended Practices for Thermomechanical Evaluation (Italy)
vi) Recommended Practices for Powder Characterisation (The Netherlands)
vii) Recommended Practices for Stack Evaluation (Japan)

Augustin McEvoy, from the Federal Institute of Technology, in Lausanne, acted as Operating Agent on behalf of the Swiss Federal Office of Energy. Continuation of Annex II is presently being discussed.

FOREWORD

FACTS & FIGURES

If modelling is the art of scrutinizing systematically all variations of interesting parameters which otherwise nobody could afford to test in real life, it requires a common data base and a reference source, that is to say, a *common language* !

The original version of Facts & Figures had been compiled by U.G. Bossel and J.P. Ferguson for the Swiss Federal Office of Energy. It has been distributed to the participants of the first IEA Workshop on Mathematical Modelling of Natural Gas Fuelled Solid Oxide Fuel Cells and Systems, at Charmey, Switzerland, from July 2 to 6, 1989. It provided a base for fruitful discussions, and, although incomplete, this compilation was recognized as a helpful document, not only for SOFC modellers, but for general use by scientists and engineers.

The document has been revised in depth within the framework of the *SOFC DATA* activity, which was led by Denmark, and the Swiss Federal Office of Energy has mandated U.G. Bossel to compile this updated version.

Berne, April 1992

SWISS FEDERAL OFFICE OF ENERGY

OPERATING AGENT - IEA SOFC TASK

CONTENTS

C ELECTROCHEMISTRY

C1 FUNDAMENTALS
- C1.1 Reforming of Hydrocarbon Fuels
- C1.2 Gibbs Voltage
- C1.3 Nernst Voltage
- C1.4 Gibbs and Nernst Efficiency

C2 FLUXES IN FUEL CELL PROCESSES

C3 LOSS MECHANISMS
- C3.1 Diffusion of O_2 through Porous Cathode
- C3.2 Charge Transfer to O_2 at Cathode-Electrolyte Interface
- C3.3 Diffusion of $O^{2=}$ through Electrolyte
- C3.4 Diffusion of Fuel Gas through Porous Anode
- C3.5 Oxidation Reaction of H_2 at Anode-Electrolyte Interface
- C3.6 Diffusion of Reaction Products through Porous Anode
- C3.7 Ohmic Voltage Loss in Cathode
- C3.8 Electron Leakage through Electrolyte
- C3.9 Ohmic Voltage Loss in Anode

D ELECTRIC CURRENT FLOW IN SOFC ELEMENTS

D1 BASICS

D2 CHARGE TRANSPORT IN LINEAR CONDUCTRORS OF CONSTANT CROSS SECTION
- D2.1 Conducting Wire
- D2.2 Charge Transport in Conductors of Variing Cross Section
- D2.3 In-plane Charge Transport by Conducting Sheets
- D2.4 Ion Current Conduction across Electrolyte Sheets
- D2.5 Cross-plane Resistance of Cathode-Electrolyte-Anode Structures

D3 CHARGE TRANSPORT IN 2-DIMENSIONAL PEN STRUCTURES
- D3.1 Differential Equation
- D3.2 Ohmic Resistance of Pen Strip with Aligned Terminals
- D3.3 Ohmic Resistance of PEN Strips with Diagonal Terminals
- D3.4 The PEN Function for PEN Strips
- D3.5 Ohmic Resistance of Circular PEN Structures

0 DEFINITIONS AND SYMBOLS

01 ELEMENTS AND MOLECULES

Only the following elements and molecules are considered:

C		Carbon
CO		Carbon monoxide
CO_2		Carbon dioxide
CH_4		Methane
H	(resp. H_2)	Hydrogen
H_2O		Water (generally in vapor state)
N	(resp. N_2)	Nitrogen
O	(resp. O_2)	Oxygen

02 REACTIONS

(R1)	2 H_2	+		O_2	$\leftrightarrow$	2 H_2O				
(R2)	2 CO	+		O_2	$\leftrightarrow$	2 CO_2				
(R3)	CH_4	+	2	O_2	$\leftrightarrow$	CO_2	+	2	H_2O	
(R4)	CH_4	+		H_2O	$\leftrightarrow$	CO	+	3	H_2	
(R5)	CH_4	+		CO_2	$\leftrightarrow$	2 CO	+	2	H_2	
(R6)	CO	+		H_2O	$\leftrightarrow$	CO_2	+		H_2	
(R7)				H_2	$\leftrightarrow$	H	+		H	
(R8)				O_2	$\leftrightarrow$	O	+		O	
(R9)			2	CO_2	$\leftrightarrow$	2 CO	+		O_2	
(R10)				CO_2	$\leftrightarrow$	C	+		O_2	
(R11)			2	CO	$\leftrightarrow$	2 C	+		O_2	
(R12)			2	CO	$\leftrightarrow$	C	+		CO_2	
(R13)				CH_4	$\leftrightarrow$	C	+	2	H_2	

03 UNITS

[m]	meter		
[s]	second		
[kg]	kilogram		
[N]	Newton	= [kg m s^{-2}]	
[Pa]	Pascal	= [N m^{-2}]	= [kg m^{-1} s^{-2}]
[J]	Joule	= [kg m^2 s^{-2}]	= [W s]
[W]	Watt	= [kg m^2 s^{-3}]	= [J s^{-1}]
[mol]	mole		
[V]	Volt		
[A]	Ampere		
[Ω]	Ohm = [V A^{-1}]		

04 DIMENSIONLESS NUMBERS

$Re = L\ u\ \rho\ \mu^{-1}$	Reynolds number
$Nu = L\ h\ \lambda^{-1}$	Nusselt number
$Gr = L^3\ g\ \beta\ \Delta T\ \rho^2\ \mu^{-2}$	Grasshoff number
$Pr = c_p\ \mu\ \lambda^{-1}$	Prandtl number
$Sc = \mu\ \rho^{-1}\ D_m^{-1}$	Schmidt number
$Pe = Re\ Pr = L\ u\ \rho\ c_p\ \lambda^{-1}$	Peclet number

05 CONSTANTS

$e = 1.602177\ 10^{-19}$	C		Elementary charge
$F = 9.6485\ 10^{4}$	C mol^{-1}		Faraday constant
$g = 9.80665$	m s^{-2}		gravitat. acceleration
$k = 1.38066\ 10^{-23}$	J K^{-1}		Boltzmann constant
$N_A = 6.02214\ 10^{23}$	mol^{-1}		Avogadro constant
$R_G = 8.31451$	J K^{-1} mol^{-1}		Gas constant
$V_0 = 2.24136\ 10^{-2}$	m^3 mol^{-1}		Normal volume perf. gas
$\sigma_S = 5.6703\ 10^{-8}$	W m^{-2} K^{-4}		Stefan-Bolzmann constant

06 SYMBOLS, ROMAN LETTERS

$A,\ A_x,\ A_e,\ A_i$	areas [m^2]
$A,\ B,\ C,\ D$	constants
A_e	empirical constant [K Ω^{-1} m^{-1}]
A_i	empirical constant [Ω^{-1} m^{-1}]
a	empirical constant [K^{-1}]
$a,\ b,\ c,\ h$	geometric lengths [m]
$a^*,\ b^*$	constants in Tafel equations
B	$E/(1+E)^2$
$B_e,\ B_i$	empirical constants [K]
C	cross-plane resistance area [Ω m^2]
C_i	compound species
c	molar density [mol m^{-3}]
c_p	specific heat, p = const [J kg^{-1} K^{-1}]
$D_m,\ D_{1,2}$	molecular diffusivity of 1 in 2 [m^2 s^{-1}]
d	diameters [m]
d_h	hydraulic diamter [m]
E	ohmic symmetry parameter
E_f	fuel gas energy fow rate [W]
$F_0,\ F_1,\ F_2$	PEN functions
f	friction coefficient

G	Gibbs free energy [J mol^{-1}]
H	enthalpy [J mol^{-1}]
h	heat transfer coefficient [W m^{-2} K^{-1}]
I	electric current [A]
i	electric current density [A m^{-2}]
J	non-dimensional strip width
j	current, general
K	ratio of activity products
K_p	equilibrium constant
L	length [m]
l, L	characteristic length [m]
M_f	mole flow rate of fuel [mol s^{-1}]
M, M_i	molar mass [kg mol^{-1}]
m, m_i	mass flux [kg m^{-2} s^{-1}]
N_{mi}	Number of moles of species "i"
N_i	fluxes [s^{-1} m^{-2}]
n_e	electrons transferred per reaction
P_i	product species
P, P_e	electric power [W]
P_f	fuel power
P_s	shunt power
P_t	thermal powers [W]
p	pressure [Pa = N m^{-2}]
Q	heat flow rate [W]
q	heat flux per unit area [W m^{-2}]
q'	heat generated per unit area [W m^{-2}]
R	radius
R	ohmic resistances [Ω]
R_G	universal gas constant, see above
R_{Gs}	specific gas constant [J kg^{-1} K^{-1}]
r	radius [m]
S	entropy [J mol^{-1} K^{-1}]
S	stochiometric ratio ("Stoich")
T	temperature [K, °C is tolerated]
t	time [s]
U	voltage [V]
U_G	Gibbs voltage [V]
U_N	Nernst voltage [V]
u	fluid flow velocity [m s^{-1}]
u_a, u_f	utilizations of air, fuel
V, V_i	volume flow rates [m^3 s^{-1}]
X	length of plate in x-direction [m]
X_i	mole fraction of constituent "i"
x	x-coordinate
Y	widths of plate in y-direction [m]
y	y-coordinate
Z	thickness of plate in z-direction [m]
z	z-coordinate

07 SYMBOLS, GREEK LETTERS

α	absorptance
α_t	thermal diffusivity [$m^2\ s^{-1}$]
β	coefficient of thermal expansion [K^{-1}]
Γ	product gas stoichiometric coefficient
Δ	symbol of difference
Δ^2	Laplace operator
$\Delta_f G$, $\Delta_f G^0$	Gibbs free energy change
$\Delta_f H$, $\Delta_f H^0$	Enthalpy change
$\Delta_f S$, $\Delta_f S^0$	Entropy change
δ	symbol for differentials
ε	emittance
ε	electrical potential (Tafel equation)
η	efficiency
η_e	electrical efficiency of SOFC system
η_G	Gibbs efficiency
η_N	Nernst efficiency
η_V	voltage efficiency
λ	thermal conductivity [$W\ m^{-1}\ K^{-1}$]
μ	dynamic ("bulk") viscosity [$kg\ m^{-1}\ s^{-1}$]
μ_{H2}	chemical potential of H_2, etc.
U	voltage [V]
υ	kinematic viscosity [$m^2\ s^{-1}$]
Π...	product ...
R	resistance [Ω]
ρ	density [$kg\ m^{-3}$]
ρ	resistivity [Ω m]
Σ...	sum ...
σ	conductivity [$\Omega^{-1}\ m^{-1}$]
Φ	oxygen stoichiometric coefficient
Ω	Ohm [$V\ A^{-1}$]

08 SUBSCRIPTS

a	air
a, an	anode
c, ca	cathode
e	electron, electronic
e, el	electrolyte
f	fuel
i	ion, ionic
i	general, i = 1, 2, 3 ...
in	input
int	internal
max	maximum
opt	optimum
out	output
t	thermal
tot	total
+	positive
-	negative
0	base

A SOFC CHEMISTRY

A1 CHEMICAL REACTIONS

A1.1 CONVERSION REACTIONS

For the conversion of natural gas only the following basic exothermic conversion reactions shall be considered:

$$H_2 + 0.5\ O_2 \leftrightarrow H_2O \quad (R1)$$

$$CO + 0.5\ O_2 \leftrightarrow CO_2 \quad (R2)$$

$$CH_4 + 2\ O_2 \leftrightarrow CO_2 + 2\ H_2O \quad (R3)$$

A1.2 REFORMING REACTIONS

CH_4 can be reformed with to CO and H_2 by reactions with H_2O and CO_2:

$$CH_4 + H_2O \leftrightarrow CO + 3\ H_2 \quad (R4)$$

$$CH_4 + CO_2 \leftrightarrow 2\ CO + 2\ H_2 \quad (R5)$$

A1.3 SHIFT REACTIONS

CO can be shifted with H_2O to CO_2 and H_2 by the exothermic shift reaction:

$$CO + H_2O \leftrightarrow CO_2 + H_2 \quad (R6)$$

A1.4 DISSOCIATION REACTIONS

Molecule dissociate under the influence of received energy:

$$H_2 \leftrightarrow H + H \quad (R7)$$

$$O_2 \leftrightarrow O + O \quad (R8)$$

$$CO_2 \leftrightarrow CO + 0.5\ O_2 \quad (R9)$$

$$CO_2 \leftrightarrow C + O_2 \quad (R10)$$

$$CO \leftrightarrow C + 0.5\ O_2 \quad (R11)$$

$$2\ CO \leftrightarrow C + CO_2 \quad (R12)$$

$$CH_4 \leftrightarrow C + 2\ H_2 \quad (R13)$$

Thermodynamic propertiers of these 13 reactions are tabulated in Chapter B. Under certain conditions, carbon containing molecules dissociate into solid carbon (sud, lamp black) and gases. Gas passages may be blocked by carbon deposits. Carbonization can be avoided by adding water to the fuel gas (reforming reaction R4).

A2 EQUILIBRIUM CONSTANTS K_p

Definition:

> The equilibrium constant "K_p" is the product of the concentrations (or activities) of the substances produced at equilibrium in a chemical reaction divided by the product of concentrations of the reacting substances, each concentration raised to that power which is the coefficient of the substance in the chemical equation.

Example: For the brutto reaction R3 of CH_4 with O_2

$$CH_4 + 2\ O_2 = CO_2 + 2\ H_2O$$

the equilibrium constant is defined for any given temperature by

$$K_p = \frac{(p_{H2O})^2 * p_{CO2}}{p_{CH4} * (p_{O2})^2} \qquad (A201)$$

In this example, the concentrations are expressed in terms of partial pressures "p_{xxx}" of the four substances involved. For any given reaction, the equilibrium constant is a function of temperature.

Table A20.1: Equilibrium constants, expressed as $\log_{10}K_p$ [1] for the selected SOFC reactions

T [K] / [°C]	298 / 25	800 / 527	1000 / 727	1200 / 927	1400 / 1127
R1	40.090	13.296	10.067	7.903	6.351
R2	45.113	13.924	10.227	7.768	6.017
R3	140.437	52.292	41.837	34.860	29.869
R4	- 24.947	- 1.522	1.409	3.383	4.798
R5	- 29.970	- 2.150	1.250	3.518	5.132
R6	5.023	0.628	0.159	- 0.135	- 0.334
R7	- 71.265	- 23.077	- 17.289	- 13.410	- 10.626
R8	- 81.242	- 26.197	- 19.608	- 15.202	- 12.048
R9	- 45.113	- 13.924	- 10.227	- 7.768	- 6.017
R10	- 69.168	- 25.845	- 20.692	- 17.253	- 14.793
R11	- 24.055	- 11.920	- 10.465	- 9.484	- 8.776
R12	21.058	2.004	- 0.238	- 1.716	- 2.759
R13	- 8.912	- 0.146	1.011	1.802	2.373

A3 CHANGE OF STATE

As a result of a chemical reaction, enthalpy, entropy and free energy of the system change. For all three changes of state[5] the following computation scheme is applied.

a. All quantities are referred to the standard temperature (298K =25°C) and the standard pressure (101 325 Pa)
b. In all cases, the unknown quantity is derived from known properties of the chemical compounds and products by a procedure which is here illustrated for the standard enthalpy change $\Delta_f H^0$:

The standard enthalpy of a substance is defined as its energy state at the standard temperature of 298 K. Consequently, the standard enthalpy change of a reaction is defined as the difference of the standard enthalpies of the reaction products "P_i" and the original compounds "C_i", i.e. for the generalized reaction

$$n_1\ C_1 + n_2\ C_2 + \ldots = m_1\ P_1 + m_2\ P_2 + \ldots$$

one obtains

$$\Delta_f H^0_{reaction} = SUM(m_i \Delta_f H^0_{Pi}) - SUM(n_i \Delta_f H^0_{Ci}) \qquad (A301)$$

Example:
For the net reaction of CH_4 with O_2, equation (R3),

$$CH_4 + 2\ O_2 = CO_2 + 2\ H_2O$$

the standard enthalpy change is obtained by computing

$$\Delta_f H^0 = (\Delta_f H^0_{CO2} + 2\ \Delta_f H^0_{H2O}) - (\Delta_f H^0_{CH4} + 2\ \Delta_f H^0_{O2}) \qquad (A302)$$

This scheme is also applied for the computation of the standard change of entropy $\Delta_f S^0$ and the standard change of Gibbs free energy $\Delta_f G^0$.

A3.1 ENTHALPY CHANGE $\Delta_f H$

The change of enthalpy resulting from a chemical reaction is denoted by $\Delta_f H$. In case of exothermic reactions, the enthalpy change is marked with a negative sign. It expresses the difference between the enthalpies of the reaction products and the compounds, all referred to the same temperature.

For practical reasons, a standard temperature has been chosen to be 289K (25°C). The standard enthalpy change $\Delta_f H^0$ of a chemical reaction is defined for this temperature. Since the enthalpies of all substances participating in the reaction are related to this base temperature, no sensible heat contributions to the enthalpy must be considered. Therefore, $\Delta_f H^0$ has a unique value for any given reaction.

By definition, the absolute value of the standard enthaply change of oxidizing reactions is equivalent to the "upper heating value" used by engineers to describe the heat release by combustion processes. In chemical thermodynamics, all conversion analyses are referred to this "upper heating value". The "lower heating value" introduced by energy engineers excludes the latent heat of condensation of reaction products. Flue gases are ejected from boilers, internal combusion engines and gas turbines at temperatures well above the saturation temperatures of the dominant condensible exhaust constituents to avoid corrosion by acidic condensates.

Table A31.1: Standard Enthalpy Change $\Delta_f H^0$ [10^3 J mol^{-1}] [1]

T [K]	298	800	1000	1200	1400
[°C]	25	527	727	927	1127
R1	-241.94	-246.58	-248.00	-249.15	-250.05
R2	-283.13	-283.41	-282.76	-281.96	-281.04
R3	-802.69	-800.24	-800.91	-802.05	-803.43
R4	206.27	222.90	225.86	227.35	227.75
R5	247.46	259.73	260.62	260.16	258.75
R6	- 41.19	- 36.83	- 34.76	- 32.81	- 31.00
R7	436.00	442.16	444.50	446.69	448.72
R8	498.35	503.85	505.36	506.66	507.81
R9	283.13	283.41	282.76	281.96	281.04
R10	393.71	394.40	394.83	395.24	395.64
R11	110.59	110.99	112.06	113.28	114.60
R12	-172.55	-172.42	-170.70	-168.67	-166.45
R13	74.91	87.31	89.92	91.48	92.30

A3.2 ENTROPY CHANGE $\Delta_f S$

The entropy of a substance is a function of temperature and chemical composition. If two or more substances react, then the entropy of the new system differs from the entropy of any of the original compounds. The change of entropy $\Delta_f S$ depends on a number of mechanisms by which energy is stored during the reaction process. On a microscopic scale, the rearrangement of atoms within the molecular structures is one of the contributing factors. But the dominating contribution to the entropy change is the amount of energy invested in the reduction or expansion of volume due to a change of the number of moles of gaseous reactants and products.

Table A32.1: Entropy Change $\Delta_f S$ [J mol^{-1} K^{-1}] [1]

T [K]	298	800	1000	1200	1400
[°C]	25	527	727	927	1127
R1	- 44.388	- 53.679	- 55.280	- 56.329	- 57.024
R2	- 86.416	- 87.703	- 86.985	- 86.250	- 85.551
R3	- 5.082	0.753	0.013	- 1.021	- 2.085
R4	214.499	249.494	252.839	254.216	254.538
R5	256.526	283.518	284.543	284.137	283.066
R6	- 42.027	- 34.024	- 31.705	- 29.922	- 28.528
R7	229.432	270.464	279.742	287.320	293.730
R8	322.166	364.232	373.580	381.198	387.632
R9	86.416	87.703	86.985	86.250	85.551
R10	- 2.968	- 1.766	- 1.289	- 0.913	- 0.599
R11	- 89.384	- 89.469	- 88.274	- 87.163	- 86.150
R12	-175.799	-177.172	-175.259	-173.413	-171.710
R13	80.727	106.345	109.284	110.724	111.364

A3.3 GIBBS FREE ENERGY CHANGE $\Delta_f G$

The Gibbs free energy change $\Delta_f G$ is the chemical energy which can be reversibly converted into electrical energy. The Gibbs free energy change $\Delta_f G$ thus becomes the determining quantity for any electrochemical process.

The difference between $\Delta_f H$ and $\Delta_f G$ constitutes the energy portion produced by the chemical reaction as heat at any given temperature. The quantities are linked by the entropy change $\Delta_f S$:

$$\Delta_f G = \Delta_f H - T * \Delta_f S \qquad \text{(A331)}$$

The following table contains values for $\Delta_f G^0$ calculated for various temperatures.

Table A33.1: Standard Gibbs free energy change $\Delta_f G^0$ [10^3 J mol^{-1}][1]

T [K]	298	800	1000	1200	1400
[°C]	25	527	727	927	1127
R1	-228.71	-203.63	-192.72	-181.55	-170.22
R2	-257.36	-213.25	-195.78	-178.46	-161.27
R3	-801.17	-800.84	-800.92	-800.82	-800.52
R4	143.32	23.30	- 26.97	- 77.71	-128.60
R5	170.97	32.92	- 23.92	- 80.81	-137.54
R6	- 28.66	- 9.62	- 3.05	- 3.09	- 8.94
R7	406.56	353.43	330.97	308.06	284.79
R8	463.47	401.20	375.36	349.24	322.91
R9	257.36	213.25	195.78	178.46	161.27
R10	394.59	395.81	396.11	396.33	396.48
R11	137.23	182.56	200.34	217.88	235.21
R12	-120.13	- 30.69	- 4.56	39.42	73.93
R13	50.84	2.23	- 19.36	- 41.39	- 63.61

B PROPERTIES OF SOFC GASES AND MATERIALS

B1 PHYSICAL PROPERTIES OF COMMON SOFC GASES

The data are presented for the gases H_2, O_2, N_2, CO, CO_2, CH_4 and H_2O_{vap} (water in the vapor state). Presented are the molar mass M, the specific gas constant R_{Gs}, the density ρ, the specific heat c_p, the dynamic (or bulk) viscosity μ, the thermal conductivity λ and the thermal diffusivity α_t. Analytic forms relating these quantities to the temperature at atmospheric pressures are given. For easy use results are tabulated for typical SOFC temperatures. These analytic results agree well with the real physical properties obtained by experiment.

B1.1 MOLAR MASS M

The molar mass M (also called "molecular weight") is defined as the amount of substance which contains exactly the same number of molelcules (Avogadro number) as 12.000 kg of ^{12}C ("carbon 12"). The following numbers were taken from the Handbook of Chemistry and Physics[2].

Table B11.1: Molar masses of common SOFC gases

		M [kg]
Hydrogen	H_2	2.017
Oxygen	O_2	32.01
Nitrogen	N_2	28.03
Carbon monoxide	CO	28.02
Carbon dioxide	CO_2	44.02
Methane	CH_4	16.05
Water vapor	H_2O_{vap}	18.03

B1.2 SPECIFIC GAS CONSTANT R_{Gs}

For a particular gas, the specific gas constant is obtained from the universal gas constant $R_G = 8.3143$ [J mol^{-1} K^{-1}] by the following relation

$$R_{Gs} = R_G / M \quad [J\ Kg^{-1}\ K^{-1}] \qquad (B121)$$

Table B12.1: Specific gas constants for SOFC gases

		R_{Gs} [10^3 J Kg^{-1} K^{-1}]
Hydrogen	H_2	4.126
Oxygen	O_2	0.260
Nitrogen	N_2	0.297
Carbon monoxide	CO	0.297
Carbon dioxide	CO_2	0.189
Methane	CH_4	0.519
Water vapor	H_2O_{vap}	0.457

B1.3 DENSITY ρ

The density is best computed by using the ideal gas law

$$\rho = p / (R_{Gs}\ T) \quad [kg\ m^{-3}] \qquad (B131)$$

Pascals [1 Pa = 1 N m^{-2} = 1 kg m^{-1} s^{-2}] should be used for the pressure p and Kelvin for the temperature T.

Table B13.1: Density ρ [kg m^{-3}] at standard pressure [p_0 = 101 325 Pa = 1 atm]

T [K]	298	800	1000	1200	1400
[°C]	25	527	727	927	1127
H_2	0.0824	0.0307	0.0246	0.0205	0.0175
O_2	1.3087	0.4874	0.3900	0.3250	0.2786
N_2	1.1459	0.4268	0.3415	0.2846	0.2439
CO	1.1455	0.4267	0.3414	0.2845	0.2438
CO_2	1.7998	0.6704	0.5363	0.4470	0.3831
CH_4	0.6560	0.2443	0.1955	0.1629	0.1396
H_2O_{vap}	liquid	0.2745	0.2196	0.1830	0.1569

B1.4 SPECIFIC HEAT c_p

c_p [J mol^{-1} K^{-1}]:

The specific heat c_p [J mol^{-1} K^{-1}] of common SOFC gases is optained by using the following empirical expression

$$c_p = A + B\,T + C\,T^2 + D\,T^3 \quad [\text{J mol}^{-1}\,\text{K}^{-1}] \qquad \text{(B141)}$$

with the following numbers

Table B14.1: Coefficients[3] for the expansion of c_p [J mol^{-1} K^{-1}]

	A	B [x 10^{-3}]	C [x 10^{-6}]	D [x 10^{-9}]
H_2	27.14	9.274	-13.81	7.645
O_2	28.11	- 0.00368	17.46	-10.65
N_2	31.15	-13.57	26.80	-11.68
CO	30.87	-12.85	27.89	-12.72
CO_2	19.80	73.44	-56.02	17.15
CH_4	19.20	52.13	11.97	-11.32
H_2O_{vap}	32.24	1.924	10.55	- 3.596

Using Equation B141 and the cefficients of Table B14.1 the following values are obtained for the specific heats of common SOFC gases:

Table B14.2: Specific heat c_p [J mol^{-1} K^{-1}]

T [K] / [°C]	298 / 25	800 / 527	1000 / 727	1200 / 927	1400 / 1127
H_2	28.88	29.64	30.25	31.59	34.03
O_2	29.27	33.54	34.55	34.41	32.59
N_2	29.18	31.47	32.70	33.27	32.63
CO	29.18	31.93	33.19	33.63	32.64
CO_2	37.16	51.48	54.37	56.89	59.88
CH_4	35.50	62.77	71.98	79.43	84.58
H_2O_{vap}	33.66	38.69	41.12	43.53	45.74

c_p [J kg^{-1} K^{-1}]:

The specific heat c_p [J kg^{-1} K^{-1}] of common SOFC gases is optained by using the following empirical expression

$$c_p = A + B\,T + C\,T^2 + D\,T^3 \quad [\text{J kg}^{-1}\ \text{K}^{-1}] \qquad \text{(B142)}$$

with the following numbers

Table B14.3: Coefficients[3] for the expansion of c_p [10^3 J kg^{-1} K^{-1}]

	A	B [x 10^{-3}]	C [x 10^{-6}]	D [x 10^{-9}]
H_2	13.4623	4.6002	-6.8502	3.7922
O_2	0.8784	-0.0001	0.5456	-0.3328
N_2	1.1117	-0.4843	0.9565	-0.4168
CO	1.1021	-0.4588	0.9957	-0.4541
CO_2	0.4499	1.6687	-1.2729	0.3897
CH_4	1.1970	3.2500	0.7463	-0.7057
H_2O_{vap}	1.7891	0.1068	0.5855	-0.1996

Using Equation B142 and the cefficients of Table B14.3 the following values are obtained for the specific heats of common SOFC gases:

Table B14.4: Specific heat c_p [10^3 J kg^{-1} K^{-1}]

T [K] / [°C]	298 / 25	800 / 527	1000 / 727	1200 / 927	1400 / 1127
H_2	14.33	14.70	15.00	15.67	16.88
O_2	0.92	1.06	1.09	1.09	1.03
N_2	1.04	1.12	1.17	1.19	1.16
CO	1.04	1.14	1.18	1.20	1.17
CO_2	0.84	1.17	1.24	1.29	1.36
CH_4	2.21	3.91	4.49	4.95	5.27
H_2O_{vap}	1.87	2.15	2.28	2.42	2.54

B5

B1.5 DYNAMIC (BULK) VISCOSITY μ

The dynamic or bulk viscosity of common SOFC gases is obtained by using the following empirical expression

$$\mu = A + B\,T + C\,T^2 \quad [\text{kg m}^{-1}\,\text{s}^{-1}] \qquad \text{(B151)}$$

with the following numbers

Table B15.1: Coefficients[3] for the expansion of μ [10^5 kg m^{-1} s^{-1}]

	A	B [x 10^{-3}]	C [x 10^{-6}]
H_2	0.3621	1.851	-0.2050
O_2	0.6570	4.990	-0.8916
N_2	0.6063	4.196	-0.8176
CO	0.9758	2.664	0.3767
CO_2	0.1321	4.818	-0.9881
CH_4	0.1768	3.379	-0.8256
H_2O_{vap}	0.3403	3.204	-0.1187

Using Equation B151 and the coefficients of Table B15.1 the following values are obtained for the dynamic or bulk viscosity of common SOFC gases:

Table B15.2: Dynamic or bulk viscosity m [10^5 kg m^{-1} s^{-1}]

T [K] / [°C]	298 / 25	800 / 527	1000 / 727	1200 / 927	1400 / 1127
H_2	0.90	1.71	2.01	2.29	2.55
O_2	2.06	4.08	4.76	5.36	5.90
N_2	1.78	3.44	3.98	4.46	4.88
CO	1.80	3.35	4.02	4.72	5.44
CO_2	1.48	3.35	3.96	4.49	4.94
CH_4	1.11	2.35	2.73	3.04	3.29
H_2O_{vap}	1.28	2.83	3.43	4.01	4.59

B1.6 THERMAL CONDUCTIVITY λ

The thermal conductivity of common SOFC gases is obtained by using the following empirical expression

$$\lambda = A + B\,T + C\,T^2 \quad [W\ m^{-1}\ K^{-1}] \qquad (B161)$$

with the following numbers

Table B16.1: Coefficients[3] for the expansion of λ [W m^{-1} K^{-1}]

	A	B [x 10^{-3}]	C [x 10^{-6}]
H_2	0.06232	0.41070	-0.04070
O_2	0.00550	0.07217	-0.00617
N_2	0.00595	0.07154	-0.01546
CO	0.00494	0.06954	-0.00770
CO_2	-0.01010	0.09388	-0.01676
CH_4	0.00859	0.05334	0.10910
H_2O_{vap}	-0.01320	0.08890	0.01250

Using Equation B161 and the coefficients of Table B16.1 the following values are obtained for the thermal conductivity of common SOFC gases:

Table B16.2: Thermal conductivities λ [W m^{-1} K^{-1}]

T [K] / [°C]	298 / 25	800 / 527	1000 / 727	1200 / 927	1400 / 1127
H_2	18.11	38.48	43.23	49.66	55.75
O_2	2.65	5.93	7.15	8.32	9.44
N_2	2.59	5.33	6.20	6.95	7.58
CO	2.50	5.56	6.68	7.73	8.72
CO_2	1.64	5.43	6.70	7.84	8.85
CH_4	3.42	12.11	17.10	22.97	29.71
H_2O_{vap}	1.44	6.59	8.82	11.15	13.58

B1.7 THERMAL DIFFUSIVITY α_t

The thermal diffusivity of common SOFC gases is obtained by using the following empirical expression

$$\alpha_t = A + B\,T + C\,T^2 \quad [m2\ s^{-1}] \qquad (B171)$$

with the following numbers

Table B17.1: Coefficients[3] for the expansion of α_t [10^{-4} m2 s^{-1}]

	A	B [x 10^{-3}]	C [x 10^{-6}]
H_2	-0.9725	6.5200	6.1470
O_2	-0.0739	0.6642	1.0890
N_2	-0.2080	1.2750	0.4861
CO	-0.3343	1.6380	0.4613
CO_2	-0.1175	0.5909	0.5357
CH_4	0.2822	-0.8031	2.4850
H_2O_{vap}	-0.1945	0.4167	1.5310

Using Equation B171 and the constants of Table B17.1 the following values are obtained for the thermal diffusivity of common SOFC gases:

Table B17.2: Thermal diffusivity α_t [10^{-4} m^2 s^{-1}]

T [K] / [°C]	298 / 25	800 / 527	1000 / 727	1200 / 927	1400 / 1127
H_2	1.52	8.18	11.69	15.70	20.20
O_2	0.22	1.15	1.68	2.29	2.99
N_2	0.22	1.12	1.55	2.02	2.53
CO	0.19	1.27	1.77	2.30	2.86
CO_2	0.11	0.70	1.01	1.36	1.76
CH_4	0.26	1.23	1.96	2.90	4.03
H_2O_{vap}	0.06	1.11	1.74	2.48	3.35

B2 COMPOSITION OF NATURAL GAS

The composition of natural gas may vary from country to country. The Swiss distributors of natural gas specify its composition by average, minimum and maximum volumetric concentrations of the constituent gases.

Table B20.1: Typical composition and properties of natural gas[4]

	Russian	Dutch	Algerian	Natural Gas
CH_4	92.00	88.85	83.00	[Vol%]
C_2H_6	3.20	4.30	7.50	[Vol%]
C_3H_8	0.85	0.90	2.00	[Vol%]
C_4H_{10}	0.20	0.30	0.80	[Vol%]
C_5H_{12} and C_6H_{14}	0.15	0.15	0.50	[Vol%]
N_2	3.30	4.20	6.00	[Vol%]
others	0.30	1.30	0.20	[Vol%]
Rel. mol. mass	17.38	17.98	19.07	[kg Mol^{-1}]
Density	0.74	0.76	0.81	[kg m^{-3}]
UHV	38.17	37.90	40.10	[10^6 J m^{-3}]
	51.58	49.87	49.51	[10^6 J kg^{-1}]
LHV	34.43	34.20	36.26	[10^6 J m^{-3}]
	46.53	44.99	44.76	[10^6 J kg^{-1}]

Table B20.2: General information on natural gas

1. Natural gas distributed to end users is normally odored with aromas containing traces of sulfur. The following sulfur contents are typical for distributed natural gas:

Unodored gas	< 2	[mg m^{-3}]
Odored gas	< 8	[mg m^{-3}]
H_2S	< 0.05	[mg m^{-3}]

2. Representative physical properties:

Bulk viscosity at 1 bar:		
0°C:	10.31	[10^{-6} kg m^{-1} s^{-1}]
20°C:	10.95	[10^{-6} kg m^{-1} s^{-1}]
Mean specific heat c_p between 0°C and 300°C:	1.91	[10^6 J m^{-3} K^{-1}]
	= 2.45	[10^6 J kg^{-1} K^{-1}]
Sutherland constant:	128	
Flammability in air:	between 5 and 15	[Vol%]
Maximum flame propagation in air:	0.39	[m s^{-1}]

B3 SOFC MATERIALS

B3.1 MATERIAL SELECTION

In today's solid oxide fuel cells the key component, the electrolyte, is made of zirconia (zirconium oxide) stabilized by Yttria and/or Ytterbia. Although other electrolytes are still under investigation, no convincing proof has been given that other materials should be considered for technical application at the present time.

The electrolyte is covered by two electrode layers which in most stack designs are electrically connected in series by an interconnect material. For a number of reasons, ceramic materials are chosen for anode, cathode and interconnect. These materials must be compatible with the electrolyte and with each other. Also, these materials must be compatible with the atmospheres to which they are exposed. Furthermore, at operating temperatures diffusion of atoms from one material to the other should be minimal. Most important is the stability of system materials over 50.000 hours or more.

These requirements make it difficult to develop new compositions for any one of the four materials. The long term compatibility of a new material with the three others has to be demonstrated before it can be accepted for technical developments.

For this reason, only materials shall be considered whose compatibility and long term stability has been convincingly established. These are:

Electrolyte:

Mat E1: Yttria stabilized zirconia
$(ZrO_2)_{0.90}$ $(Y_2O_3)_{0.10}$

Ceramic technology of 1980:
Crushed powders, processed by dry pressing

Mat E2: Yttria stabilized zirconia
$(ZrO_2)_{0.92}$ $(Y_2O_3)_{0.08}$

Ceramic technology of 1990:
Fine powders, processed by tape casting or EVD

Mat E3: Yttria and ytterbia stabilized zirconia
$(ZrO_2)_{0.92}$ $(Y_2O_3)_{0.04}$ $(Yb_2O_3)_{0.04}$

Cathode:

Mat C1: Strontium doped lanthanum manganite
$La_{0.84}\ Sr_{0.16}\ MnO_3$

Anode:

Mat A1: Nickel zirconia cermet
$Ni_{0.35}\ (ZrO_2)_{0.65}$

Interconnect:

Mat I1: Strontium doped lanthanum chromite
$La_{0.84}\ Sr_{0.16}\ CrO_3$

Support:

Mat S1: Calcia stabilized zirconia
$(ZrO_2)_{0.85}\ (CaO)_{0.15}$

Mat S2: Magnesium alumina spinell
$MgAl_2O_4$ (= $MgO \cdot Al_2O_3$)

B3.2 MECHANICAL PROPERTIES OF SELCTED MATERIALS

The most significant material properties for the five components listed above are:

Table B20.1: Properties of ceramic materials[15] used in solid oxide fuel cells (data typical for 800°C to 1000°C)

Material:	bulk density [kgm^{-3}]	specific porosity [Vol-%]	specific heat [$Jkg^{-1}K^{-1}$]	thermal conduct. [$WK^{-1}m^{-1}$]	thermal expansion [$10^{-6}K^{-1}$]
Mat E1 and Mat E2:	5900	0	500-600*	2	9.9
Mat E3:	6100	0	500-600*	2	9.9*
Mat C1:	6580	> 30	300*	2-4*	9.3-10.1*
Mat A1:	6950	> 30	400*	3*	11.7
Mat I1:	6600	0	400*	3-4*	9.6
Mat S1:	5400	> 40	350*	2*	10.0*
Mat S2:	3400	> 40	600-700*	3-4*	9.0*

* = guessed by extrapolation and interpolation of documented data

The following mechanical properties are not sufficiently known:

- σ_y yield strength
- σ stress distribution near crack front
- m Weibull Modulus
- n slow crack growth exponent
- t_B time to failure due to subcritical crack growth

B4 ELECTRICAL AND IONIC CONDUCTION OF SOFC MATERIALS

The ion conductivity σ_i of the electrolyte and the electron conductivity σ_e of anode, cathode and interconnect materials or their inverse, the resistivity ρ_i or ρ_e, depend not only on the temperature, but also on powder preparation, pressing or casting techniques, processing and sintering conditions or even on the origin of the materials (impurities). The theory of ion or electron conduction in ceramic materials is complex. There are temperature regimes of transition between two conduction mechanisms. For a simplified analysis the temperature dependence is described by simple exponential equation.

Normally, so called "Arrhenius diagrams", i.e. $\log(\sigma_i)$ vs. $1/T$ or $\log(\sigma_e T)$ vs. $1/T$, are used to display the dependence of the ion or electron conductivities or resistivities on the temperature. Plotted in this manner, experimental data points should fall on straight lines, thereby proving the validity of the exponential laws. But it is diffucult to extract useful engineering information from Arrhenius diagrams. Therefore, a presentation suggested by Figure B40.1 appears to be more revealing for practical SOFC work. This presentation of $\log(\sigma_i)$ vs. T or $\log(\sigma_e)$ vs. T shows that in the range of concern the ion conductivity of the ceramic electrolyte is a strong function of temperature, while the electron conductivity of anode, cathode and interconnect materials remains practically unchanged between 600°C and 1200°C.

For both types of conduction simple equations are proposed. Both exponental forms are based on two empirical parameters.

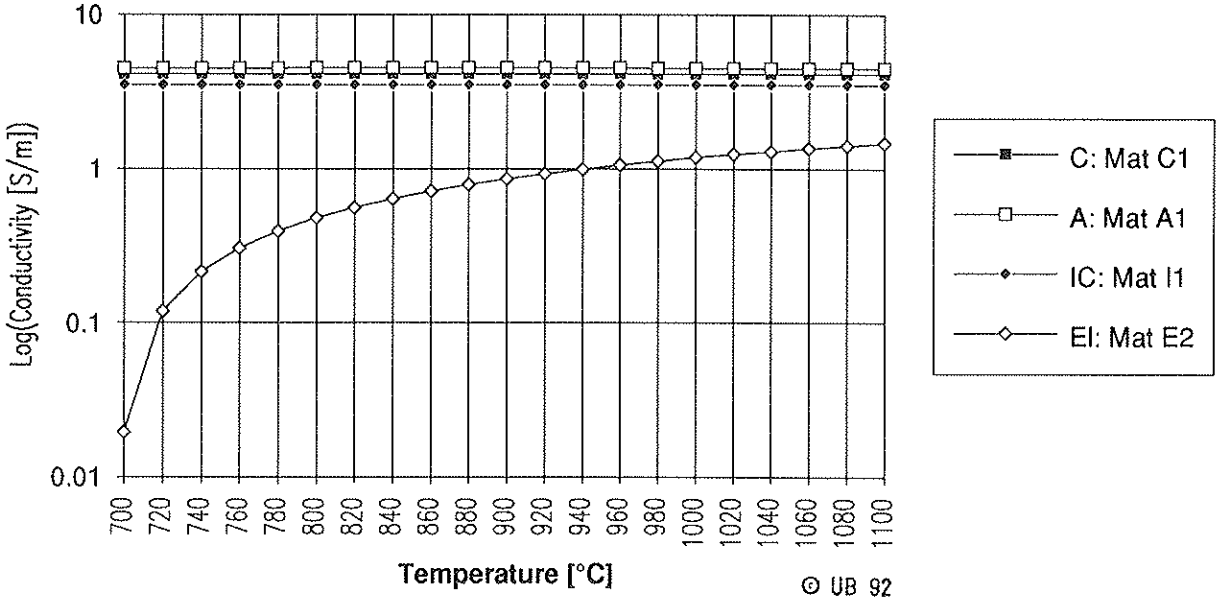

Figure B40.1: Conductivities of representative electrolyte, electrode and interconnect materials

B4.1 ION CONDUCTING ELECTROLYTE MATERIALS

Theory and experiment suggest for the ion conducting electrolyte materials the following equation for the ionic conductivity σ_i:

$$\sigma_i = A_i \exp(- B_i/T) \quad [S\ m^{-1}] \qquad (B411)$$

Note that the conductivity is defined as the inverse of the resistivity ρ_i , i.e. $\rho_i = 1/\sigma_i$ [Ω m].

For the two common SOFC electrolytes listed above the constants A_i and B_i are:

Table B41.1: Ion conduction parameters[16,17,18,19]

	Mat E1	Mat E2	Mat E3
A_i [S m^{-1}]	33.4 10^3	85.0 10^3	27.8 10^3
B_i [K]	10.3 10^3	11.0 10^3	9.3 10^3

With these parameters, Equation B411 yields the following results:

Table B41.2: Ion conduction σ_i of typical electrolyte materials

Temperature:	Mat E1 [S m^{-1}]	Mat E2 [S m^{-1}]	Mat E3 [S m^{-1}]
700 [°C]	0.844	1.046	1.904
800 [°C]	2.264	3.000	4.653
900 [°C]	4.407	6.111	8.507
1000 [°C]	10.23	15.02	18.24
1100 [°C]	18.44	28.18	31.11

These results are also presented in Figure B41.1.

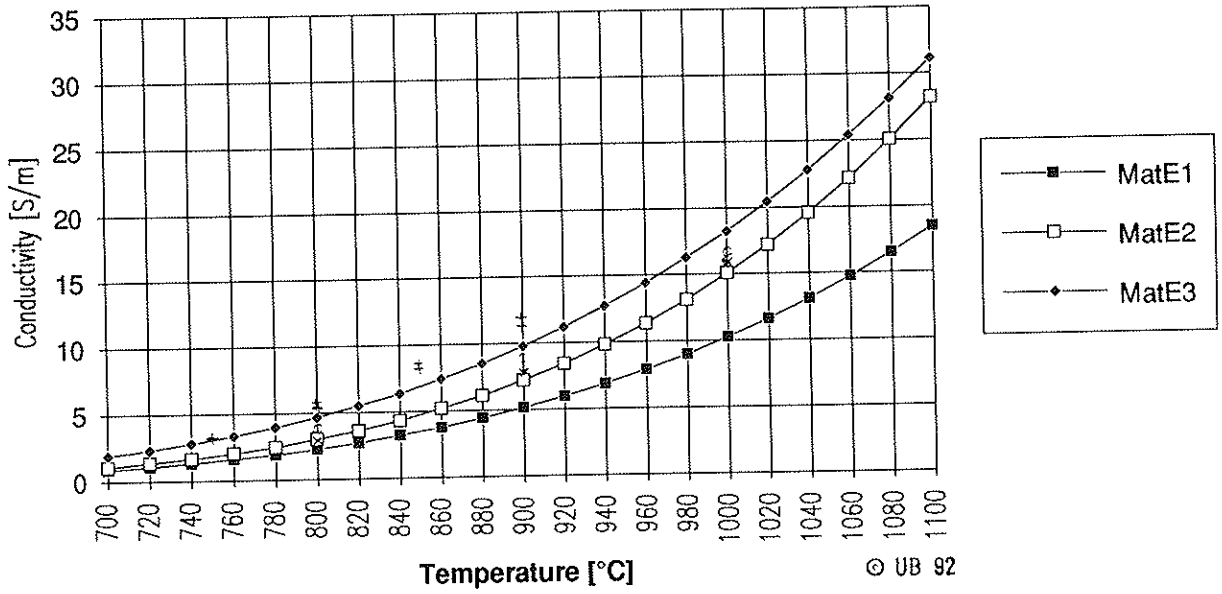

Figure B41.1: Conductivity of ion conducting materials as a function of temperature

Legend:
+ data obtained from [17]
o data obtained from [18]
x data obtained from [19]
Mat E1: based on data obtained from [16]
Mat E2: based on data obtained from [17, 18, 19]
Mat E3: based on data obtained from [16]

B4.2 ELECTRON CONDUCTING CERAMIC MATERIALS

Theory and experiment suggest for the electron conducting anode, cathode and interconnect materials the following relationship for the electronic conductivity σ_e:

$$\sigma_e = A_e/T * \exp(- B_e/T) \quad [S\ m^{-1}] \qquad (B421)$$

Note that the conductivity is defined as the inverse of the resistivity ρ_e, i.e. $\rho_e = 1/\sigma_e$ [Ω m].

For the three common SOFC electron conducting materials listed above the constants A_e and B_e are:

Table B42.1: Electron conduction parameters[16]

	Mat C1	Mat A1	Mat I1
A_e [K S m^{-1}]	42.0 10^6	95.0 10^6	9.3 10^6
B_e [K]	1.2 10^3	1.15 10^3	1.1 10^3

With these parameters, Equation B421 yields the following results:

Table B42.2: Electronic conductivity σ_e for typical cathode, anode and interconnect materials

Temperature:	Mat C1 [10^3 S m^{-1}]	Mat A1 [10^3 S m^{-1}]	Mat I1 [10^3 S m^{-1}]
700 [°C]	12.57 10^3	29.94 10^3	3.09 10^3
800 [°C]	12.76 10^3	30.27 10^3	3.11 10^3
900 [°C]	12.87 10^3	30.39 10^3	3.11 10^3
1000 [°C]	12.85 10^3	30.24 10^3	3.08 10^3
1100 [°C]	12.77 10^3	29.94 10^3	3.04 10^3

The temperature dependence of these three materials is negligible in the temperature range of concern. The conductivities of these electron conductors exhibit shallow maxima at temperatures between 800°C and 1000°C.

It appears to be permissible to use constant conductivities in SOFC modelling and analyses. The following values should be acceptable:

Cathode:	Mat C1	σ_e =	12.8 10^3	[S m^{-1}]
		or ρ_e =	78.1 10^{-6}	[Ω m]
Anode:	Mat A1	σ_e =	30.3 10^3	[S m^{-1}]
		or ρ_e =	33.0 10^{-6}	[Ω m]
Interconnect:	Mat I1	σ_e =	3.1 10^3	[S m^{-1}]
		or ρ_e =	325 10^{-6}	[Ω m]

These results are also presented in Figure B42.1.

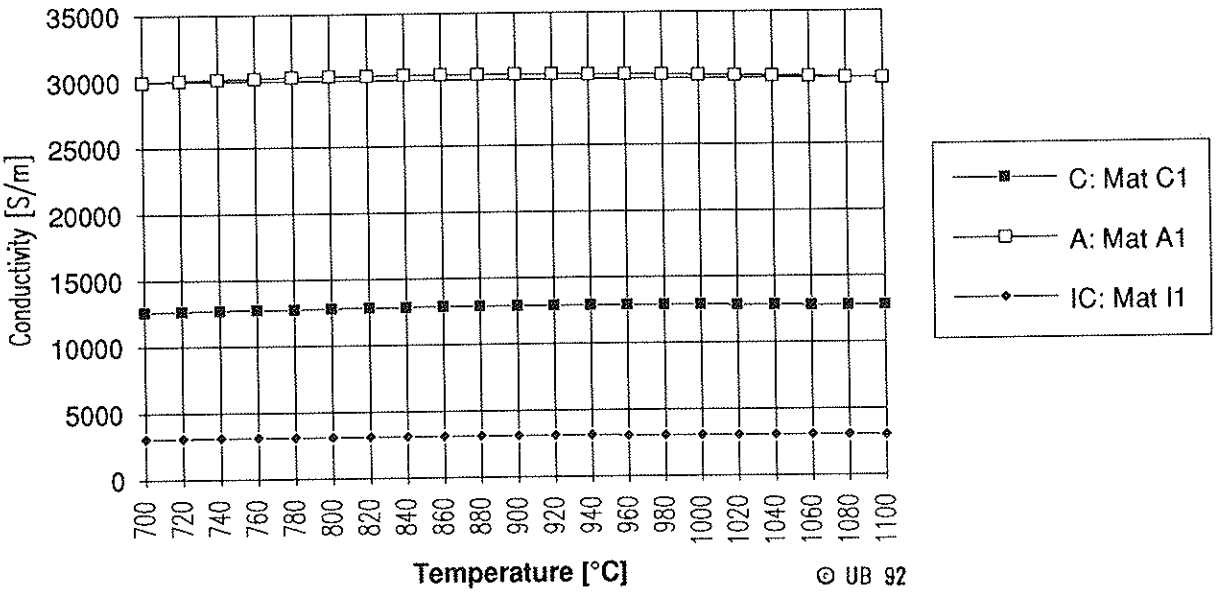

Figure B42.1: Conductivity of electron conducting materials as a function of temperature

B4.3 CONDUCTIVITY OF SELECTED METALS AND CARBON

The electrical conductivity σ_e of metals is orders of magnitude better than that of advanced ceramic electrode and interconnect materials. Therefore, the use of ceramic conductors should be limited to the necessary minimum, while metals should be used for the conduction of electric currents over longer distances. Care must be taken to properly select and protect the metallic conductors from various forms of corrosion by the hot atmospheres to which they are subjected in SOFC applications.

Table B43.3: Conductivity of selected metals and materials used in SOFC applications[2]

Material:	Temperature [°C]	Resistivity ρ_e [Ω m]	Conductivity σ_e [S m^{-1}]
Constantan	400	$0.448\ 10^{-6}$	$2.23\ 10^{6}$
Copper	1000	$0.942\ 10^{-6}$	$1.06\ 10^{6}$
Gold	1000	$0.125\ 10^{-6}$	$7.99\ 10^{6}$
Iron	400	$0.433\ 10^{-6}$	$2.31\ 10^{6}$
Platinum	1000	$0.470\ 10^{-6}$	$2.13\ 10^{6}$
Tungsten	727	$0.253\ 10^{-6}$	$3.95\ 10^{6}$
also:			
Graphite	1000	$8.70\ 10^{-6}$	$0.12\ 10^{6}$
Carbon	1000	$21.0\ 10^{-6}$	$0.05\ 10^{6}$

The electrical properties of metals and alloys are a function of temperature. Reliable data are obtained from the supplier of the material.

B4.4 CONDUCTIVITY OF STRUCTURAL CERAMIC MATERIALS

Only materials with insulating properties can be used for the porous support of electrically conducting ceramic materials (electrodes, electrolytes, interconnects). Otherwise, electric currents may find conducting paths within the SOFC element. This would then contribute to the internal losses and to a reduction of the useful electric power delivered to the grid.

In Table B44.1, the electric properties of common ceramic materials used for electrolyte support or structural applications are listed. These materials have negligible ionic and very low electronic conductivities.

Table B44.1: Electrical properties of ceramic structural materials used in SOFC application

Material:	Temperature [°C]	Resistivity ρ_e [Ω m]	Conductivity σ_e [S m^{-1}]
Mat S1	1000	> 0.5	< 2
Mat S2	1000	> 10	< 10^{-1}
Al_2O_3	1000	10^6	10^{-6}
MgO	1000	10^5	10^{-5}

B5 DIFFUSION COEFFICIENTS FOR GASES IN GASES

For the diffusion of gases in gases the following coefficients $D_{1,2}$ of species "1" in species "2" (also called "diffusivity") can be found in the literature [26,27].

Table B50.1: Diffusion Coefficients*) $D_{1,2}$

System	Temperature [K]	calculated [10^{-4} m^2 s^{-1}]	measured [10^{-4} m^2 s^{-1}]
O_2 - N_2	273	0.178	0.181 [26,27]
H_2 - H_2O	273	0.753	0.75 [27]
	293	0.852	0.85 [26]
H_2 - CO	273	0.637	0.651 [26,27]
H_2 - CO_2	273	0.547	0.550 [26,27]
	298	0.637	0.646 [27]
H_2 - CH_4	273	0.590	0.625 [26,27]
H_2O - CO	273	0.222	-
H_2O - CO_2	273	0.181	0.138 [27]
	298	0.210	0.164 [26]
H_2O - CH_4	273	0.230	-
CO - CO_2	273	0.138	0.137 [27]
CO - CH_4	273	0.186	-
CO_2 - CH_4	273	0.154	0.153 [26]
O_2 - H_2	773	4.12	4.2 [27]
O_2 - H_2O	723	1.24	1.3 [27]
O_2 - CO	723	0.959	1.0 [27]
O_2 - CO_2	773	0.856	0.9 [27]
O_2 - CH_4	773	1.17	1.1 [27]

*) Data compiled by A. Solheim, SINTEF, Trondheim/Norway

C ELECTROCHEMISTRY

C1 FUNDAMENTALS

The modeling of electrochemical processes which occur in a solid oxide fuel cell can be accomplished in several ways. The approach used here is intended to provide a basic, yet simple description in terms which are readily conceptualized and understood from a physical and intuitive point of view. Consequently, the use of equivalent electrical networks, impedances, etc. which facilitate solution procedures and/or compress the modeling are avoided. Hopefully, what remains is a unified, complete description containing basic equations describing the physical processes. These equations are intended to aid the engineer in the design of a solid oxide fuel cell.

Certain aspects of the SOFC electrochemistry are not completely understood at this time and are often modeled semi-empirically. Consequently, various constants appear in the equations (e.g. effective diffusion coefficients, activation energies, reaction rate constants etc.) which must be determined experimentally. While some values can be found in the literature, others have yet to be measured. More experimental data are needed to determine these values as well as a clearer experimental insight into the physics of the processes. Consequently, although the equations can provide a solution, they ultimately depend on reliable experimental evidence.

At operating temperatures of the SOFC the hydrocarbons of natural gas tend to decompose into lighter species. In fact, in the absence of oxygen solid carbon may be formed causing not only blockage of gas passages but also changes in the conversion electrochemisty. Details are not yet fully understood, but it is clear that conventional chemical and electrochemical processes occur simultaneaously and effect each other via rate constants, partial pressures, concentration gradients etc.

Therefore, the gas conversion chemistry shall be presented first.

C1.1 REFORMING OF HYDROCARBON FUELS

At the nominal SOFC operating temperature (e.g. 1200 K), the equilibrium constants for the reforming (R4 and R5) and shift reactions (R6) are:

$\log_{10}(K_p) = 3.383$ for $CH_4 + H_2O \leftrightarrow CO + 3H_2$ (R4)

$\log_{10}(K_p) = 3.518$ for $CH_4 + CO_2 \leftrightarrow 2CO + 2H_2$ (R5)

$\log_{10}(K_p) = -0.135$ for $CO + H_2O \leftrightarrow CO_2 + H_2$ (R6)

The numbers indicate that methane is primarily decomposed into H_2 and CO by two reforming reactions which are likely to occur simulataneously in the presence of H_2O and CO_2. If water vapor is added to the fuel stream, the "steam reforming" reaction R4 becomes dominant.

One of the attractive features of high temperature fuel cells is their potential to run on unreformed or partially reformed hydrocarbon fuels such as methane or natural gas. But it is still not clear whether

- methane oxidizes directly with oxygen at the electrolyte-anode interface
- methane first undergoes a series of reforming reations (R4 and R5) to form hydrogen and carbon monoxide which are then oxidized at the electrolyte-anode interface
- carbon monoxide is further shifted by reaction R6 and only hydrogen oxidizes at the electrolyte-anode interface
- all three types of reactions occur simultaneaously in the anode chamber
- reforming and shifting can be performed inside the anode chamber or external reactors must be used for the fuel processing.

In any event, reforming chemistry is an important part of the fuel cell process, but not an electrochemical reaction of the fuel cell itself.

Moreover, reforming reactions can occur at different locations within an SOFC system. The following three typical process locations are identified:

- **External reforming**: The reforming reactions occur in a chemical reactor physically separated from and not in thermal contact with the SOFC. The reactant H_2O (and/or CO_2) and the necessary heat are supplied to the reformer from external sources. Heat may be exchanged with the hot SOFC exhaust.

- **Internal reforming**: The reforming reactions occur in a region within the SOFC containment which is in thermal contact with the SOFC element. The reactant H_2O (and/or CO_2) are externally supplied, while the heat comes from the SOFC itself. Normally, the heat is conducted to the reformer region by structural SOFC stack components, i.e. by internal heat exchange.

- **In situ reforming**: The reforming reactions occur in the anode chambers of the SOFC stack or even on the anode surface itself. The reactants H_2O and CO_2 come from the conversion reactions and locally generated heat is utilized.

In all cases, if sufficient water vapor is present, the amount of CO can be minimized. This is necessary to prevent solid carbon formation as a result of fuel dissociation in the absence of oxygen, i.e. by reactions R11 and R12[7]. Carbon would fill the pores of the anode or block the flow passages in the anode chamber. Both could lead to a failure of the cell. To avoid such events, water vapor must be added or some fuel cell exhaust must be recycled to the fuel gas stream. Steam addition to the fuel gas not only triggers the reforming process, but also creates favorable condition for the shifting of carbon monoxide. As a consequence, hydrogen may be the dominant fuel for the electrochemical anode reaction even in cases where natural gas is uses as fuel for the SOFC.

In the following sections describing SOFC loss mechanisms, hydrogen is used as a typical fuel. In principle, the oxidation of CO and CH_4 could have been added but, by doing so, the mathematics would have become more complex without providing any additional understanding of the fundamental processes. The reforming of methane and the shifting of carbon monoxide are chemical processes of sufficient complexity to be dealt with separately.

C1.2 GIBBS VOLTAGE U_G

When the dynamics of the chemical reactions in the fuel cell (e.g. partial pressures of reactants and products) are not considered, the ideal fuel cell voltage is directly related to the Standard Gibbs free energy change $\Delta_f G^0$. This voltage or "standard potential", here called "Gibbs voltage" and denoted by U_G, shall therefore be used as reference voltage. It is computed by using the equation:

$$U_G = \frac{-\Delta_f G^0}{n_e F} \qquad \text{(C121)}$$

where:

$\Delta_f G^0$ = Standard Gibbs free energy change for reaction

n_e = number of electrons per molecule participating in the eloctrochemical exchange process:

n_e = 2 for reaction (R1)
= 2 for reaction (R2)
= 8 for reaction (R3)

F = Faraday constant

Both the Gibbs free energy change and the Gibbs voltage depend on the temperature at which the reaction occurs. For the fuel gases H_2, CO and CH_4, the Gibbs voltages are presented as a function of temperature in Table C13.1 and Figure C13.1.

C1.3 NERNST VOLTAGE

But to generate power an SOFC must be operated under conditions which reflect practical considerations (e.g. operation with atmospheric air fixes the O_2 partial pressure to 0.2 atm), fuel properties (e.g. reactions R1, R2 or R3) or engineering design (e.g. pressurized anode chamber). As a consequence, Equation C121 for the ideal Gibbs voltage, must be modified to include reaction kinetics of the chemical processes involved.

Therefore, the Gibbs voltage is corrected by a term decribing the chemical dynamics. The "Nernst voltage" U_N ,the actual cell voltage when the electrodes are at equilibrium, is defined by:

$$U_N = U_G - \frac{R_G T}{n F} \ln(K) \qquad \text{(C131)}$$

where K assumes in the general form:

$$K = \frac{\Pi[\text{product activities}]}{\Pi[\text{reactant actvities}]} \qquad (C132)$$

or applied to the reaction R1:

$$= \left[\frac{p_{H2O}}{p_{H2}\,(p_{O2})^{0.5}}\right] \qquad (C133)$$

with:

U_G = Gibbs voltage (C121)
R_G = Gas constant
F = Faraday constant
n = number of electrons participating in the reaction
p = partial pressures of O_2, H_2 and H_2O

To illustrate the difference between the two voltages, the following conditions are assumed for the three conversion reactions (R1, R2 and R3) of pure hydrogen, carbon dioxide or methane with air at atmospheric pressure in both cathode and anode chamber:

$p_{H2O} = p_{H2} = 0.5\ p_{at}$ (for $u_f = 1$)
$p_{O2} = 0.2\ p_{at}$ (for air)

The results are presented in Table C13.1 and Figure C13.1 The difference between the two voltages is recognizable for all three conversions.

Table C13.1: Gibbs and Nernst voltages [V] ($u_f = 1$)

Temperature [K]	800	1000	1200	1400
[°C]	527	727	827	1127
Reaction R1:				
U_G	1.055	0.999	0.941	0.882
U_N	1.028	0.964	0.899	0.834
Reaction R2:				
U_G	1.105	1.015	0.925	0.836
U_N	1.077	0.980	0.883	0.787
Reaction R3:				
U_G	1.038	1.038	1.037	1.037
U_N	1.034	1.033	1.032	1.030

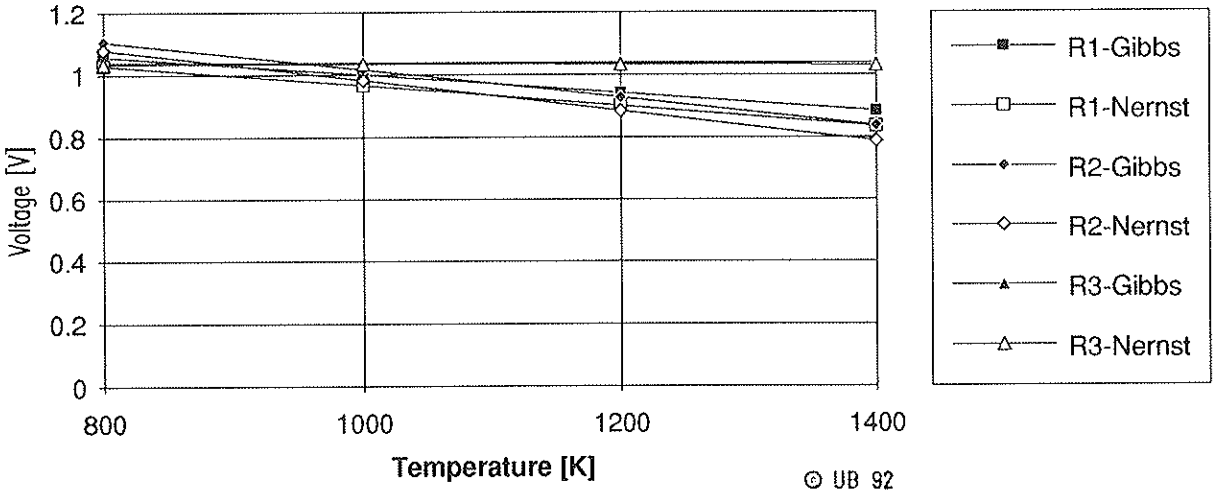

Figure C13.1: Gibbs and Nernst voltages for the reactions R1, R2 and R3

For the atmospheric H_2/O_2 reaction R1 and full fuel utilization the Nernst voltage is about 30 mV below the Gibbs voltage.

C1.4 GIBBS AND NERNST EFFICIENCY

The ideal fuel cell efficiencies are defined by the Gibbs free energy or the Nernst potential. Consequently, the terms "Gibbs efficiency" and "Nernst efficiency" are introduced and denoted by η_G (sometimes also called the "thermal" efficiency[6]) and η_N.

The Gibbs efficiency η_G is defined as the ratio of the freely convertible energy $\Delta_f G$ to the available enthalpy change $\Delta_f H$ of a particular reaction:

$$\eta_G = \frac{\Delta_f G}{\Delta_f H} = \frac{\Delta_f H - T * \Delta_f S}{\Delta_f H}$$

$$= 1 - \frac{T * \Delta_f S}{\Delta_f H} \qquad \text{(C141)}$$

The Nernst efficiency η_N relates a Gibbs function modified by the Nernst term to the available enthalpy change:

$$\eta_N = \frac{\Delta_f G - R_G T \ln(K)}{\Delta_f H} \qquad \text{(C142)}$$

At absolute zero temperature, both efficiencies are equal to unity for all chemical reactions. They changes with temperature. This change is dominated by the linear departure from unity. The slope of that departure depends on the chemical reaction. The weak dependence of $\Delta_f S$ and $\Delta_f H$ on temperature does not play a significant role over the temperature range of interest.

For the three prominent fuel reactions R1 to R3 the computed efficiencies are listed in Table C14.1 as a function of the temperature at which the conversion occurs:

Table C14.1: Gibbs and Nernst efficiencies [-] (u_f = 1)

Temperature [K]	800	1000	1200	1400
[°C]	527	727	927	1127
Reaction R1:				
η_G	0.826	0.777	0.729	0.681
η_N	0.804	0.750	0.696	0.643
Reaction R2:				
η_G	0.752	0.692	0.633	0.574
η_N	0.733	0.669	0.604	0.540
Reaction R3:				
η_G	1.001*	1.000*	0.998	0.996
η_N	0.997	0.995	0.993	0.990

*) whereas heat is produced in common H_2/O_2 fuel cells as a result of entropy production, in the CH_4/O_2 reaction energy is absorbed from the environment. Therefore, efficiencies above unity do not violate thermodynamic principles.

In Figure C14.1 the Gibbs and Nernst efficiencies of the three elementary reactions are depicted as a function of temperature. One should note that the Gibbs efficiency is the upper limit of a fuel conversion under stoichiometric conditions. Stoichiometry requires complete fuel utilization at zero air access (S = 1). As a consequence, stoichiometric conditions can not be accomplished. Therefore, the role of the Gibbs efficiency for fuel cells is comparable to the role of the Carnot efficiency in conventional heat engine processes.

Although Equations C131 and C142 suggest that the Nerst voltage and efficiency are always lower than the respective Gibbs properties, this is not generally true. In fact, at low fuel utilization the Nernst results may exceed the Gibbs voltage or efficiency.

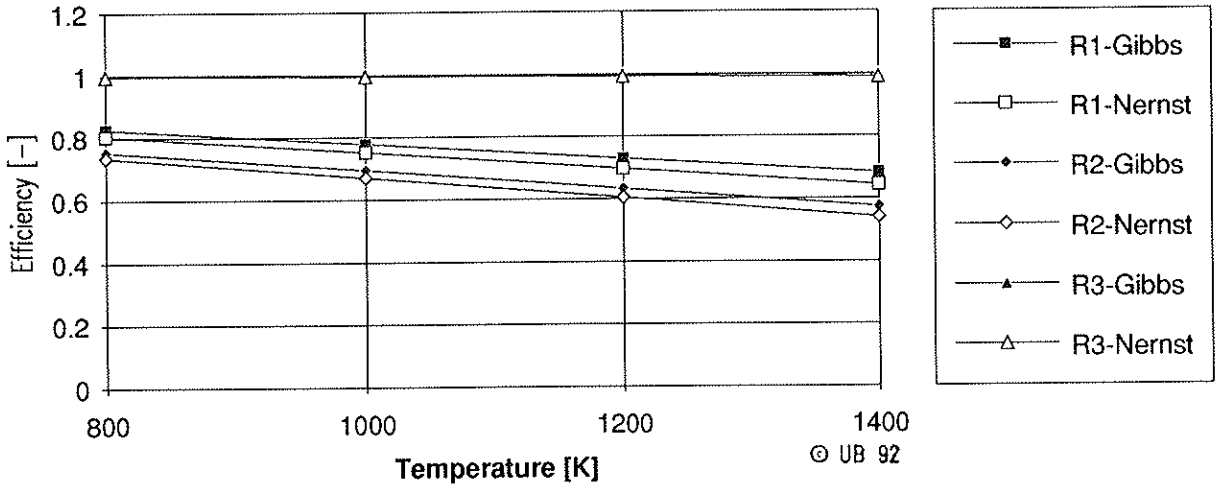

Figure C14.1: Gibbs and Nernst efficiencies for the reactions R1, R2 and R3

Because of the significance of the Gibbs efficiency as a limiting quantity for fuel cell applications, the following simplified expression has been derived for the three reactions R1, R2 and R3:

$$\eta_G \cong 1 - a * T \qquad \text{(C143)}$$

with $a = 0.2229 * 10^{-3}\ K^{-1}$ for hydrogen conversion
$a = 0.3076 * 10^{-3}\ K^{-1}$ for cabon monoxide conversion
$a = 0.0010 * 10^{-3}\ K^{-1}$ for direct methane conversion

C2 FLUXES IN FUEL CELL PROCESSES

In this section, the processes which determine the performance of the solid oxide fuel cell are described. A one-dimensional analysis is considered and only the processes occurring between the outer surfaces of the cathode and anode are considered. The extension to two or three dimensions is straightforward. The various mechanisms are illustrated in Figure C20.1 for the oxidation of hydrogen. The depletion of H_2 and O_2 in the fuel and oxidant supply streams are not considered since these are geometry dependent and hence difficult to include in a general way.

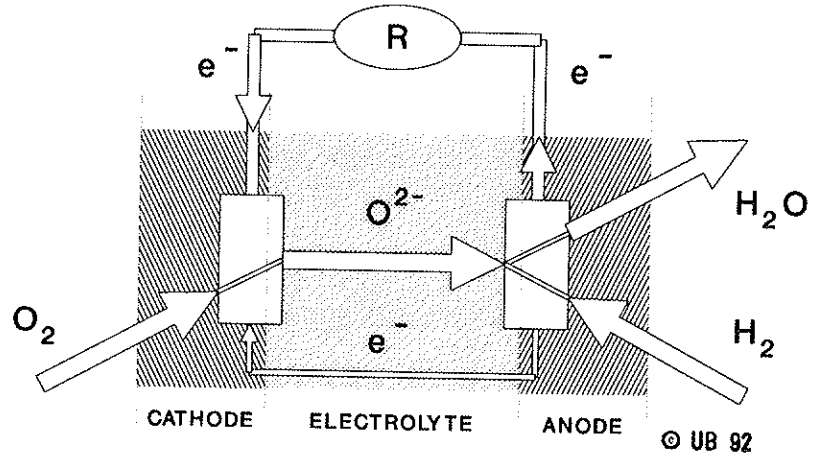

Figure C20.1: Flux of mass and charges in solid oxide fuel cells (e.g. H_2/O_2 reaction)

The six fundamental processes involving mass transport and the location of their occurrence are depicted schematically in Figure C20.2.

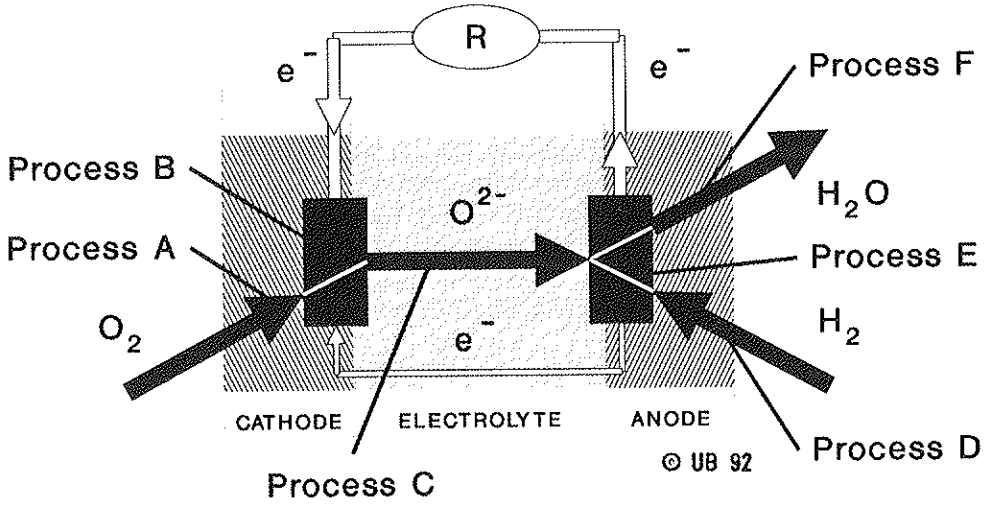

Figure C20.2: SOFC processes involving mass transport (e.g. H_2/O_2 reaction)

Process A: Diffusion of O_2 through porous cathode
Process B: Charge transfer to O_2 at cathode-electrolyte inferface
Process C: Diffusion of O^{2-} through electrolyte
Process D: Diffusion of H_2 through anode
Process E: Oxidation reaction of H_2 at anode-electrolyte interface
Process F: Diffusion of H_2O through anode

For each process an expression is given desribing the flux of the pertinent chemical species through that section. The fluxes are all related through the stoichiometry of the chemical reactions:

$$O_2 + 4\,e^- \leftrightarrow 2\,O^{2-}$$

$$H_2 + O^{2-} \leftrightarrow H_2O + 2\,e^-$$

Hence,

$$N_{O2} = 0.5\,N_{O2-}$$

$$N_{O2-} = N_{H2O}$$

and $$N_{H2} = N_{H2O} \qquad \text{(C201)}$$

In addition to the six voltage loss mechanisms related to the flow of neutral and charged atoms/molecules, three voltage loss mechanisms related to the flow of electrons are identified in Figure C20.3. These include the ohmic losses due to electric current flux in anode and cathode layers as well as the leakage of electrons back through the electrolyte from anode to cathode, i.e. against the stream of oxygen ions.

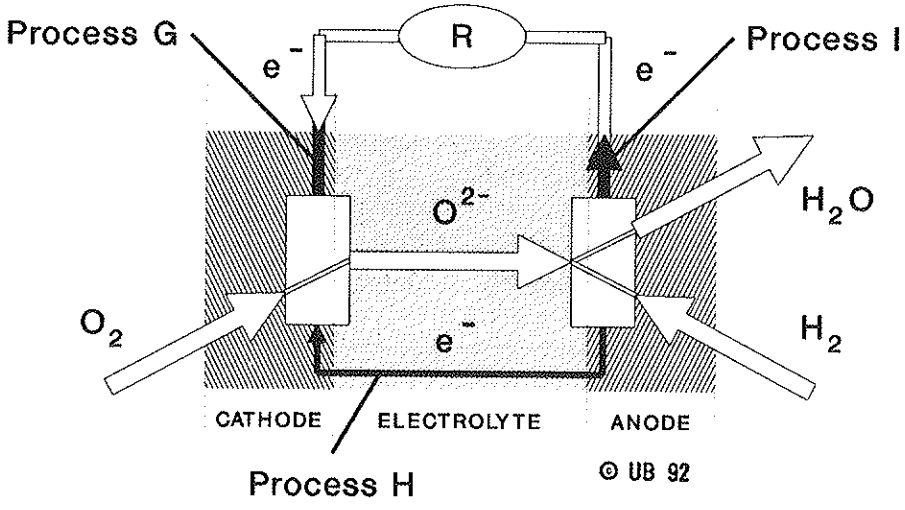

Figure C20.3: Processes involving only electric current flows (e.g. H_2/O_2 reaction)

Process G: Ohmic voltage loss in cathode
Process H: Electron leakage through electrolyte
Process I: Ohmic voltage loss in anode

The external electrical current, of course, is determined from the flux of electrons. It is equal to the flux of O^{2-} minus the internal leakage current. All fluxes of matter can be related to the electrical current.

Once the various species fluxes are determined from the supply concentration of H_2 and O_2, concentration profiles can be computed for each species in the appropriate fuel cell section for a given current. The concentration profiles are then used to determine the voltage reductions from the ideal fuel cell voltage, i.e. the Gibbs voltage U_G . Then for various external loads (or electrical currents) voltage-current curves can be computed yielding the desired information on fuel cell performance.

C3 LOSS MECHANISMS

C3.1 PROCESS A: DIFFUSION OF O_2 THROUGH POROUS CATHODE

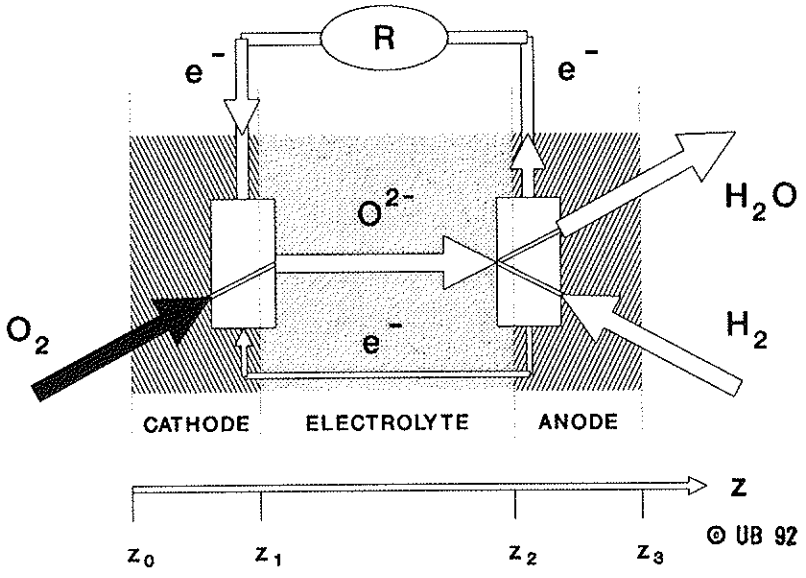

Figure C31.1: Diffusion of O_2 through cathode (e.g. H_2/O_2 reaction)

The flux of O_2 passing through the porous cathode is modeled as diffusion through a stagnant gas film[8]. The flux is then given by Ficks Law.

$$N_{O2,z} = -c\, D_{O2} \frac{dX_{O2}}{dz} + X_{O2}\,(N_{O2,z} + N_{N2,z}) \qquad (C311)$$

where

$N_{i,z}$ = flux of "i" in the "z" direction [mol m^{-2} s^{-1}]
c = the molar density of the mixture [mol m^{-3}]
D_{O2} = the effective diffusion coefficient of O_2 through the cathode [m^2 s^{-1}]
Xi = the mole fraction of component "i"

The term "$-c\, D_{O2}\, dX_{O2}/dz$" represents the flux due to a concentration gradient of O_2 while the term "$X_{O2}\,(N_{O2,z} + N_{N2})$" represents the flux due to the bulk motion of the mixture. In the stagnant gas film within the porous cathode there is no motion of N_2 (i.e. $N_{N2,z} = 0$). Equation C311 can then be rearranged to give

$$N_{O2,z} = \frac{-c\ D_{O2}}{1 - X_{O2}} * \frac{dX_{O2}}{dz} \qquad (C312)$$

The effective diffusion coefficient D_{O2} is a function of the binary diffusion coefficient of O_2 in N_2, $D_{O2,N2}$, the porosity of the cathode material Pc and a characteristic diameter d_{pc} of the pores

$$D_{O2} = f(D_{O2,N2},\ Pc,\ d_{pc}) \qquad (C313)$$

From conservation of mass considerations, the flux of O_2 must be the same at all "z" locations within the cathode. Consequently,

$$dN_{O2,z}/dz = 0 \qquad (C314)$$

Substituting Equation C312 in this expression gives

$$d\left(\frac{-c\ D_{O2,N2}}{1 - X_{O2}} * dX_{O2}/dz\right)/dz = 0 \qquad (C315)$$

The solution is

$$\left(\frac{1 - X_{O2}}{1 - X_{O2,z0}}\right) = \left(\frac{1 - X_{O2,ZiC}}{1 - X_{O2,Z0}}\right)^{z/z_1} \qquad 0 \le z \le z_1 \qquad (C316)$$

where use has been made of the boundary conditions

$$X_{O2}(z=0) = X_{O2,z0} \qquad (C317)$$

$$X_{O2}(z=z_1) = X_{O2,Z1C} \qquad (C318)$$

to evaluate the constants of integration and assuming C and $D_{O2,N2}$ are constants. The flux of O_2 is obtained by evaluation of the derivative in Equation C312 to yield

$$N_{O2,Z} = \frac{c\ D_{O2}}{z_1} \ln\left(\frac{1 - X_{O2,Z1C}}{1 - X_{O2,Z0}}\right) \qquad (C319)$$

C3.2 PROCESS B: CHARGE TRANSFER TO O_2 AT CATHODE-ELECTROLYTE INTERFACE

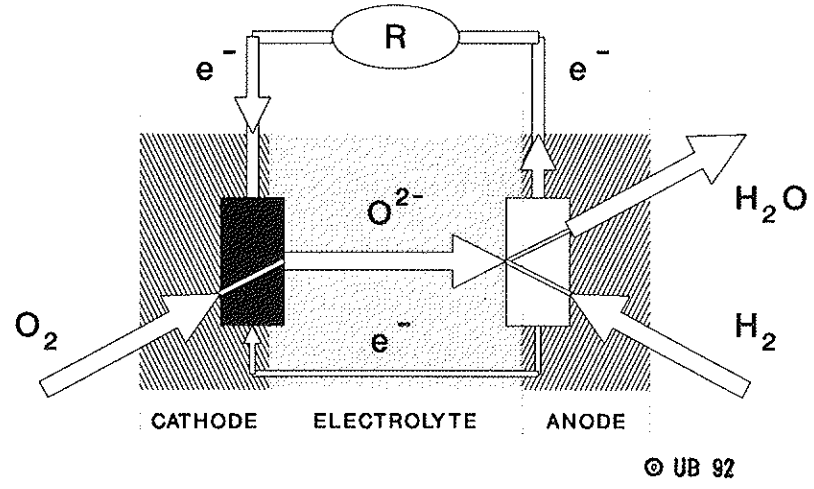

Figure C32.1: Charge transfer to O_2 at cathode-electrolyte interface (e.g. H_2/O_2 reaction)

At the cathode-electrolyte interface, oxygen moelcules are split into oxygen atoms which acquire two electrons each as they enter the solid electrolyte. The solid electrolyte is able to conduct oxygen ions due to oxygen vacancies and defects in its structure. The mechanisms by which this charge transfer and ion conduction occurs are complex and not fully understood. However, semi-empirical models have been developed and used successfully to describe the losses (resistance to current flow) by this process.

At the electrode-electrolyte interface the net current is expressed as the sum of two currents per unit area flowing in opposing directions, j_+ and j_-. Each of the currents is in turn assumed to be proportional to the concentration of O_2 or O^{2-}, depending on current direction, and on an associated Boltzmann factor, $\exp(-E_i/RT)$, accounting for the activation energies. The net current is then given[9] by

$$j = j_+ + j_-$$

$$j = K_+ \, c_{O2-} \exp\left(a\varepsilon \frac{F}{R\,T}\right) - K_- \, c_{O2} \exp\left(-(1-a)\varepsilon \frac{F}{R\,T}\right) \qquad \text{(C321)}$$

where

K_+, K_-	=	proportionality constants
c_{O2}, c_{O2-}	=	molar density of O_2 or O^{2-} at interface [mol m^{-3}]
F	=	Faraday constant
R	=	universal gas constant
T	=	temperature [K]
ε	=	electrical potential across interface [V]
a	=	charge transfer constant
j	=	electric current per unit area or current density [A m^{-2}]

When the net voltage loss ε is relatively large, one of the two terms in Equation C321 can be neglected in comparison to the other. At the cathode the second term, dominates while at the anode the first term is dominant. Hence, at the cathode the current is given by

$$j = K_- \, C_{O2} \exp\left(-(1-a)\varepsilon \frac{F}{R\,T}\right) \qquad \text{(C322)}$$

or alternately

$$\varepsilon = -\frac{R\,T}{(1-a)\,F} * \ln\left(\frac{j}{K_- \, C_{O2}}\right) \qquad \text{(C323)}$$

$$\varepsilon = a^* + b^* \ln(j) \qquad \text{(C324)}$$

This last equation expressing the losses due to the charge transfer process has the form of a "Tafel Equation"[6,8]. The Tafel slope "b^*" and the intercept "a^*" are determined from semi-logarithmic plots of experimental data.

The current flux is related to the molar flux of O^{2-} ions, N_{O2-} through the relation

$$j = 2 \, e \, N_A \, N_{O2-} = 2 \, F \, N_{O2-} \qquad \text{(C325)}$$

where

e	=	electrical charge of an electron
N_A	=	Avogadro's number
N_{O2-}	=	flux of O^{2-} ions through electrolyte [mol m^{-2} s^{-1}]

C3.3 Process C: DIFFUSION OF O^{2-} THROUGH ELECTROLYTE

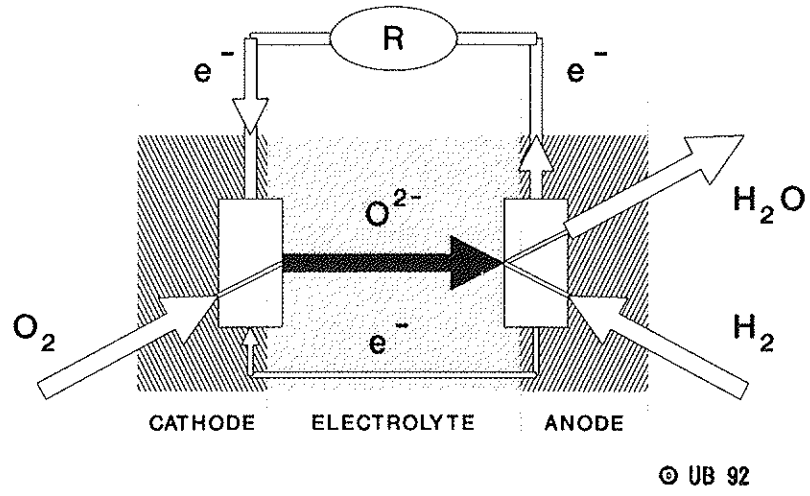

Figure C33.1: Diffusion of O^{2-} through electrolyte (e.g. H_2/O_2 reaction)

The flux of O^{2-} is also modeled with Fick's law of diffusion. However, since the electrolyte is a solid, there is no bulk[ ] motion of fluid and the O^{2-} flux results only from a concentration gradient. The equation is

$$N_{O2-,z} = - c D_{O2-,el} * dX_{O2-}/dz \qquad (C331)$$

where

$N_{O2-,z}$ = flux of O^{2-} in the z direction
$D_{O2-,el}$ = diffusion coefficient of O^{2-} in electrolyte
c = molar density of mixture

From conservation of mass considerations, the flux of O^{2-} is the same at all "z" locations in the electrolyte. Consequently

$$dN_{O2-,z}/dz = 0 \qquad (C332)$$

Substituting Equation C331 into this expression gives

$$d(- c D_{O2-,el} * dX_{O2-}/dz)/dz = 0 \qquad (C333)$$

The solution is

$$\frac{X_{O2-} - X_{O2-,z1el}}{X_{O2-,z2el} - X_{O2-z1el}} = \frac{z - z_1}{z_2 - z_1}, \qquad z_1 \le z \le z_2 \qquad \text{(C334)}$$

where

X_{O2-} = the mole fraction of O^{2-}
$X_{O2-,z1el}$ = the mole fraction of O^{2-} in the electrolyte at $z = z_1$
$X_{O2-,z2el}$ = the mole fraction of O^{2-} in the electrolyte at $z = z_2$

The flux of O^{2-} is then found by evaluating the derivative in equation C331

$$N_{O2-,z} = - c\, D_{O2-,el} * \frac{X_{O2-,z2el} - X_{O2-,z1el}}{z_2 - z_1} \qquad \text{(C335)}$$

By identifying the total flux of oxygen ions N_{O2-} with a current I, the concentration difference $c(X_{O2-,z2el} - X_{O2-,z1el})$ with a voltage potential ΔU and the inverse of the diffusion coefficient $D_{O2-,el}$ with a resistance R_i, an equivalent expression describing this process appears as Ohm's Law

$$I = \Delta U / R_i \qquad \text{(C336)}$$

C3.4 PROCESS D: DIFFUSION OF FUEL GAS THROUGH POROUS ANODE

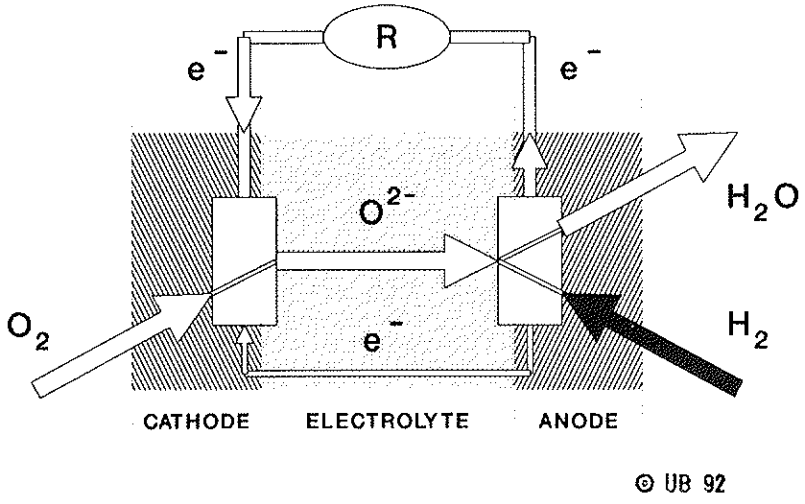

Figure C34.1: Diffusion of fuel gas (H_2) through anode (e.g. H_2/O_2 reaction)

The flux of fuel gas, in this case hydrogen, through the anode is modeled with Fick's law of diffusion[18]

$$N_{H2} = -c\, D_{H2} * dX_{H2}/dz + X_{2H}\,(N_{H2} + N_{H2O}) \qquad (C341)$$

where

N_i = the flux of compound "i" in the "z" direction
c = the molar density of the mixture [mol m^{-3}]
D_{H2} = the effective diffusion coefficient of H_2 through anode
X_i = the mole fraction of compound "i"

In this situation H_2 is diffusing towards the anode-electrode interface (negative z-direction) while H_2O is diffusing away from the interface. From the stoichiometry of the reaction

$$H_2 + O^{2-} \leftrightarrow H_2O + 2e$$

we know that $N_{H2} = - N_{H2O}$ at steady state. Making this substitution into Equation C341 and solving for N_{H2} gives

$$N_{H2} = - c\, D_{H2} * dX_{H2}/dz \qquad (C342)$$

Conservation of mass requires that the flux of H_2 be constant at each "z" location. Consequently

$$dN_{H2}/dz = 0$$

$$d(-c\ D_{H2} * dX_{H2}/dz)/dz = 0$$

The solution to this equation is

$$\frac{X_{H2} - X_{H2,z2a}}{X_{H2,z3a} - X_{H2,z2a}} = \frac{z - z_2}{z_3 - z_2} \qquad z_2 \le z \le z_3 \qquad \text{(C345)}$$

where

$X_{H2,z2a}$ = the mole fraction of H_2 in the anode at $z = z_2$

$X_{H2,Z3a}$ = the mole fraction of H_2 in the anode at $z = z_3$

The flux of H_2 is found by evaluating the derivative of Equation C342

$$N_{H2} = - c\ D_{H2} * \frac{X_{H2,z3a} - X_{H2,z2a}}{z_3 - z_2} \qquad \text{(C346)}$$

The effective diffusion coefficient includes the effects of anode porosity and pore geometry as in Process A (see section C3.1).

C3.5 PROCESS E: OXIDATION REACTION OF H_2 AT ANODE-ELECTROLYTE INTERFACE

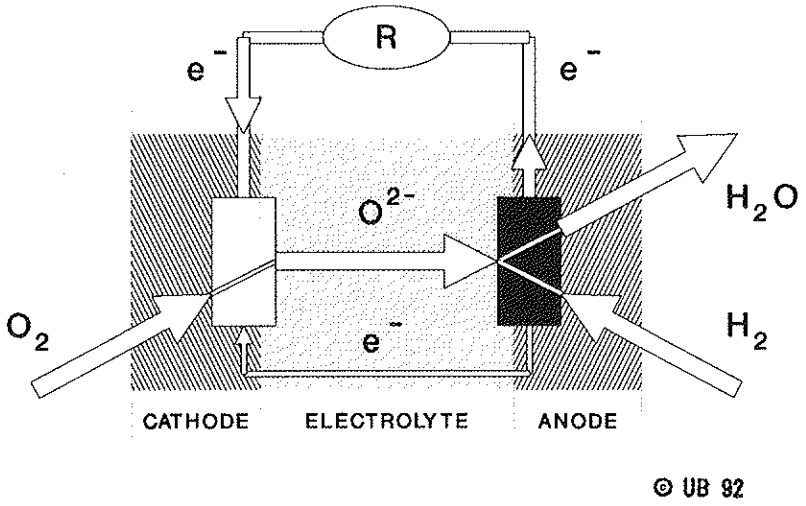

Figure C35.1: Oxidation reaction of H_2 at anode-electrolyte interface (e.g. H_2/O_2 reaction)

At the anode-electrolyte interface, oxygen ions give up two electrons and combine with an H_2 molecule to form H_2O. Along this interface, these 3 phases (electrolyte with O^{2-}ions, anode and H_2) must come together simultaneously before the reaction can occur. The mechanisms by which the O^{2-}ions give up electrons (i.e. a charge transfer process) and combine with H_2 molecules (i.e. an oxidation reaction) are complex and not fully understood. Here, the charge transfer process is assumed to occur much faster than the oxidation reaction. Consequently, the oxidation reaction is assumed to be the rate determining step and the charge transfer process is neglected[6,9,10,11].

Assuming the charge transfer process produces "O" atoms from "O^{2-}" ions, the oxidation reaction is modelled semi-empirically using the reaction of molecular hydrogen with **atomic** oxygen

$$H_2 + O \leftrightarrow H_2O \qquad (C351)$$

The rate of formation of H_2O is assumed to be driven by some function of the chemical potential difference between product and reactants. Often a linear

$$N_{H2O} = C\ \Delta\mu_{rx} \qquad (C352)$$

or exponential

$$N_{H2O} = A\ [\exp(\frac{B\,\Delta\mu_{rx}}{RT}) - 1] \qquad \text{(C353)}$$

rate law is assumed, where A, B and C are constants determined from experimental data. The chemical potential of the reaction ΔG_{rx} is computed by summing the chemical potentials of the constituents

$$\Delta G_{rx} = \Sigma \nu_i \mu_i = \mu_{H2O} - \mu_{H2} - \mu_O \qquad [J\ mol^{-1}] \qquad \text{(C354)}$$

where the chemical potential of each species μ_i is given by

$$\mu_i = \mu_0 + RT * \ln(X_i) \qquad \text{(C355)}$$

μ_i may be considered the Gibbs free energy of species i, X_i is the mole fraction, T is the temperature and R is the unversal gas constant.

Hence the chemical potential for the reaction of hydrogen molecules with atomic oxygen (C351) becomes

$$\Delta G_{rx} = \Delta_f G^0 + RT \ln(\frac{X_{H2O}}{X_{H2}\ X_O}) \qquad \text{(C356)}$$

$\Delta_f G$ for reaction C351 is <u>not</u> listed in Table A33.1.

If the charge transfer proces produces O_2 molecules instead of O atoms similar computations would be made but the chemical potential of O_2 would replace μ_O and the oxidation would follow the reaction

$$H_2 + 0.5\ O_2 \leftrightarrow H_2O$$

The chemical potential for this reaction becomes

$$\Delta G_{rx} = \Delta_f G^0{}_{H2O} + RT \ln(\frac{X_{H2O}}{X_{H2}\ X_{O2}{}^{0.5}}) \qquad \text{(C357)}$$

$\Delta_f G^0{}_{H2O}$ is given in Table B40.1.

Furthermore, if the exponential expression is the proper expression describing the formation rate of H_2O then this expression may be put into a Tafel form by recognizing that $D\mu$ is a driving force proportional to a voltage difference ε and that the flux of H_2O, N_{H2O}, is proportional to the current density i . Hence an equation of the form

$$\varepsilon = a^* + b^* \ln(i) \qquad \text{(C358)}$$

C3.6 PROCESS F: DIFFUSION OF REACTION PRODUCTS THROUGH POROUS ANODE

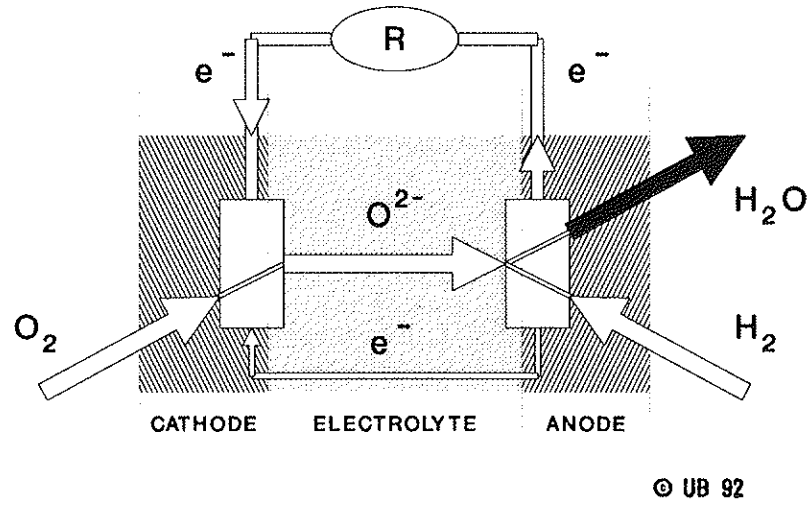

Figure C36.1: Diffusion of reaction products (H_2O) through porous anode (e.g. H_2/O_2 reaction)

The flux of the reaction products, in this case H_2O, through the porous anode can be modeled using Fick's law of diffusion[6,8]

$$N_{H2O} = -c\, D_{H2O} * dX_{H2O}/dz + X_{H2O}\,(N_{H2O} + N_{H2}) \qquad (C361)$$

where

N_i = the flux of "i" in the "z" direction
c = molar density of the mixture [mol m^{-3}]
D_{H2O} = the effective diffusion coefficient of H_2O through anode
X_i = the mole fraction of compound "i"

The solution is the complementary half of Process D, the diffusion of H_2 through the porous anode. There it was recognized that H_2 and H_2O were diffusing in opposing directions.

From the stoichiometry of the reaction

$$H_2 + O^{2-} = H_2O + 2e$$

it was noted that $N_{H2} = - N_{H2O}$. Consequently, the resulting flux of H_2O may be written directly from the result of Process D or a similar derivation performed. In either case, the H_2O molar fraction profile is given by

$$\frac{X_{H2O} - X_{H2O,z2a}}{X_{H2O,z3a} - X_{H2O,z2a}} = \frac{z - z_2}{z_3 - z_2} \qquad \text{(C362)}$$

and the H_2O molar flux by

$$N_{H2O} = - c\, D_{H2O} * \frac{X_{H2O,z3a} - X_{H2O,z2a}}{z_3 - z_2} \qquad \text{(C363)}$$

where it is noted that

$$N_{H2O} = - N_{H2}$$

C3.7 PROCESS G: OHMIC VOLTAGE LOSS IN CATHODE

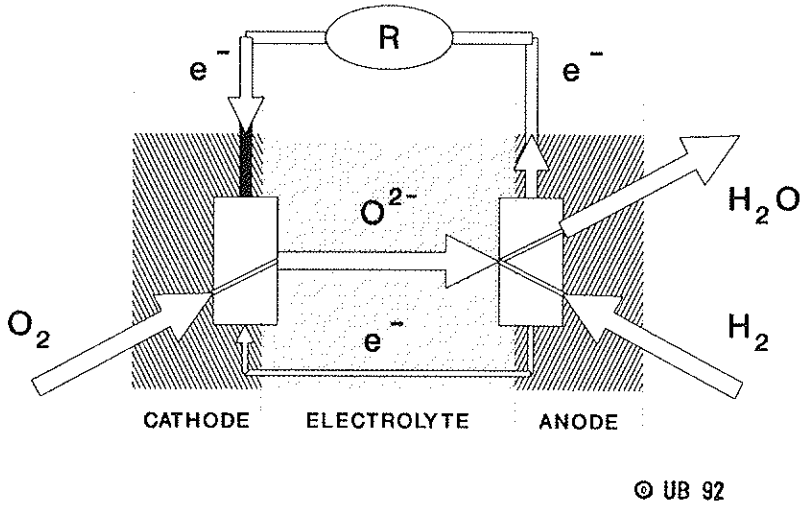

Figure C37.1: Ohmic voltage loss in cathode (e.g. H_2/O_2 reaction)

The voltage losses resulting from the flow of electrical currents along the length of the cathode depend on the geometry of the positive electrode-electrolyte-negative electrode ("PEN") configuration. These losses may be a dominant contributor to the inefficiency of SOFC elements, stacks and systems.

Since it is the function of electrodes to collect electrons from the entire electrolyte area, the conducted electric currents vary from point to point. Generally speaking, the electric currents are highest at the electric current collectors or interconnects of SOFC elements and decrease with distance from these terminals.

The ohmic losses in cathodes are thus also related to the PEN geometry. Typical PEN configurations are analyzed in Chapter D.

C3.8 PROCESS H: ELECTRON LEAKAGE THROUGH ELECTROLYTE

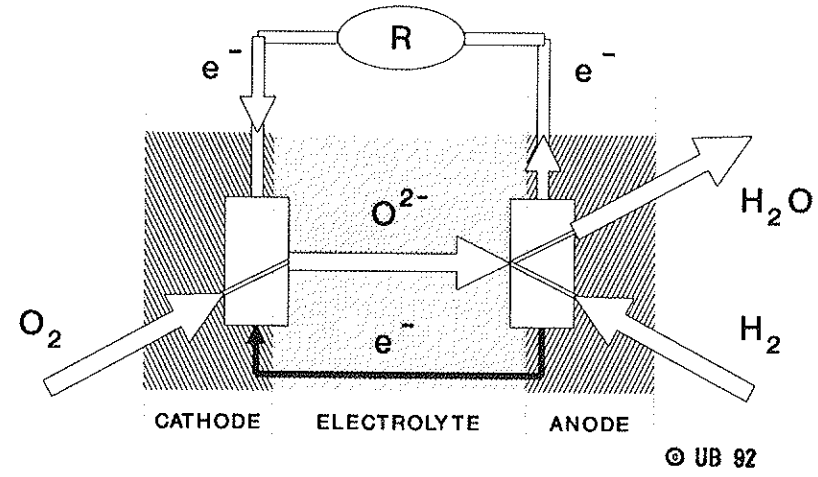

Figure C38.1: Electron leakage through electrolyte (e.g. H_2/O_2 reaction)

The passage of electrons through the electrolyte from the anode to the cathode instead of passing throught the external load, can be modeled in the same manner as the passage of oxygen ions through the electrolyte. Fick's law of diffusion gives[6,8]

$$N_e = - D_{e,el} \, dc_e/dz \qquad (C381)$$

where the term accounting for the bulk motion of fluid is omitted since the electrolyte is a solid. In this case the electron flux is proportional to a leakage current, i.e., the diffusion coefficient $D_{e.el}$ is proportinal to the electron conductance of the electrolyte and the concentration gradient dc_e/dz is proportional to the voltage difference between the anode and cathode. Consequently the total electron leakage may also be described by Ohm's law

$$I_e = \Delta U \; / \; R_e \qquad (C382)$$

where

I_e = electron leakage current [A]
ΔU = voltage difference between anode and cathode [V]
R_e = electron resistance of the electrolyte
$R_e = \rho_e \, Z_e/A_e$ [Ω]
ρ_e = electron resistivity of the electrolyte [Ω m]
Z_e = thickness of the electrolyte [m]
A_e = active electrolyte area [m^2]

The effect of this inefficiency is not a reduction of the electric current available at the fuel cell terminals.

C3.9 PROCESS I: OHMIC VOLTAGE LOSS IN ANODE

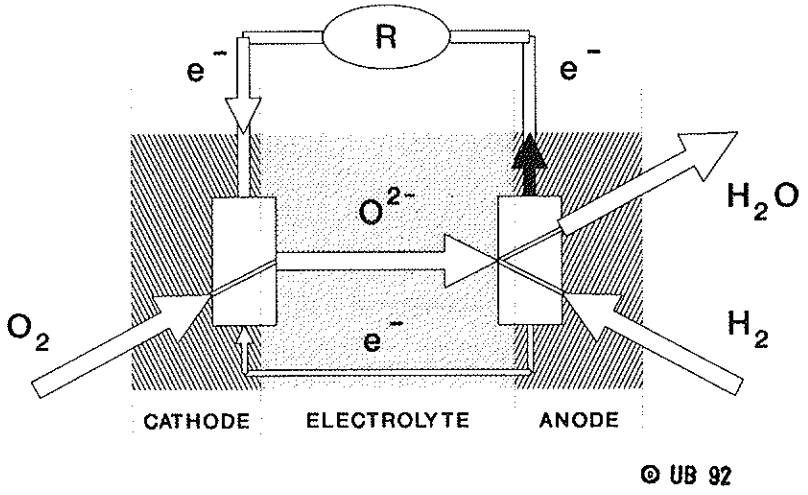

Figure C39.1: Ohmic voltage loss in anode
(e.g. H_2/O_2 reaction)

As in Process G, the voltage losses resulting from the flow of electron currents along the length of the anode also depend on the geometry of the positive electrode-electrolyte-negative electrode ("PEN") configuration.

Since it is the function of electrodes to collect electrons from the entire electrolyte area, the conducted electric currents vary from point to point. Generally speaking, the electric currents are highest at the electric current collectors or interconnects of SOFC elements and decrease with distance from these terminals.

The ohmic losses in anodes are thus also related to the PEN geometry. Typical PEN configurations are analyzed in Chapter D.

Again, the ohmic losses in the anode layer may contribute significantly to the inefficiency of the system. But losses due to sheet resistance of electrodes are not of electrochemical nature. They can be reduced by proper design of the SOFC element, by choice of materials and fabrication methods.

D ELECTRIC CURRENT FLOW IN SOFC ELEMENTS

D1 BASICS

In fuel cells, electric charges are conducted at a number of places either by electron or by ion currents. The subscripts "e" and "i" shall be used to identify electronic or ionic transport processes, respectively. Although the conduction mechanisms are of a different nature, both charge transport phenomena obey Ohm's law

$$\Delta U = I\,R \qquad \text{(D101)}$$

where

ΔU = $U_1 - U_2$, driving voltage difference [V]
I = charge current: I_e = electron current [A]; I_i = ion current [A]
R = resistance: R_e = electronic resistance [Ω]; R_i = ionic resistance [Ω]

In fuel cell work, the total current I is frequently related to the current flow cross sectional area A. For both types of charge transport a current density i (a better name would be "charge flux intensity") is defined by

$$i_e = \frac{I_e}{A} \quad \text{or} \quad i_i = \frac{I_i}{A} \qquad \text{(D102)}$$

For given total current I and voltage drop ΔU the power loss by ohmic dissipation ΔP is given by

$$\Delta P = I\,\Delta U = I^2\,R = i^2\,A^2\,R \qquad \text{(D103)}$$

One of the most important task of SOFC design is to minimize the total internal resistance R_{tot} of an SOFC stack or module. These building blocks are composed of a number of conducting elements each one resisting the flow of electrons or ions. In general, the resistance of any one of these resistors is given by

$$R_e = \rho_e \frac{L_e}{A_e} \quad \text{or} \quad R_i = \rho_i \frac{L_i}{A_i} \qquad \text{(D104)}$$

where

ρ = resistivity [Ω m] (formerly [Ω cm])
L = current path length [m]
A = current path cross section [m^2]

In many applications the conductivity σ [Ω^{-1} m^{-1} = S m^{-1}] is used. It is defined as the inverse of the resistivity, $\sigma = 1/\rho$.

Some materials conduct both electrons and ions at the same time. For electron conductors, the electronis conductivity σ_e is orders of magnitude higher than the ionic conduction σ_i . The opposite is true for electrolytes. Ionic conduction dominates over electronic conduction.

In SOFC stacks or modules a large number of resistor elements are arranged in series or parallel. The electric circuit depends on the SOFC configuration considered. The total resistance of an SOFC stack or module is thus determined by two types of arrangements of the elemental resistor.

Serial connection of resistances R_1, R_2, R_3, ... R_n

$$R_{tot} = R_1 + R_2 + R_3 + \ldots + R_n$$

or $$R_{tot} = \Sigma[R_n] \qquad \text{(D105)}$$

Parallel connection of resistances R_1, R_2, R_3, ... R_n

$$1/R = 1/R_1 + 1/R_2 + 1/R_3 + \ldots + 1/Rn$$

or

$$R_{tot} = \frac{1}{\Sigma[1/R_n]} \qquad \text{(D106)}$$

Equations D101 to D106 suffice to analyze elementary SOFC networks, Chapter D2. For two-dimensional current flows in real SOFC structures, the same basic laws are cast into differential forms and second order differential equations must be dealt with.

D2 CHARGE TRANSPORT IN LINEAR CONDUCTORS OF CONSTANT CROSS SECTION

D2.1 CONDUCTING WIRE

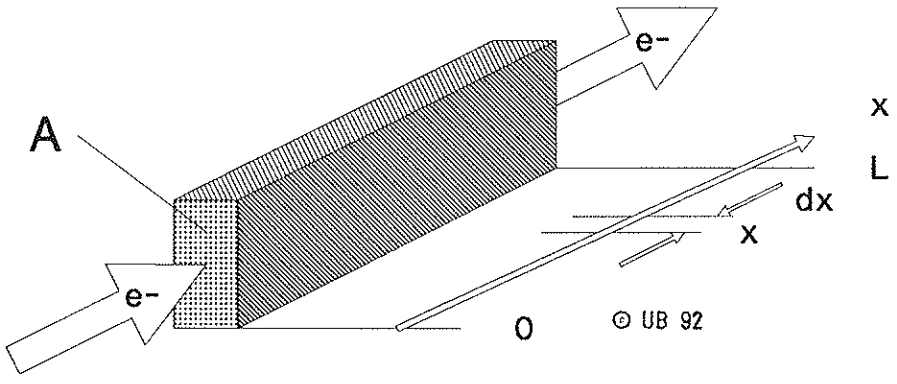

Figure D21.1: Electron current transport by a linear conductors of uniform cross section

The analysis applies to the conventional electonic conduction by wires as well as the ionic conduction through channels of constant cross section filled with stagnant electrolytes. For an electron conductor of length L one obtains for the resistance:

$$dR_e(x) = \frac{\rho_e \, dx}{A}$$

$$R_e = \frac{\rho_e \, L}{A} \qquad \text{(D211)}$$

D2.2 CHARGE TRANSPORT IN CONDUCTORS OF VARIING CROSS SECTIONS

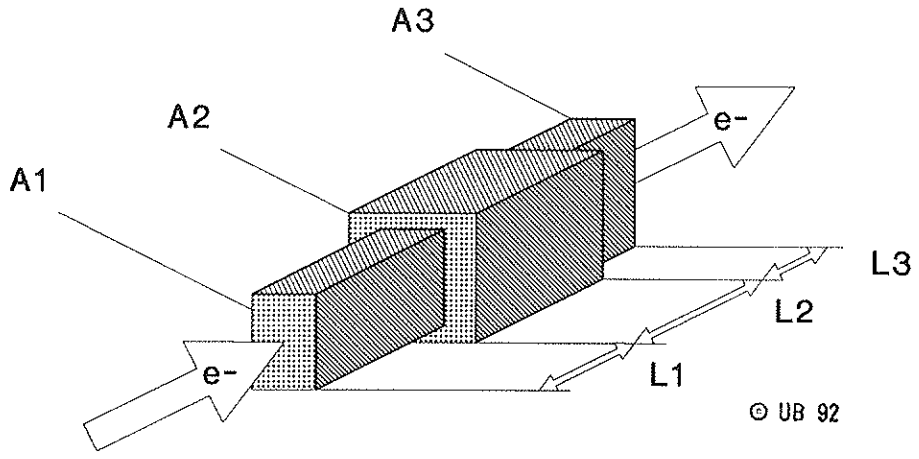

Figure D22.1: Charge transport in a conductor of variing cross section

The conductor may be modelled as a series of conducting elements of different lengths L_n all having different, but constant cross sections A_n .

$$R = R_1 + R_2 + R_3 + \ldots + R_n$$

$$= \rho\, L_1/A_1 + \rho\, L_2/A_2 + \rho\, L_3/A_3 + \ldots + \rho\, L_n/A_n$$

$$= \rho\, \Sigma[L_n/A_n] \qquad \text{(D221)}$$

D2.3 IN-PLANE CHARGE TRANSPORT BY CONDUCTING SHEETS

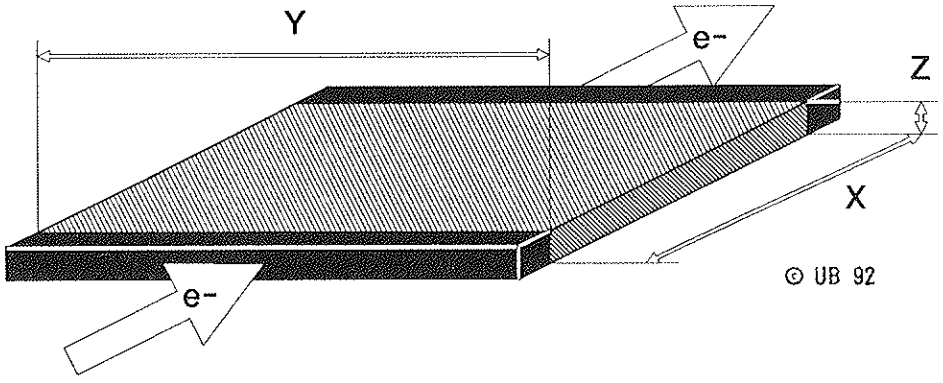

Figure D23.1: In-plane charge transport by conduction sheets

In SOFC configurations, such sheets may be interconnect strips or the electrochemically "passive" edges of anodes or cathodes which conduct the current from the "active" region to the interconnect. The resistance of such cunducting sheets is found by analogy with Equation D21.1

$$R = \rho_e \frac{L_e}{A} = \rho_e \frac{X}{Y\ Z} \qquad \text{(D231)}$$

where

X = sheet length in current direction [m]
Y = sheet width normal to current direction [m]
Z = sheet height nomral to current direction [m]

D2.4 ION CURRENT CONDUCTION ACROSS ELECTROLYTE SHEETS

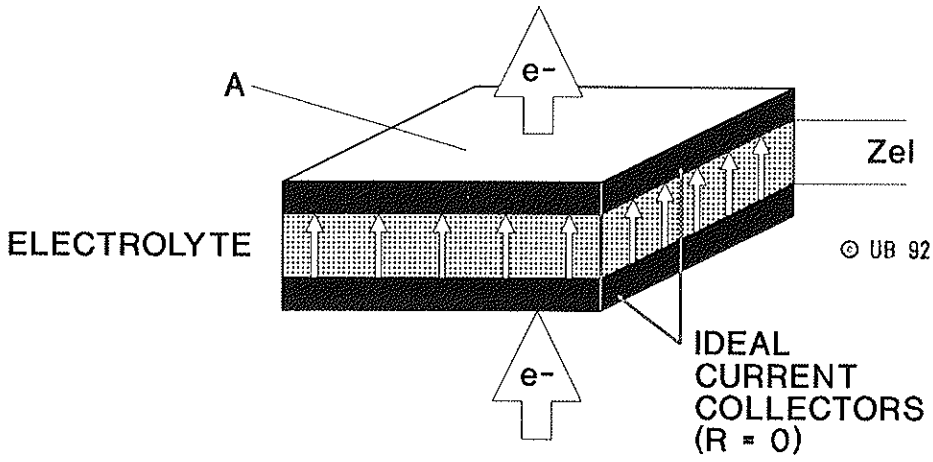

Figure D24.1: Charge current conduction across sheets

The analysis for ion current flows across electrolyte sheets of thickness Z_{el} is similar to that for the conducting wire. One obtains for the electrolyte resistance to cross-plane ion flow:

$$R_{el} = \frac{\rho_{el}\, Z_{el}}{A} = \frac{\rho_{el}\, Z_{el}}{X\ Y} \qquad \text{(D241)}$$

The effective electrolyte resistivity ρ_{el} is the difference of ionic and electronic resistivity of the electrolyte material at given temperature. As ion and electron currents are parallel both drawing from the same potential, the effective electrolyte resistivity is computed using the inverse of the resisitivities of the conductivities σ

$$\sigma_{el} = \sigma_i + \sigma_e$$

or

$$1/\rho_{el} = 1/\rho_i + 1/\rho_e \qquad \text{(D242)}$$

D2.5 CROSS-PLANE RESISTANCE OF CATHODE-ELECTROLYTE-ANODE STRUCTURES

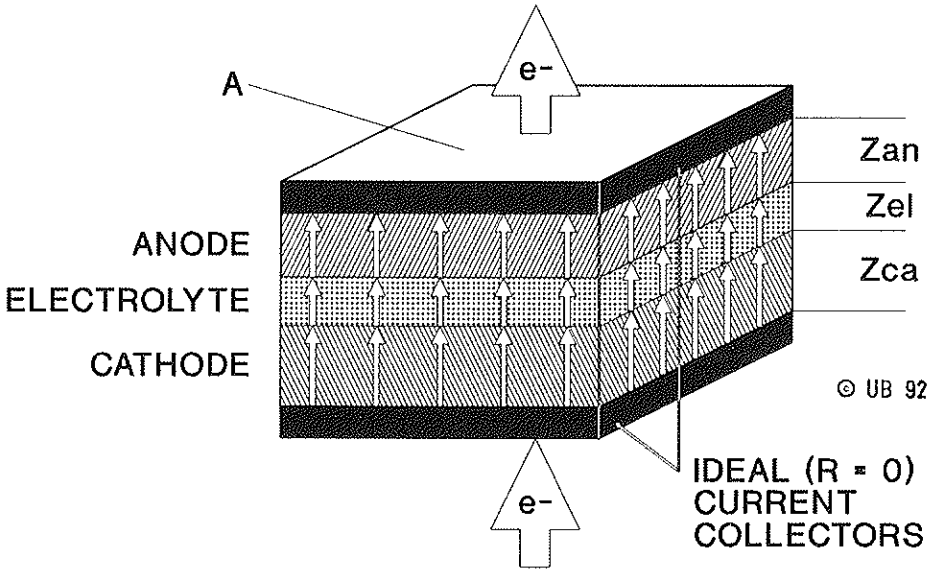

Figure D25.1: Cross-plane charge flow through an active SOFC element consisting of cathode, electrolyte and anode sheets

Neglecting interfaction resistances, the cross-plane resistances R_{ca} of the cathode, R_{el} of the electrolyte and R_{an} of the anode layers are added as suggested by Equation D105.

$$R_{tot} = R_{ca} + R_{el} + R_{an}$$

$$= \rho_{ca}Z_{ca}/A + \rho_{el}Z_{el}/A + \rho_{an}Z_{an}/A \qquad (D251)$$

This expression has been presented in the form

$$C = R_{tot}\ A$$

$$= \rho_{ca}Z_{ca} + \rho_{el}Z_{el} + \rho_{an}Z_{an} \quad [\Omega\ m2] \qquad (D252)$$

with C called the "cross-plane resistance area"[20]. In some publications, the misleading term "area-specific resistance" is still in use.

D3 CHARGE TRANSPORT IN 2-DIMENSIONAL PEN STRUCTURES

The abbriviation "PEN" has been introduced for the **p**ositive electrode, **e**lectrolyte, **n**egative electrode tri-layer of active electrochemical elements. A "PEN structure" is such a tri-layer to which terminals or interconnects have been attached so that the two-dimensional current flow field is uniquely defined.

In reality, the charge transport in SOFC elements is always two-dimensional. It is composed of "in-plane" as well as "cross-plane" conductance as defined in the previous two chapters. While ions are conducted directly across the electrolyte, the electrons must move some distance along the electrodes towards a terminal or the interconnect.

Considering the thickness of the three layers, the in-plane current paths may exceed the cross-plane current paths by orders of magnitude. For a 15 mm wide PEN strip with 0.05 mm thick electrodes the in-plane current path is up to 300 times longer than the cross-plane distance. As a consequence, ohmic resistance in the electrode sheets may become the dominant loss contribution of "in-plane conducting" SOFC configurations.

D3.1 DIFFERENTIAL EQUATION

The Figures D32.1, D33.1, D35.1, D35.2 and D35.3 presented below all illustrate that the electron current introduced to the PEN structure at the cathode terminal is dissipated into the electrolyte while it is collected at the anode and appears again in full strength at the anode terminal. Thus, the electron currents in the electrodes are not uniform, but decrease with distance from the terminals.

Also, to make the currents flow along the electrodes, a driving voltage gradient must not only exist, but it must be alligned with the direction of current flow. For the case depicted by Figure D32.1 the cathode potential must be higher at the cathode terminal than at the right edge of the PEN structure. Similarly, the potential on the right edge of the anode must be higher than at the anode terminal, otherwise electrons would not move towards the terminal.

Because of the different conductivities of anode and cathode materials, the potential gradients along along both electrodes may differ. As a consequence, if an exernal voltage is impressed upon the PEN structure, the voltage potential across the electrolyte may also become a function of location, i.e. the ion

flux distribution over the electrolyte surface also becomes non-uniform.

But in the case of fuel cells the electrochemical potential is the driving force and remains constant across the electrolyte surface as long as effects like fuel depletion (Nernst potential) remain insignificant.

For the SOFC the following 2nd order differential equation can be derived[20,21,22,23]. It applies to arbitirary geometries:

$$\Delta^2 U = U/L^2 \qquad \text{(D311)}$$

where
Δ^2 = is the Laplace operator
U = voltage potential [V]
L = characteristic length [m]

Filling in the details yields for the characteristic length L the following expression:

$$L = [(\rho_{el} Z_{el})/(\rho_{an}/Z_{an} + \rho_{ca}/Z_{ca})]^{1/2} \text{ [m]} \qquad \text{(D312)}$$

where
Z_{el}, Z_{an} and Z_{ca} = sheet thicknesses of electrolyte, anode and cathode
ρ_{el}, ρ_{an} and ρ_{ca} = resistivities of electrolyte, anode and cathode

The spatial dependence of the voltage potential is thus scaled by a parameter formed by the resistivities and sheet thicknesses of the three PEN layers cathode, electrolyte and anode.

For PEN strips and PEN disks Equation D311 has closed form solutions. These depend on the boundary conditions, i.e. on the attachment of the terminals to the PEN structure. Solutions can be found for two strip and three disk configurations. For other geometries the differential equation must be solved numerically.

The solutions describe the voltage potential between the two terminals. The voltage drop can be related to the internal ohmic resistance of the investigated PEN structure. In the following, only the internal ohmic resistance shall be presented. But the reader is referred to[21] for further details on the analysis.

D3.2 OHMIC RESISTANCE OF PEN STRIP WITH ALIGNED TERMINALS

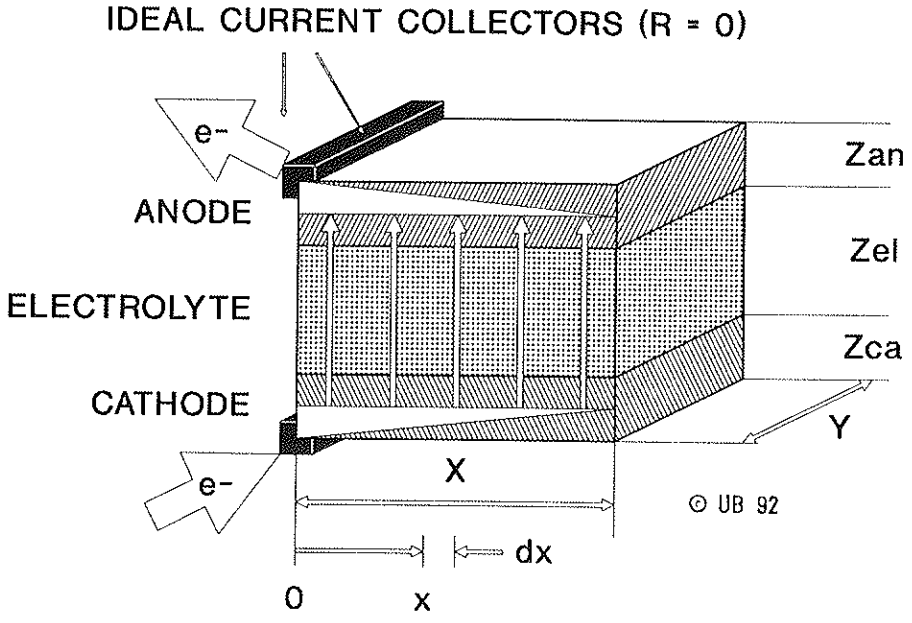

Figure D33.1 PEN strip with aligned terminals

The general solution of the one-dimensional form of the differential equation D311 is a combination of hyperbolic functions. For the investigated PEN configuration the following expression is obtained for the overall resistance area R_{tot} A :

$$R_{tot}\ A = [\rho_{ca}Z_{ca}+\rho_{el}Z_{el}+\rho_{an}Z_{an}]\ J\ \coth(J)$$

$$= C\ J\ \coth(J) \qquad (D321)$$

where

A = X Y = active electrolyte area [m^2]
C = [..] = cross-plane resistance area [$\Omega\ m^2$]
Equation D253
J = X/L = non-dimensional strip width
= PEN strip width scaled by characteristic length of PEN layer [-]

The term "PEN function", for this case denoted by F_1, shall be introduced for the dependence of the overall resistance area of a PEN configuration on the non-dimensional strip width J:

$$F_1 = J\ \coth(J) \qquad (D322)$$

For strips of negligible width (i.e. for $J \rightarrow 0$) F1 approaches unity and the cross-plane resistance area C is recoverd. For large J the PEN function F_1 becomes linear with J, in fact, for large J, $F_1 = J$.

D3.3 OHMIC RESISTANCE OF PEN STRIP WITH DIAGONAL TERMINALS

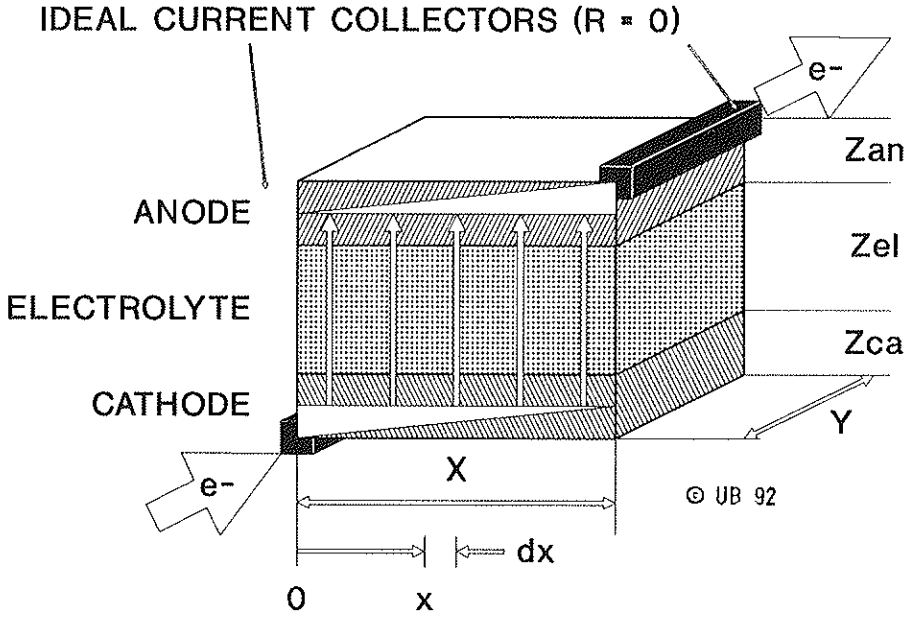

Figure D33.1: PEN strip with diagonal terminals

Again, the general solution is given by a combination of hyperbolic functions. In analogy with the previous case, the following solution shall be quoted[20]:

$$R_{tot}\ A = C\ J\ \{\coth(J) + B[J - 2\tanh(J/2)]\} \qquad (D331)$$

with

$C = \rho_{ca}Z_{ca}+\rho_{el}Z_{el}+\rho_{an}Z_{an}$ = cross-plane resistance area Equation D253

$B = E/(1+E)^2$ with the "ohmic symmetry parameter" $E = (\rho_{an}/Z_{an})/(\rho_{ca}/Z_{ca})$

For this PEN configuration the PEN function F_2 is introduced:

$$F_2 = J\ \{\coth(J) + B[J - 2\tanh(J/2)]\} \qquad (D332)$$

Again, for strips of negligible width (i.e. $J \rightarrow 0$) the cross-plane resistance area C is recoverd, while for large values of J and reasonable ohmic symmetry ($E \cong 1$) this PEN function may be approximated by the simple quadratic equation[20]. In fact, for large J, $F_2 = 1 + (1/3)J^2$.

D3.4 THE PEN FUNCTION FOR PEN STRIPS

Based on logic, the PEN function of the cross-plane conducting PEN configuration may be termed J_0 . It is independent of J and equal to unity, i.e. $F_0 = 1$. Figure D34.1 depicts all three PEN functions F_0, F_1 and F_2 for the three basic configuration of one-dimensional planar PEN structures: cross-plane conducting, aligned terminals and diagonal terminals.

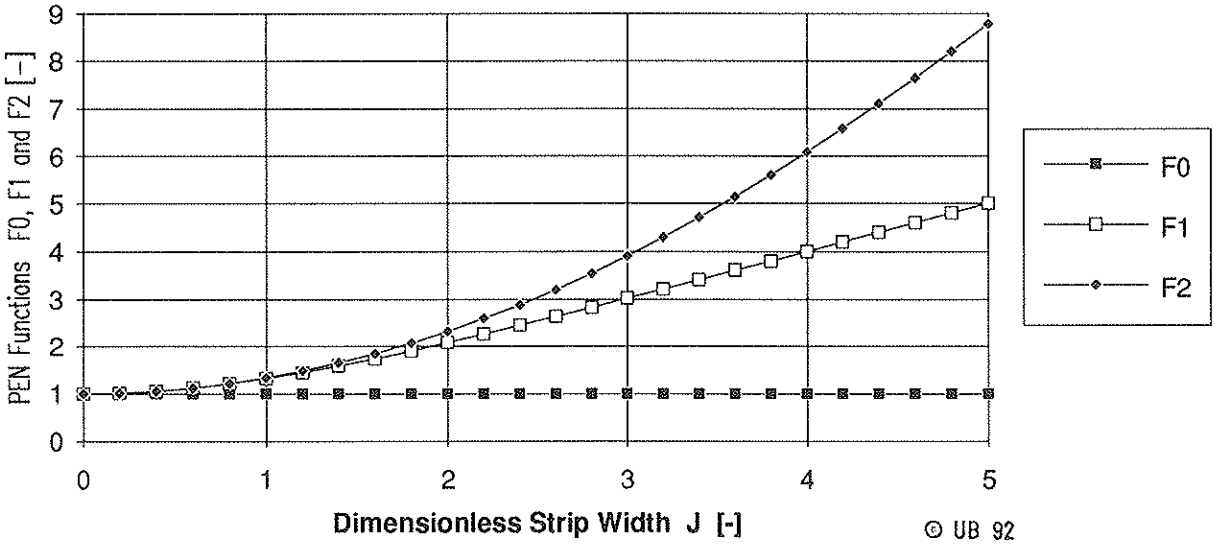

Figure D34.1: PEN functions for 1-D planar PEN structures

For diagonal terminals, the PEN function also depends on the ohmic symmetry E of the structure. Figure D34.2 shows the PEN function F_2 for various values of E. Note that for the unrealistic case of E = 0 the PEN function F_2 reduced to F_1.

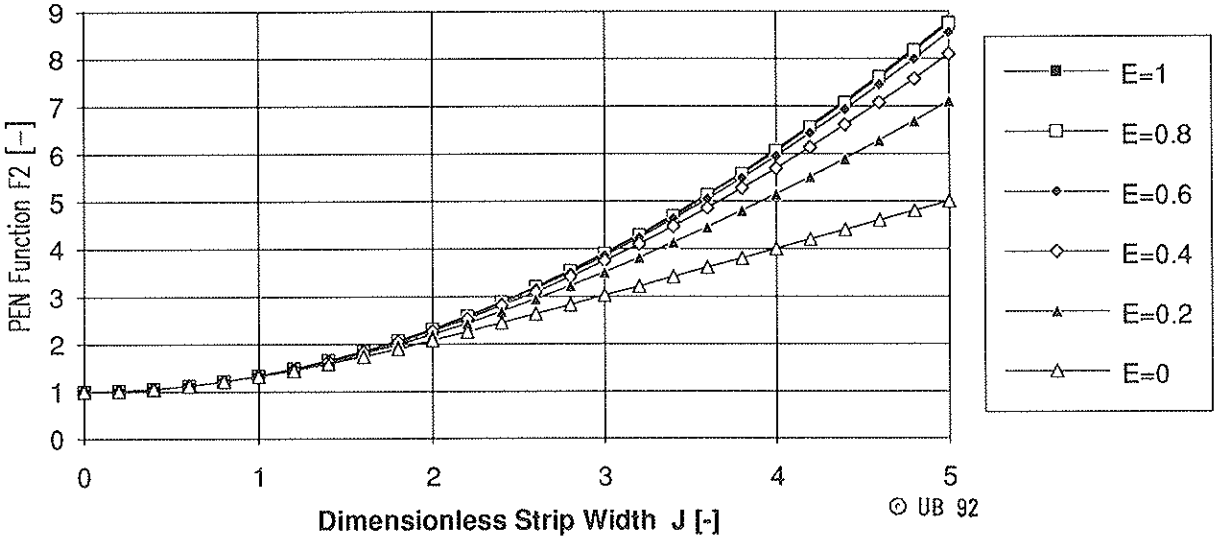

Figure D34.2: PEN function F_2 for different values of E

D3.5 OHMIC RESISTANCE OF CIRCULAR PEN STRUCTURES

For circular geometries the Laplace operator of the second order differential equation D311 must be expressed in polar coordinates with R being the radius of the perimeter. Now the radial distance is scaled by the characteristic length L (Equation D312) of the PEN structure, i.e. J = R/L . For all circular PEN disks the general solution is then given by a combination of modified Bessel functions[22,24].

As circular SOFC arrangements are not in common use, except perhaps, for characterization experiments in some laboratories, this geometry shall not be further analyzed. But is should be noted that three circular PEN structures can be obtained by different attachment of the current terminals. These three configurations are shown in Figures D35.1, D35.2 and D35.3.

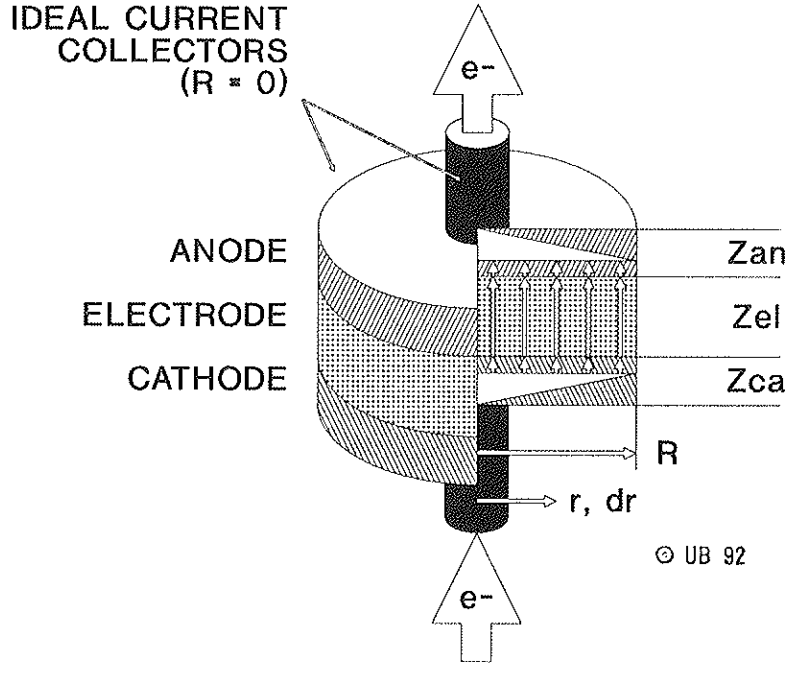

Figure D35.1: PEN disk with opposed terminals at center

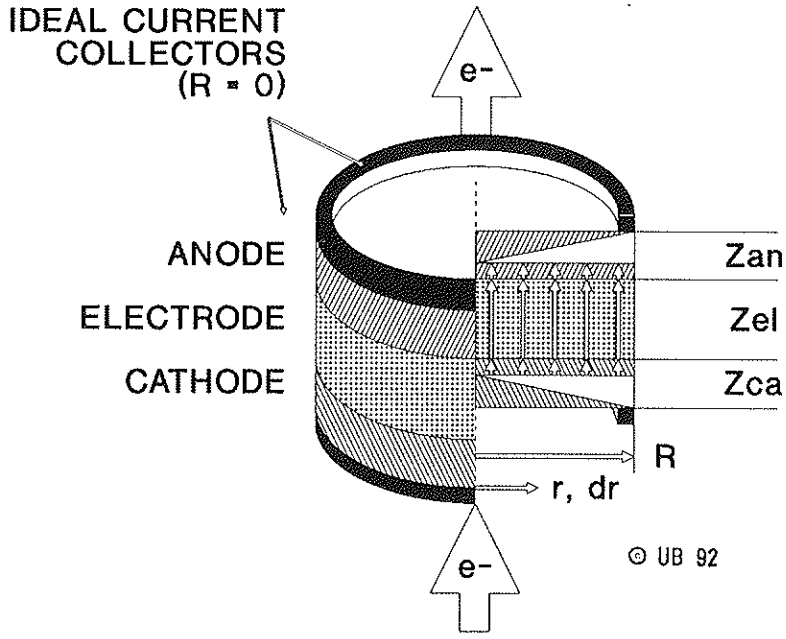

Figure D35.2: PEN disk with opposed terminals at rim

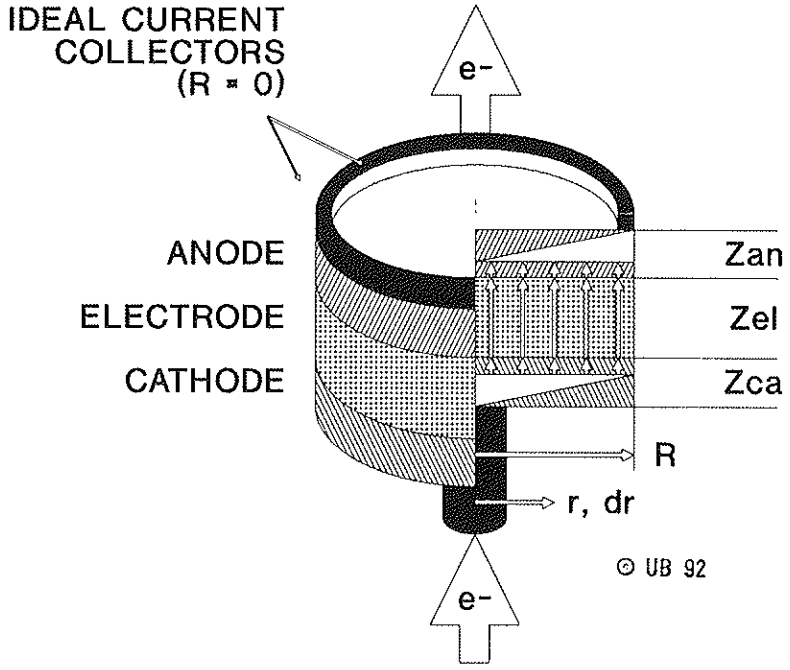

Figure D35.3: PEN disk with terminals at center and rim

E SOFC CONFIGURATIONS

E1 CONCEPT CHARACTERIZATION

Many different concepts have been proposed for SOFC elements and stacks. There is a large number of names which more or less characterize specific configurations without contributing to a general classification of configuration and design principles. To end this confusion a scheme is suggested for a systematic characterization of SOFC concepts according to their most significant features.

According to this suggestion, the characterization of SOFC concepts should always be composed of a limited number of significant building blocks [...] and read

"[A].,.[B]..[C] concept with [D]..[E] electrolyte"

where each block contains a significant statement. For these statements, the following options are suggested:

[A]:
- in-plane conducting
- cross-plane conducting

[B]:
- all-ceramic
- metal-ceramic hybrid

[C]:
- planar
- tubular
- cylindrical
- matrix

[D]:
- self-supporting
- supported

[E]:
- thick-film (t > 0.020 mm)
- thin-film (t < 0.020 mm)

The well-known Westinghouse tubular design, Figure E20.1, would then be described by:

"In-plane conducting, all-ceramic tubular concept with self-supported thin-film electrolyte"

Important SOFC concepts are described using the characterization scheme proposed above.

E2 SOFC CONCEPTS

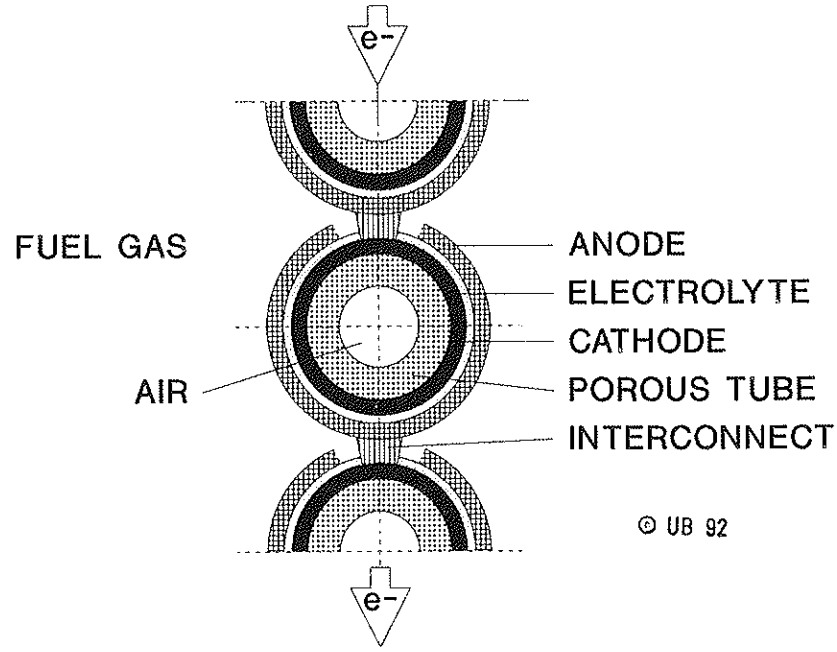

Figure E20.1: In-plane conducting, all-ceramic tubular concept with supported thin-film electrolyte

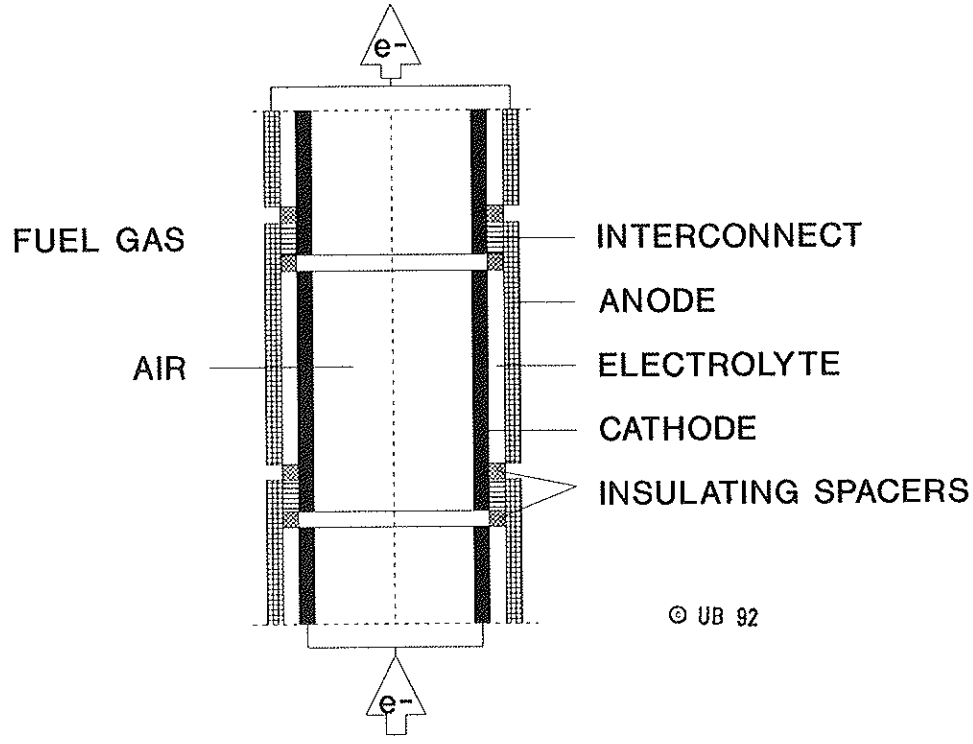

Figure E20.2: In-plane conducting, all-ceramic cylindrical concept with self-supporting thick-film electrolyte

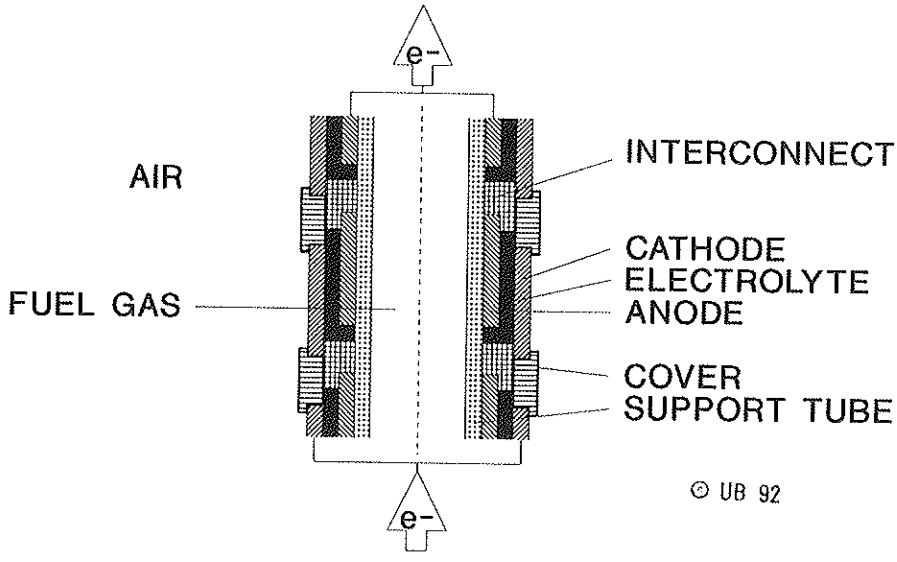

Figure E20.3: In-plane conducting, all-ceramic tubular concept with supported thick-film electrolyte

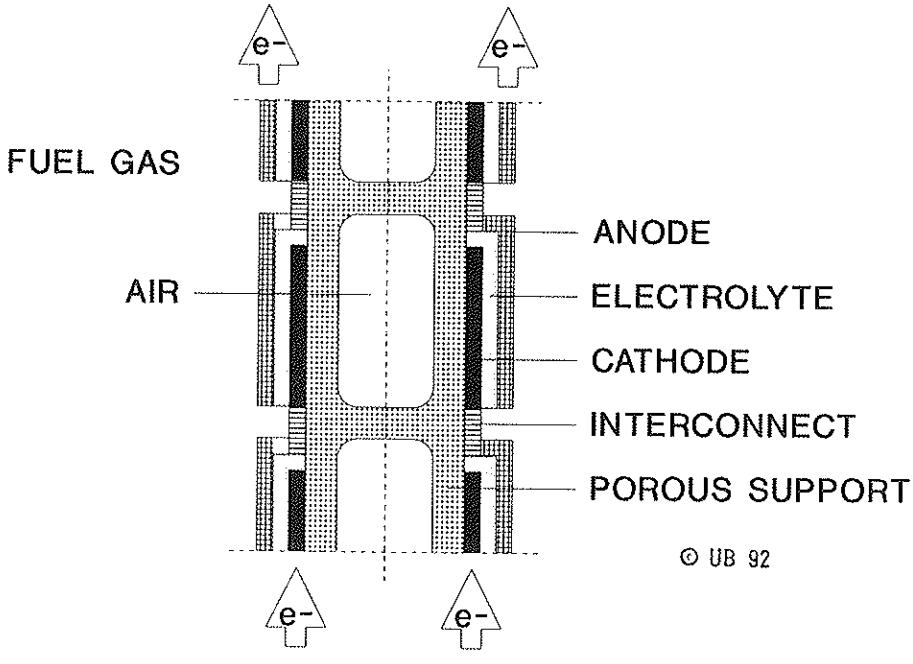

Figure E20.4: In-plane conducting, all-ceramic planar concept with supported thin-film electrolyte

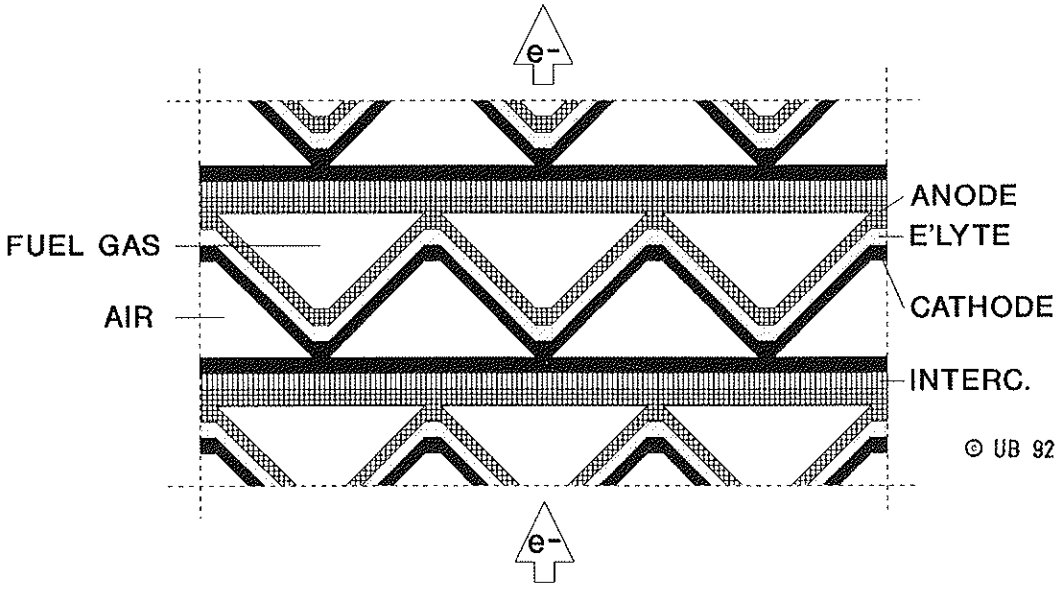

Figure E20.5: In-plane conducting, all-ceramic planar concept with self-supporting thick-film electrolyte (air and gas flow parallel)

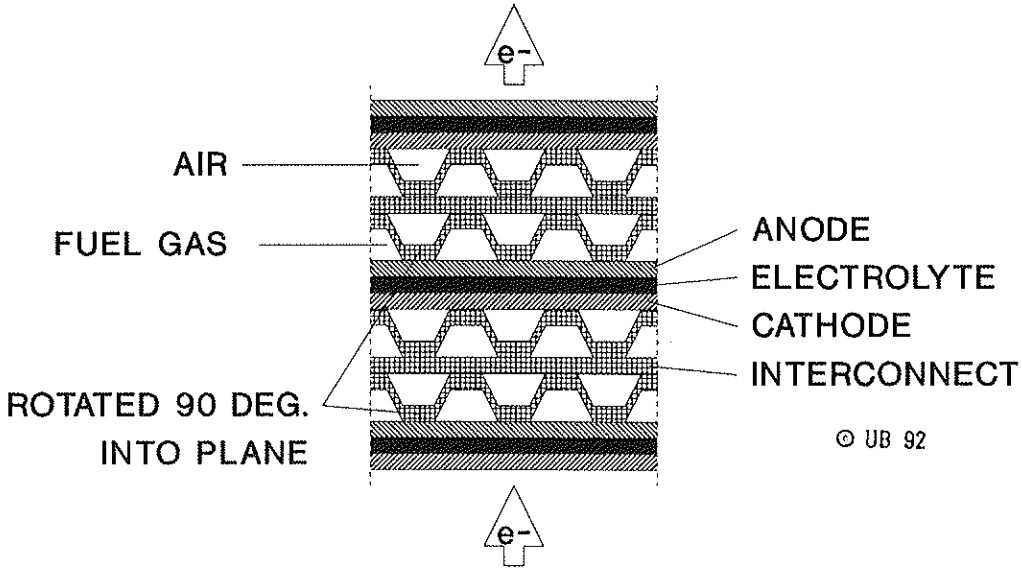

Figure E20.6: In-plane conducting, all-ceramic matrix concept with self-supporting thick-film electrolyte (air and gas flow crossing)

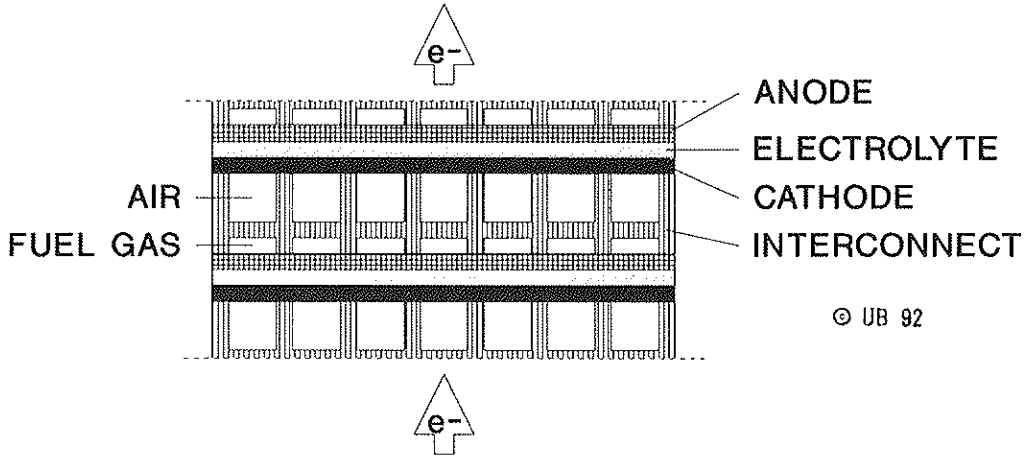

Figure E20.7: Cross-plane conducting, all-ceramic planar concept with self-supporting thick-film electrolyte

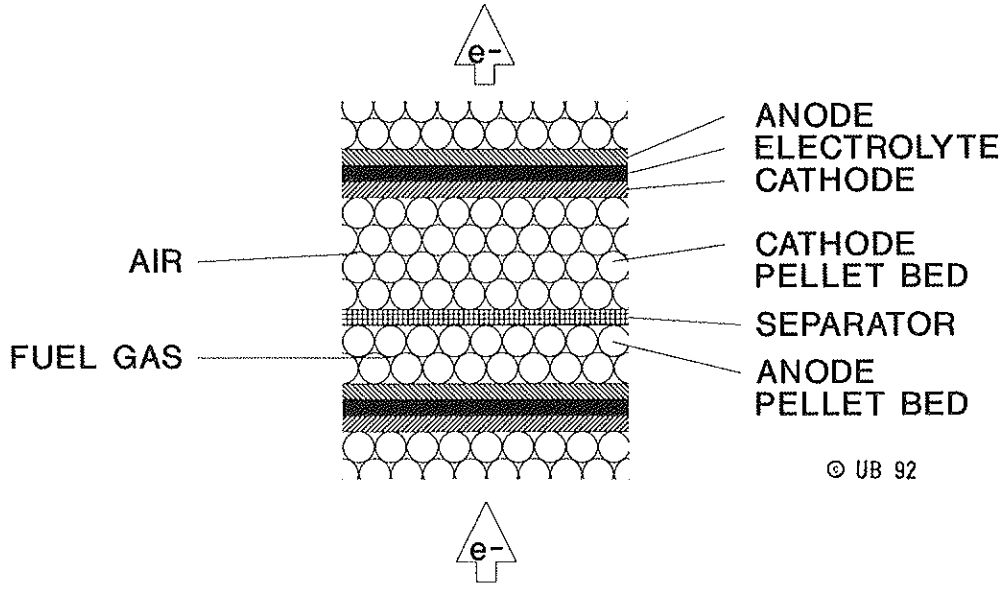

Figure E20.8: Cross-plane conducting, all-ceramic planar concept with self-supporting thick-film electrolyte (electrode chambers filled with granulated cathode or anode material)

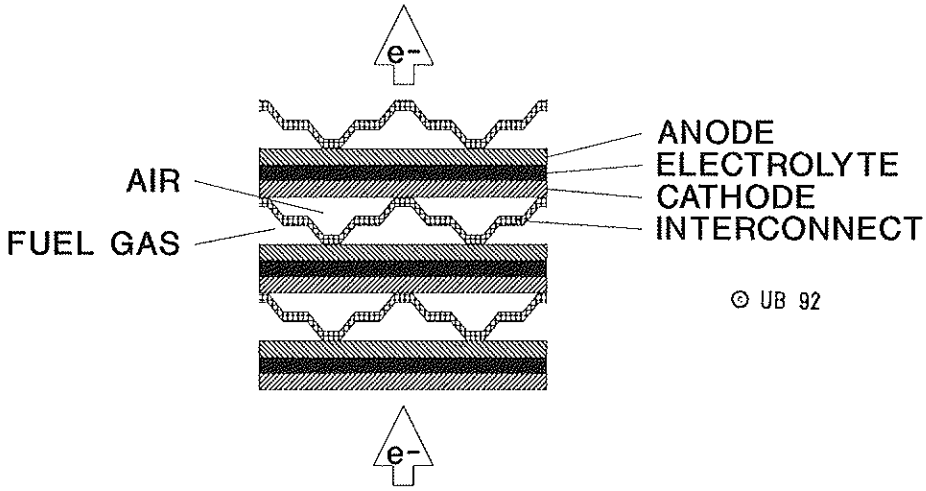

Figure E20.9: In-plane conducting, metal-ceramic hybrid concept with self-supporting, thick-film electrolyte

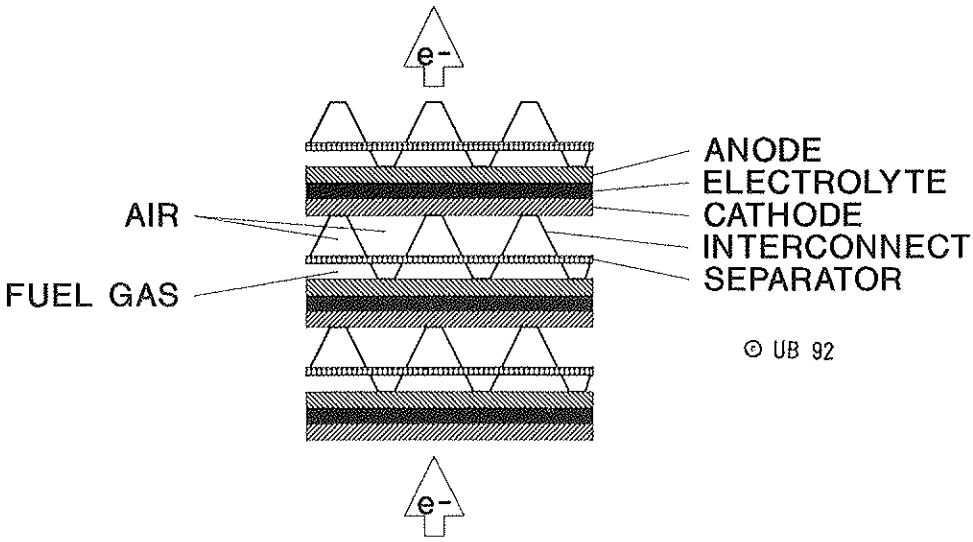

Figure E20.10: Cross-plane conducting, metal-ceramic hybrid concept with self-supporting, thick-film electrolyte

E3 CONCEPT PERFORMANCE COMPARISON

It would be difficult to evaluate the performance of all SOFC concepts presented above on the basis of a single computer analysis. But it is likely that all SOFC configuration will be evaluated by computer modelling in the development process to obtain preliminary data for stack design and optimization.

Modelling must include many levels of analyis. Micro-models of the exchange processes at the electrode-electrolyte interfaces may reveal useful information as well as makro-models of the overall system dynamics.

Experience shows that modelling of flow phenomena associated with the supply of air and gas to as well as the discharge of exhaust from SOFC elements has frequently been neglected. In fact, the thermal control of the high temperature fuel cell requires a skillful handling of many heat transfer options.

In the following Chapter F the mass flow phenomena in SOFC cells, stacks and systems are listed and guidelines are presented for preliminary analyses of flow-related effects like pressure losses and heat transfer.

F MASS FLOW PHENOMENA

F1 AIR EXCESS AND FUEL UTILIZATION

Practicality requires that solid oxide and other fuel cells are operated with excess fuel gas and oxygen. Otherwise the supply streams are depleted in the downstream region of the conversion element. As a result, the electrochemical process may be inhibited locally on the conversion element. This leads to a local voltage drop and stray currents within the electrodes of a fuel cell element.

F1.1 AIR EXCESS

Excess air must also be supplied for cooling purposes. As a rule, three to ten times more air or oxygen passes through the SOFC than would be required for oxidizing the fuel gas. Stack temperature control must be accomplished by adjusting the air stream to the cooling requirements rather than to the stoichiometry of the chemical reactions.

The air excess, measured in "stoichs", is denoted by S :

$$S = \frac{\text{moles of oxygen supplied with air}}{\text{moles of oxygen needed for stoichiometry}} \qquad \text{(F111)}$$

where the air needed is determined from the amount of oxygen required for stoichiometric conversion of the fuel.

Under stoichiometric conditions $S = 1$. Values of $3 < S < 10$ have been reported. One should aim for small values of S to minimize pumping requirements, voluminous ducting etc. If all fuel supplied is oxidized, the surplus oxygen remaining in the gas stream is given by the term $S-1$. For S less than unity, the combustion is said to be lean or incomplete.

F1.2 FUEL UTILIZATION

For fuel cell applications the fuel gas must always be in surplus on the entire electrode surface. If this is not the case, the electrochemical processes are quenched. Therefore, more fuel gas is supplied than can be converted. This has led to the definition of the fuel utilization u_f:

$$u_f = \frac{\text{moles of fuel gas consumed}}{\text{moles of fuel gas supplied}} \qquad \text{(F112)}$$

For the fuel utilization factor u_f values close to unity are desired (e.g. $0.85 < u_f < 0.95$) to obtain high overall efficiencies of the electrochemical conversion.

F1.3 AIR UTILIZATION

Similarly, oxygen must alway be in surplus on the air side of the fuel cell. If this is not the case, the electrochemical processes are quenched. The air utilization u_a is defined by:

$$u_a = \frac{\text{moles of air consumed}}{\text{moles of air supplied}} \qquad \text{(F113)}$$

But in all practical applications much more air must be supplied to the fuel cell for cooling purposes than is needed for the electrochemical conversion. Therefore, the air exceess is generally presented by stoichs S rather than indicated by the utilization u_a .

F2 FLOW OF MASS, MOLES AND VOLUMES

F2.1 GENERAL CONSIDERATIONS

A solid oxide fuel cell operates by transporting oxygen from the cathode through the electrolyte to the anode where it oxidizes fuel generating electric current in the process. Normally, oxygen is extracted from an air stream which steadily sweeps the cathode side of the fuel cell system. For solid oxide fuel cells industrial quality air can be used. Because oxygen is removed from the air stream, the mass flow rate of the air stream decreases from inlet to outlet.

On the other side of the electrolyte, a fuel gas stream steadily sweeps past the anode surface. This gas stream undergoes significant changes as a result of chemical processes.

1. The fuel gas may be decomposed ("dissociated") by the influence of heat, but in the absence of oxygen. This process generally leads to a change of molar flux at no increase of mass flux. Typical dissociation reactions are listed in Chapter A1.4.

2. Hydrocarbon fuels may be converted ("reformed") into elementary fuel gases such as hydrogen or carbon monoxide. These are endothermic reactions R4 and R5, requiring the presence of water vapor or carbon dioxide. The reforming process generally leads to an increase of molar fluxes. The mass flux remains constant if the reactants are already present in the flow.

3. Carbon monoxide generated by the reforming reaction R4 and R5 may be further converted ("shifted") to carbon dioxide in the presence of water vapor. Hydrogen is produced in the process, reaction R6. The shift reaction does not change the molar flux, nor the mass flux.

4. The elementary fuel gasses (hydrogen, carbon monoxide and methane) are oxidized to water vapor and carbon dioxide by combining with oxygen which is supplied by the air stream and transported through the electrolyte. This process produces electric current and heat. Because oxygen is added, the mass flux is increased, while the molar fluxes remain unchanged for the reactions R1 and R2, but triples for the reaction R3.

These processes occur simultaneously. Water vapor and carbon dioxide generated by the oxidation reaction is partially absorbed for reforming or shifting. The details of these chemical reactions depend on a number of parameters, e.g. system geometry, temperature fields, surface structure, electrochemical properties of surface materials, mass fluxes etc.

For a preliminary analysis the methane conversion reaction R3

$$CH_4 + 2\ O_2 \leftrightarrow CO_2 + 2\ H_2O$$

shall be considered. For 1 mole of CH_4 supplied 2 moles of O_2 are withdrawn from the air stream and 3 moles of exhaust leave the system. For 1 mole of methane (16 g) consumed by the fuel cell, 2 moles of oxygen (64 g) must migrate from the air stream through the electrolyte to the fuel gas stream. While (for $S = 6$) the mass flux on the air side is diminished by only 3.8%, the mass flux on the gas side is increased by a factor of 5. This change of mass flux is related to a corresponding change of volumetric flow rates with consequences on fluid dynamics, heat transfer, pumping requirements, and other aspects of system design.

F2.2 MOLAR FLUXES FOR FUEL CELL SYSTEMS

Excess air and partial fuel utilization modify the stoichimetric conditions of an idealized chemical reaction. The actual mole fluxes depend on the stoichs S , the fuel utilization u_f as well as on the reaction itself. Furthermore, the process design must be considered for the molar flux analysis. Two typical process configurations are considered.

F2.2.1 AFTERBURNER IN MAIN AIR STREAM

Both air and fuel streams merge after leaving the fuel cell. The unspent fuel is oxidized with excess oxygen in a conventional combustion process. The region where the unspent fuel is burned is generally referred to as the "afterburner". Heat is generated in the process which is illustrated in Figure F22.1.

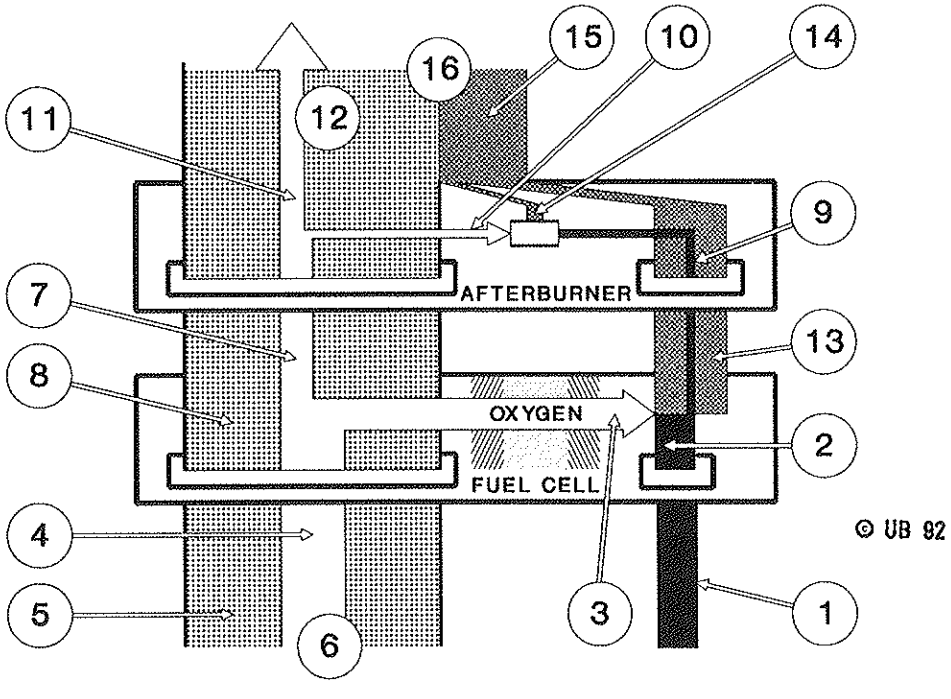

Figure F22.1: Molar fluxes for configuration with afterburner in main air stream

For the depicted situation the fluxes are determined by the following set of equations. The following definitions are used:

Φ = oxygen stoichiometric coefficient
Γ = product gas stoichiometric coefficient

For the standard reactions R1, R2 and R3 of H_2, CO and CH_4 with oxygen, respectively, these coefficients assume the following values:

Table F22.1

Reaction:	R1	R2	R3
Φ =	0.5	0.5	2.0
Γ =	1.0	1.0	3.0

Since the molar composition of atmospheric air is 21.00% O_2, 78.04% N_2, 0.93% Ar and 0.03% CO_2, the following molar ratios appear in the analysis:

inert components : oxygen = 3.7619 ($\cong$ 3.76)
air : oxygen = 4.7619 ($\cong$ 4.76)

For M_f moles of fuel gas and m_a moles of air the following set of equations is derived from Figure F22.1.

(1)	total flow of fuel gas to system	M_f
(2)	fuel gas converted in fuel cell	$M_f\ u_f$
(3)	O_2 consumed in fuel cell conversion	$M_f\ \Phi\ u_f$
(4)	total O_2 supplied to fuel cell	$M_f\ \Phi\ S$
(5)	total N_2 supplied to fuel cell	$M_f\ \Phi\ S\ 3.76$
(6)	total air supplied to fuel cell (4+5)	$M_f\ \Phi\ S\ 4.76$
(7)	O_2 leaving fuel cell (4-3)	$M_f\ \Phi\ (S-u_f)$
(8)	"air" leaving fuel cell (6-3)	$M_f\ \Phi\ (4.76S-u_f)$
(9)	fuel gas converted in afterburner	$M_f\ (1-u_f)$
(10)	O_2 consumed in afterburner	$M_f\ \Phi\ (1-u_f)$
(11)	O_2 leaving afterburner (7-10)	$M_f\ \Phi\ (S-1)$
(12)	"air" leaving afterburner (11+5)	$M_f\ (4.76S-1)$
(13)	fuel exhaust leaving fuel cell	$M_f\ \Gamma\ u_f$
(14)	fuel exhaust generated in afterburner	$M_f\ \Gamma\ (1-u_f)$
(15)	total fuel exhaust (13+14)	$M_f\ \Gamma$
(16)	total exhaust (12+15)	$M_f\ \{\Gamma+[4.76S-1]\ \Phi\}$

For this set of equations: (F221)

F2.2.2 AFTERBURNER IN BYPASS AIR STREAM

In this configuration, two independent air streams are supplied to the fuel cell and the afterburner, respectively. Both "air" streams and the fuel exhaust gas merge downstream of the fuel cell and the afterburner. Both air streams can be controlled individually. Providing the afterburner with its own combustion air may be necessary for larger installations such as fuel cell combined cycle power plants, where the cold bypass air to the afterburner is needed to control the inlet temperature of the gas turbine. The proposed process is illustrated in Figure F22.2.

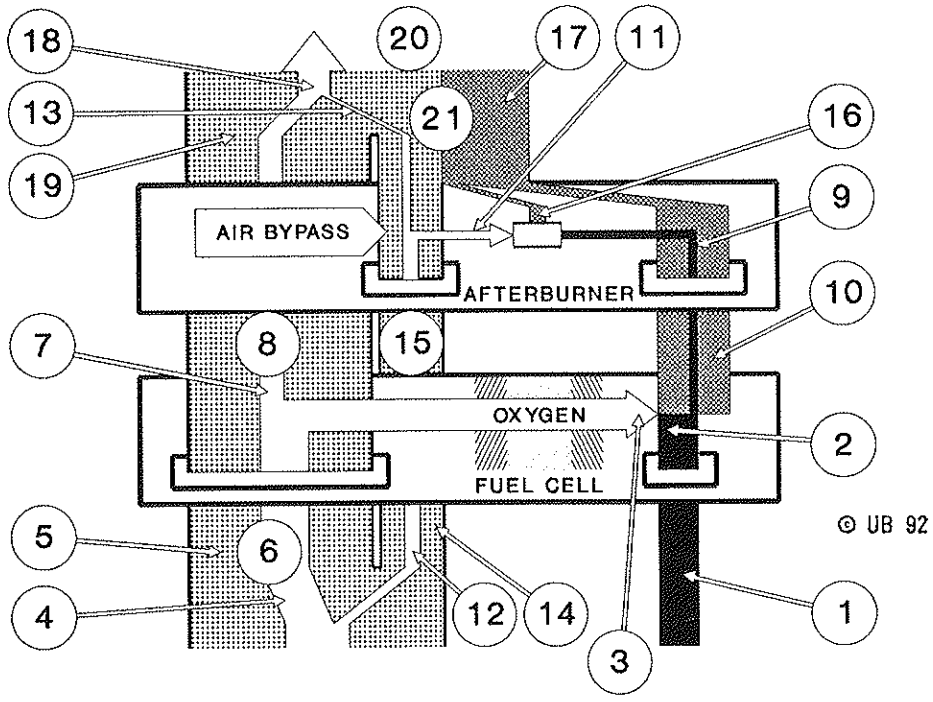

Figure F22.2: Molar fluxes for configuration with afterburner in bypass air stream

Using the symbols defined above the flux equations for this configuration are listed below. Here S stands for the air excess at which the fuel cell ("FC") is operated while β specifies the portion of the total air flow M_a to the system which is directly supplied to the afterburner ("AB") by means of a bypass ("BP").

(1)	total fuel gas to system	M_f
(2)	fuel gas converted in FC	$M_f\ u_f$
(3)	O_2 consumed in FC conversion	$M_f\ \Phi\ u_f$
(4)	O_2 supplied to FC	$M_f\ \Phi\ S$
(5)	N_2 supplied to FC	$M_f\ \Phi\ S\ 3.76$
(6)	air supplied to FC (4+5)	$M_f\ \Phi\ S\ 4.76 \quad = M_a\ (1-\beta)$
(7)	O_2 from FC to AB (4-3)	$M_f\ \Phi\ (S-u_f)$
(8)	"air" from FC to AB (6-3)	$M_f\ \Phi\ (4.76S-u_f)$
(9)	unspent fuel from FC to AB	$M_f\ (1-u_f)$
(10)	fuel exhaust from FC to AB	$M_f\ \Gamma\ u_f$
(11)	O_2 consumed in AB	$M_f\ \Phi\ (1-u_f)$
(12)	O_2 supplied to AB via BP	$M_f\ \Phi\ S\ \beta/(1-\beta)$
(13)	O_2 available in AB (7+12)	$M_f\ \Phi\ \{S[1+\beta/(\beta-1)]-u_f\}$
(14)	N_2 supplied to AB via BP	$M_f\ \Phi\ S\ 3.76\ \beta/(1-\beta)$
(15)	air supplied to AB via BP	$M_f\ \Phi\ S\ 4.76\ \beta/(1-\beta) = M_a\ \beta$
(16)	fuel exhaust generated in AB	$M_f\ \Gamma\ (1-u_f)$
(17)	fuel exh. leaving SY (10+16)	$M_f\ \Gamma$
(18)	O_2 leaving SY (13-11)	$M_f\ \Phi\ [(S(1+\beta/(1-\beta)-1]$
(19)	N_2 leaving SY (5+14)	$M_f\ \Phi\ S\ 3.76[1+\beta/(1-\beta)]$
(20)	"air" leaving SY (18+19)	$M_f\ \Phi\ \{S\ 4.76[1+\beta/(1-\beta)]-1\}$
(21)	total gas leaving SY (17+20)	$M_f\ \{\Phi\ \{S\ 4.76[1+b/(1-\beta)]-1\}+\Gamma\}$

For this set of equations: (F222)

Legend: FC = fuel cell
AB = afterburner
BP = bypass
SY = system

F2.3 CONVERSION OF FLUXES

The number N_{mi} of moles of all species participating in a particular reaction is determined by the reaction (e.g. R1, R2 or R3) and the total input of chemical power. The equation R3 for the oxidation of methane indicates that for one mole/second of CH_4, two moles/second of O_2 must be supplied to produce one mole/second of CO_2 and two moles/second of H_2O.

Since the weight per mole of a particular chemical species is characterized by its molar mass M, the mass fluxes are given by:

$$m_i = N_{mi} * M_i \qquad \text{(F231)}$$

The volumetric flow rate is the ratio of mass flux and density:

$$V_i = m_i / \rho_i \qquad \text{(F232)}$$

For reactions with enthalpy changes $\Delta_f H$, the chemical energy associated with M_f moles of fuel is given by:

$$E_f = M_f * \Delta_f H \qquad \text{(F233)}$$

For fuel mass flux m_i this equation gives the power supplied:

$$P_f = m_f * \Delta_f H \qquad \text{(F234)}$$

With these four equations the material and energy fluxes in a fuel cell system can be related.

F2.4 OUTPUT-RATED FLUX EQUATION

For most technical applications the fluxes are related to the useful power output of the system. For a fuel cell stack, this could be the DC power generated. For a fuel cell system, this should be the AC power deliverd to the grid. This accounting is based on the overall electric efficiency η_e

$$\eta_e = \frac{\text{electric power out, } P_e \text{ (W)}}{\text{chemical power in, } P_f \text{ (W)}} \qquad \text{(F241)}$$

Consequently, the chemical energy Q_f contained in one mole of fuel M_f is converted to only $Q_e = \eta_e Q_f$ of electric energy. Therefore, all Equations of set F221 and set F222 must be divided by η_e to relate them to the useful electric output of the system.

F2.5 MOLAR, MASS AND VOLUMETRIC FLOW RATES FOR STOICHIOMETRIC CONVERSIONS

The following tables summarize the mole, mass and volumetric flow rates for an "ideal" fuel cell operating on hydrogen or methane assuming for both cases:

i.	fuel utilization:	$u_f = 1.0$
ii.	stoichiometry:	$S = 1.0$
iii.	electrical efficiency:	$\eta_e = 0.6$
iv.	pressure:	$p = 10^5$ Pa ($\cong$ 1 atm)
v.	isothermal operation:	$T_{in} = T_{out} = 1200$ K
vi.	power output:	$P_e = 1$ kW$_e$

These assumptions imply an energy consumption rate by the fuel cell of 1.67 kW of which 0.67 kW is converted into heat and 1.00 kW is converted into power.

The following tables serve to provide a feeling for the order of magnitude of typical gas flows in solid oxide fuel cells.

Table F25.1: Flow rates for an ideal, 60% efficient, 1 kW$_e$ fuel cell operated with H_2

		molar flow [mol s^{-1}]	mass flow [kg s^{-1}]	volume flow [m^3 s^{-1}]
Inlet:				
Anode side:	H_2	$6.70\ 10^{-3}$	$13.4\ 10^{-6}$	$0.657\ 10^{-3}$
Cathode side:	O_2	$3.35\ 10^{-3}$	$107.2\ 10^{-6}$	$0.330\ 10^{-3}$
	N_2	$12.60\ 10^{-3}$	$352.8\ 10^{-6}$	$1.241\ 10^{-3}$
	Air	$15.95\ 10^{-3}$	$460.0\ 10^{-6}$	$1.571\ 10^{-3}$
Total in:		$22.65\ 10^{-3}$	$473.4\ 10^{-6}$	$2.228\ 10^{-3}$
Outlet:				
Anode side:	H_2	-	-	-
	H_2O	$6.70\ 10^{-3}$	$120.6\ 10^{-6}$	$0.660\ 10^{-3}$
Cathode side:	O_2	-	-	-
	N_2	$12.60\ 10^{-3}$	$352.8\ 10^{-6}$	$1.241\ 10^{-3}$
Total out:		$19.30\ 10^{-3}$	$473.4\ 10^{-6}$	$1.901\ 10^{-3}$

For the ideal conversion of methane a similar set of numbers can be given:

Table F25.2: Flow rates for an ideal, 60% efficient, 1 kW_e fuel cell operated with CH_4

		molar flow [mol s^{-1}]	mass flow [kg s^{-1}]	volume flow [m^3 s^{-1}]
Inlet:				
Anode side:	CH_4	$2.08\ 10^{-3}$	$33.3\ 10^{-6}$	$0.204\ 10^{-3}$
Cathode side:	O_2	$4.16\ 10^{-3}$	$133.1\ 10^{-6}$	$0.401\ 10^{-3}$
	N_2	$15.64\ 10^{-3}$	$438.0\ 10^{-6}$	$1.540\ 10^{-3}$
	Air	$19.80\ 10^{-3}$	$571.1\ 10^{-6}$	$1.945\ 10^{-3}$
Total in:		$21.88\ 10^{-3}$	$604.4\ 10^{-6}$	$2.149\ 10^{-3}$
Outlet:				
Anode side:	CH_4	-	-	-
	H_2O	$4.16\ 10^{-3}$	$74.9\ 10^{-6}$	$0.410\ 10^{-3}$
	CO_2	$2.08\ 10^{-3}$	$91.5\ 10^{-6}$	$0.205\ 10^{-3}$
	sum	$6.24\ 10^{-3}$	$166.4\ 10^{-6}$	$0.615\ 10^{-3}$
Cathode side:	O_2	-	-	-
	N_2	$15.64\ 10^{-3}$	$438.0\ 10^{-6}$	$1.540\ 10^{-3}$
Total out:		$21.88\ 10^{-3}$	$604.4\ 10^{-6}$	$2.145\ 10^{-3}$

Notes:

1. The air requirements given in the above tables are based upon stoichiometric requirements. In practice, much more air is used (typically, 4 to 10 times more) because of cooling requirements.

2. The volumetric and molar flow rates between the inlet and exit of the CH_4 fuel cell may exceed the inlet and outlet values given here since the reforming and shifting reactions (R4, R5 and R6) may occur considerably faster than the oxidation reactions producing larger mole numbers.

F3 PRESSURE LOSSES IN SOFC CONFIGURATIONS

The pressure losses occurring within a fuel cell are dependent upon the geometry of the flow confining ducts and the flow conditions (laminar or turbulent). In this section, the pressure losses for a few selected geometries bringing oxidant and fuel streams to the electrodes are discussed. Both laminar and turbulent conditions and the criteria determining the flow conditions are considered. The streams are considered to have fully developed velocity profiles. Entrance and exit effects are not considered. Typically, the flow conditions in a fuel cell are laminar unless excessive cooling air is required, in which case the oxidant stream may become turbulent.

For the analysis of ducted flows in fuel cell configurations the four basic geometries shall be considered.

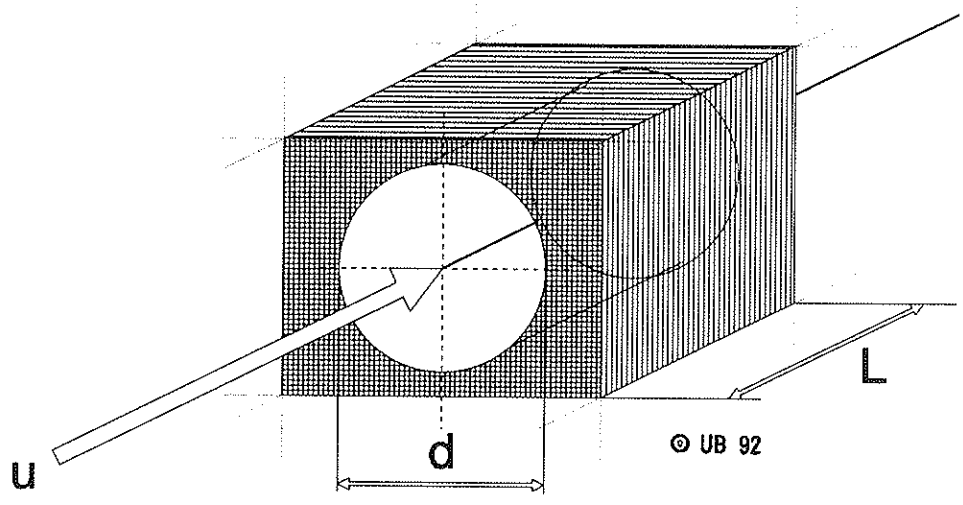

Figure F30.1: Channels with circular cross section

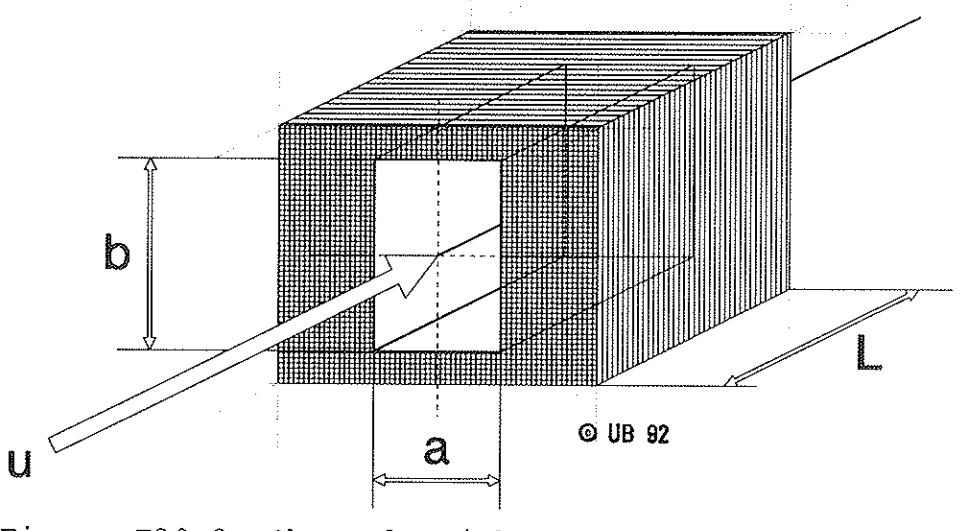

Figure F30.2: Channels with rectangular cross section

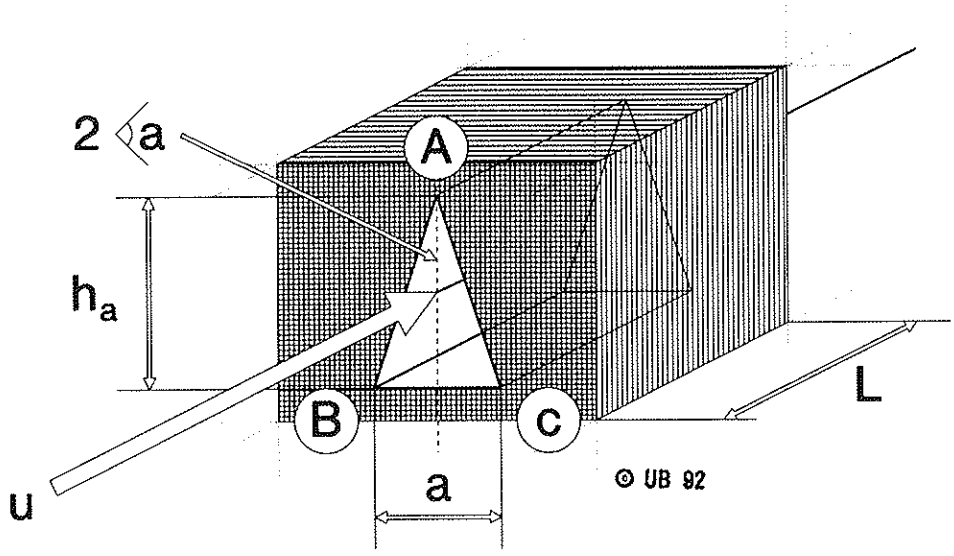

Figure F30.3: Channels with triangular cross section

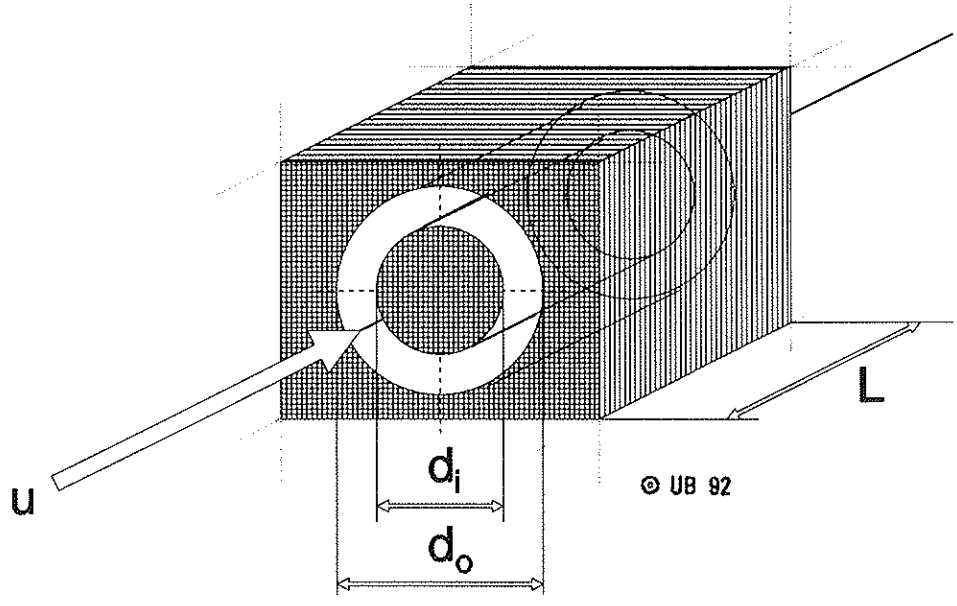

Figure F30.4: Channels with annular cross sections

F3.1 FLOW CONDITIONS

Before calculating the pressure loss through a duct one must first determine the flow condition. The flow condition can be either laminar or turbulent. The flow condition is determined from the Reynolds number Re . Above the critical Reynolds number Re_{crit} the flow is considered to be fully turbulent and below the flow is laminar. In reality, there is a transition region from laminar to turbulent around the critical Reynolds number where the flow exhibits instability and alternates between bursts of turbulent activity and calm laminar flow. This highly complex flow regime is not treated here.

The Reynolds number is defined as

$$Re = \frac{\rho \, u \, d_h}{\mu} \qquad \text{(F311)}$$

where

ρ = fluid density
u = fluid average velocity
d_h = hydraulic diameter
μ = dynamic (or bulk) viscosity of the fluid

The hydraulic diameter d_h is used as the length scale so that similar equations can be applied to various geometrical cross sections. The hydraulic diameter is defined as[12]

$$d_h = 4 * \frac{\text{cross sectional area}}{\text{wetted perimenter}} \qquad \text{(F312)}$$

Hydraulic diameters for some of the more common cross sections are given in Table F31.1.

Table F31.1: Hydraulic diameter for basic cross sections

type	d_h
circular	d
rectangular	2ab/(a+b)
triangular	2ah/(a+b+c)
annular	d_o-d_i

Once the Reynolds number has been determined for a particular flow field, the flow condition is found by comparison with the critical Reynolds number. Re_{crit} values are determined experimentally. For the four common cross sections Re_{crit} values are given in Table F31.2. One should expect

laminar flow for $Re < Re_{crit}$

turbulent flow for $Re > Re_{crit}$ (F313)

Table F31.2: Critical Reynolds numbers[12,13]

cross section		Re_{crit}
circular (Figure F30.1)		2100
rectangular (Figure F30.2)		
smooth entrance:	b/a = 1	4300
	3	6000
	5	7000
	10	4400
abrupt entrance:	b/a = 1	2200
	5	2500
	10	2500
triangular (Figure F30.3)		
isosceles, 23°		1800
acute triangle		2000 - 2360
right isosceles		2800
equilateral		2800
annular (Figure F30.4)		1800

F3.2 PRESSURE LOSSES

For the flow through a duct of length L the pressure losses are then computed from[12]

$$\Delta p = \frac{4 f}{d_h} * \frac{\rho u^2}{2} * L \qquad \text{(F321)}$$

where f is the friction factor. It depends on the Reynolds number and flow condition. Generally, the pressure losses will be considerably reduced when the flow is laminar. Some laminar friction factors are given in Table F32.1 for the four basic geometries. The friction factors for turbulent flow are given in Table F32.2.

Note that only a simplified analysis has been presented here. For all four elementary duct geometries, the approach is valid only for fully developed flows. Leading edge, separation phenomena and velocity profile developments must be studied in detail by detailed analysis or experiment.

Table F32.1: Laminar friction factors[13]

cross sections		f * Re
circular (Figure F30.1):		16
rectangular (Figure F30.2): inverse aspect ratio, a/b =	1.0	14.2
	0.9	14.3
	0.8	14.4
	0.7	14.6
	0.6	15.0
	0.5	15.5
	0.4	16.3
	0.3	17.4
	0.2	19.0
	0.1	21.1
	0	24.0
triangular (Figure F30.3): isosceles, apex angle 2 =	0°	12.0
	10°	12.5
	20°	12.8
	30°	13.1
	40°	13.2
	50°	13.3
	60°	13.3
	70°	13.3
	80°	13.2
	90°	13.1
annular (Figure F30.4): inner/outer diam. di/do =	0.0001	17.94
	0.001	18.67
	0.01	20.03
	0.05	21.56
	0.10	22.34
	0.15	22.79
	0.20	23.09
	0.30	23.46
	0.40	23.46
	0.50	23.79
	0.60	23.89
	0.70	23.94
	0.80	23.98
	0.90	23.99
	1.00	24.00

Table F32.2: Turbulent friction factors[12,13]

cross section	f
circular (Figure F30.1):	
smooth tube walls	
$5*10^3 < Re < 3*10^4$	$f = 0.079\ Re^{-0.25}$
$3*10^4 < Re < 1*10^6$	$f = 0.046\ Re^{-0.20}$
rough tube walls	$f = [1.75\ \ln(d/e)+2.28]^{-2}$ e = roughness factor
rectangular (Figure F30.2):	$f = 0.046\ Re^{-0.20}$
triangular (Figure F30.3):	$f = 0.25\ C\ Re^{-0.25}$
where C is given for isosceles by:	
for 2α = 0°	C = 0.240
8°	0.261
16°	0.280
24°	0.289
32°	0.295
40°	0.300
48°	0.304
56°	0.309
64°	0.311
annular (Figure F30.4):	$f = 0.085\ Re^{-0.25}$

F4 HEAT TRANSFER IN SOFC CONFIGURATIONS

Due to SOFC process inefficiencies, the fuel cell produces heat during the production of electric power. This heat must be removed to keep the fuel cell temperature within the electrolyte operating temperature range. This can be a significant quantity of heat requiring significant cooling.

Furthermore, solution of the heat tranfer problem also yields temperature distributions which are needed to determine thermal stresses.

A fuel cell operating at 60% efficiency with a power density of 2 kW m^{-2} produces 1.33 kW m^{-2} of heat. Assuming cooling air is available at 20°C and can be distributed through and collected from the fuel cell such that the cell is maintained at 1200 K, the minimum amount of air required is

$$m = \frac{Q}{c_p \, \Delta T} = \frac{1.33 \text{ kW m}}{1.09 \text{ kJ kg}^{-1} \text{ K}^{-1} \text{ (1200-293)K}} \qquad \text{(F401)}$$

$$= 1.34 \; 10^{-3} \text{ kg s}^{-1} \text{ m}^{-2}$$

This is approximately 17% more air than is required for the stoichiometric oxidation of methane. Typically in practice, 4 to 10 times more air is needed for cooling than stoichiometry requires. This air is warmed to a moderate intermediate temperature before entering the fuel cell to prevent the large thermal gradients and consequent stresses which can occur by bringing in room temperature air.

The following three sections discuss the pertinent mechanisms (conduction, radiation and convection) by which a fuel cell is cooled. The relevant equations and heat transfer parameters involved are also presented.

F4.1 HEAT TRANSFER BY CONDUCTION

Conduction describes the method by which heat is transported through materials by molecular vibration. Within an SOFC, heat generated by process inefficiencies in the solid electrolyte and electrodes is conducted to fuel, oxidant and possibly a separate coolant stream channels. The differential equation describing the conduction of heat through solids is[8]

$$\frac{1}{\alpha_t}\frac{\delta T}{\delta t} = \frac{\delta^2 T}{\delta x^2} + \frac{\delta^2 T}{\delta y^2} + \frac{\delta^2 T}{\delta z^2} + \frac{q'}{k} \qquad \text{(F411)}$$

where:

T	=	temperature
q'	=	heat generation per unit volume
k	=	thermal conductivity
α_t	=	thermal diffusivity
t	=	time
x,y,z	=	spatial coordinates

The solution of this equation, with appropriate boundary conditions, provides information on temperature distribution and heat flow through the fuel cell components.

For fuel cell configurations with a supporting structure three dimensional heat conduction must be considered for the flow of heat through the porous structure. Self supporting electrolytes are normally sufficiently thin that there is a negligible temperature difference across the structure. Consequently, Equation F411 reduces to

$$\frac{\delta^2 T}{\delta x^2} + \frac{\delta^2 T}{\delta y^2} + \frac{q'}{k} = 0 \qquad \text{(F412)}$$

describing the temperature distribution and flow of heat along the electrolyte and electrode structure.

If the oxidant and fuel mass flows are sufficiently slow, the conduction of heat in the solid parallel to these flows may be significant. The heat flux is given by

$$q_x = k\frac{\delta T}{\delta x}, \qquad q_y = k\frac{\delta T}{\delta y} \qquad \text{(F413)}$$

If the electrolyte and electrodes reside upon a supporting ceramic structure, the "thinness" assumption reducing the three dimensional equation to two dimensions may not apply. In this case, the original three-dimensional conduction Equation F411 dimensions may need to be solved.

F4.2 HEAT TRANSFER BY RADIATION

Radiation heat transfer is the name given to the process by which two or more bodies exchange energy in the form of electromagnetic waves or photons. The energy exchange between any two bodies is proportional to the difference of the 4th power of the temperatures of each body (i.e. $T_2^4 - T_1^4$). Within a SOFC, the electrode and electrolyte of adjacent components are expected to posses very small temperature differences (ideally, the fuel cell assembly is isothermal). Consequently, the heat transferred by radiation may be neglected compared to that transfered by convection (next section) inspite of the 4th power dependence. Likewise, the path length of the radiation is too short for either the fuel or oxidant streams to absorb significant amounts of heat transferred via radiation.

However, radiative heat transfer may play a significant role between a completed SOFC assembly and the vessel in which it is contained. In this situation the heat flux is given[8] by

$$q = S_{FC-V} (\varepsilon_{FC} \sigma_S T_{FC}^4 - \alpha_{FC} \sigma_S T_V^4) \qquad (F421)$$

where:

q = heat flux per unit surface area of fuel cell
ε_{FC} = emittance of fuel cell
α_{FC} = absorptance of fuel cell
σ_S = Stephan-Bolzmann constant
T_{FC} = surface temperature of fuel cell
T_V = surface temperature of vessel
S_{FC-V} = shape factor

For gray bodies $\varepsilon = \alpha$. Since the SOFC assembly is completely contained within the vessel, the shape factor from the fuel cell to the vessel is 1.0. Assuming the fuel cell assembly and vessel surfaces to be "gray" surfaces and assuming an emittance of 0.8 (typical of ceramics) the heat flux is $\cong$ 64 kW m^{-2} of exterior assembled surface area. Hence, a smaller quantity of cooling air is required.

F4.3 HEAT TRANSFER BY CONVECTION

The transport of heat by fluid movement is called convective heat transfer. Within a fuel cell assembly, it is the dominant mode of heat transfer. If the fluid movement is caused by some mechanical means, such as a fan, the term "forced convection" is used. When the fluid motion is induced by density differences ("buoyancy") the term "natural convection" is given to the heat transfer process. Each of these classifications is divided further into laminar and turbulent categories.

The decision to place a convection process into the forced or natural categories is determined by the value of the dimensionless Reynolds Re and Grashof Gr numbers. They are defined as

$$Re = \frac{\rho u l}{\mu} \qquad \text{(F431)}$$

$$Gr = \frac{\rho^2 g \beta \Delta T l^3}{\mu^2} \qquad \text{(F432)}$$

where

ρ = fluid density
u = fluid velocity
μ = bulk viscosity
β = coefficient of thermal expansion
l = characteristic length
g = gravitational acceleration
ΔT = temperature difference

The process is considered to be entirely "forced" or "natural" when the heat flux does not deviate by more than 10% from the heat flux when considering both heat transfer modes combined. The system most studied examining the effects of forced and natural convection is vertical tubes. Figure F43.1 illustrates the various flow regimes for vertical tubes as functions of the Reynolds and Grashof numbers. The characteristic length is the diameter D of tubes of length L.

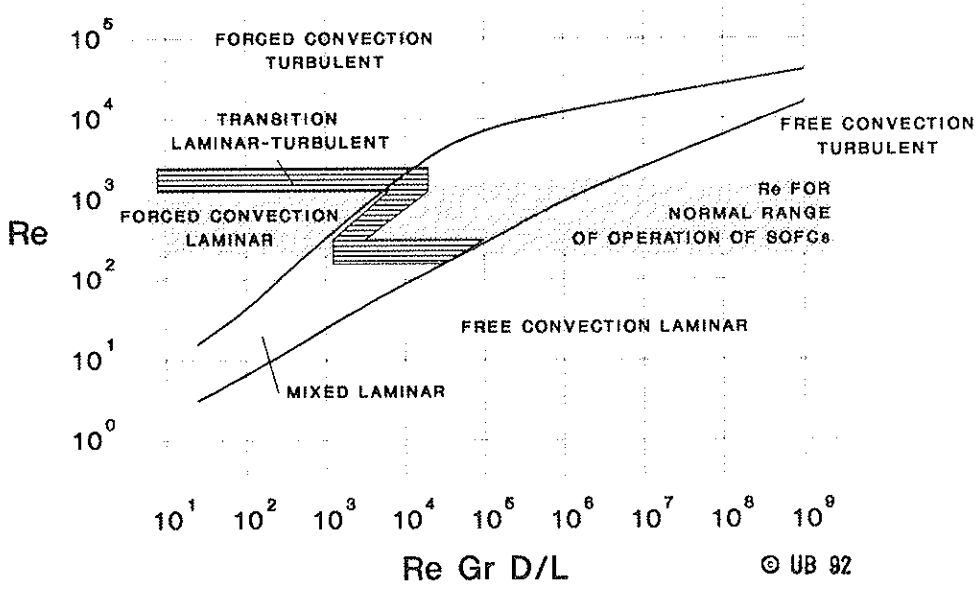

Figure F43.1: Regimes of free, forced and mixed convection for flow through vertical tubes[14]
Boundary conditions: uniform heat flux
uniform wall temperture

Operation of the SOFC is expected to fall in laminar forced convection and, perhaps in the mixed-laminar regions depending on the individual design. Turbulent forced convection heat transfer is also possible and is included in the following sections for completeness.

FORCED CONVECTION

The local heat flux is assumed to be proportional to the temperature difference between the surface and fluid far from the surface. In a duct, the average or fluid bulk temperature is used in computing the temperature difference. The heat flux is then given by Newton's law of cooling,

$$q = h\,(T_s - T_f) \qquad \text{(F433)}$$

where

q = heat flux [W m^{-2}]
h = heat transfer coefficient [W m^{-2} K^{-1}]
T_s = surface temperature [K]
T_f = fluid bulk temperature [K]
$= 0.5\,(T_{out} + T_{in})$

Normally, convective heat transfer problems are posed in terms of the dimensionless numbers

$$Nu = \frac{h\, d_h}{\lambda} = \text{Nusselt number}$$

$$Re = \frac{\rho\, u\, d_h}{\mu} = \text{Reynolds number}$$

$$Pr = \frac{c_p\, \mu}{\lambda} = \text{Prandtl number}$$

where d_h is the hydraulic diameter (see Chapter F3.1).

For a given geometry, flow rate and flow condition, one computes the Reynolds and Prandtl numbers and then finds the Nusselt number from a relation

$$Nu = f(Re, Pr) \quad \text{forced convection}$$

$$Nu = f(Gr, Pr) \quad \text{natural convection}$$

for some prescribed boundary conditions. Once the Nusselt number is known, h can be computed and the heat flux calculated.

Many types of boundary conditions are possible. The three most common are constant wall temperature, constant heat flux and insulated walls. The third, insulated boundary, is actually a constant heat flux boundary condition with $q = 0$, but sufficiently common to consider separately.

For fluids with Prandtl number of $Pr \cong 1$ or greater, the Nusselt number for two types of boundary conditions approach the same value at higher Reynolds numbers as Figure F43.2 indicates. In laminar flow, the Nusselt number is independent of Reynolds number. Consequently, the correlations which follow tend to treat only one of the two boundary conditions in turbulent flow and neglect the influence of Reynolds number in laminar flow. Furthermore, all correlations given are for fully developed velocity and temperature profiles.

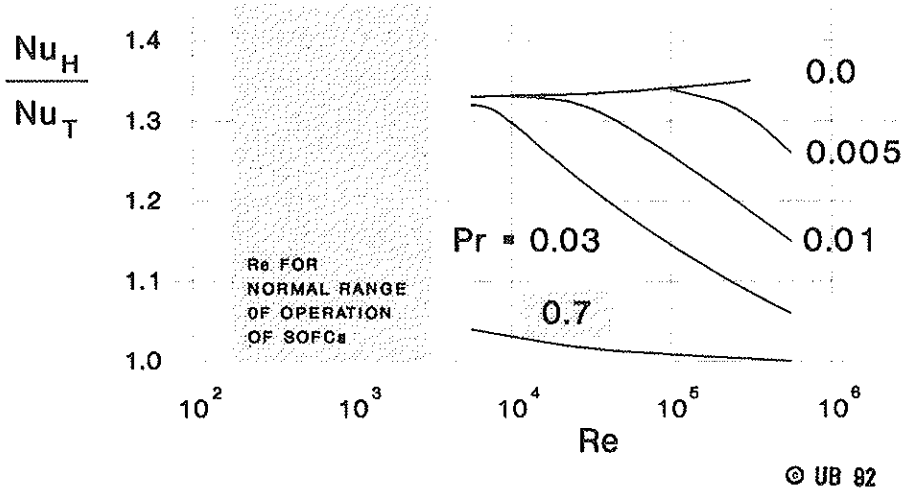

Figure F43.2: Ratio of the Nusselt number for constant heat rate to Nusselt number for constant surface temperature for turbulent fully developed conditions in a circular tube[13]

For the four common geometries and for laminar flow conditions the Nusselt numbers are given in Table F43.1. Note the lack of Reynolds number dependence. The Nusselt numbers for turbulent flow conditions are given in Table F43.2.

Once the Nusselt number has been deterimined, the heat transfer coefficient is computed from

$$h = Nu \frac{\lambda}{d_h} \qquad \text{(F437)}$$

and the heat flux from Equation F433 is found. Often the outlet temperature of the fluid is the unknown. To obtain a solution, Equation F433 must be solved together with

$$Q = q\,A = m_{air}\, c_p\, (T_{fout} - T_{fin}) \qquad \text{(F438)}$$

where A is the heat transfer surface area.

Table F43.1: Laminar flow Nusselt numbers[13]

cross section	Nusselt number
circular (Figure F30.1):	
- constant surface temperature:	Nu = 3.656
- constant heat flux:	Nu = 4.364

rectangular (Figure F30.2):

aspect ratio b/a	Nu for boundary conditions: A	B	C
1.0	2.98	3.61	3.09
1.4	3.08	3.73	
2.0	3.39	4.12	3.02
3.0	3.96	4.79	
4.0	4.44	5.33	2.93
8.0	5.60	6.49	2.90
10.0		6.78	2.90
	7.54	8.235	

case A: Wall temperature constant in flow direction and around periphery
case B: Constant heat input per unit length and constant peripheral wall temperature at a given axial position
case C: Constant het input per unit length and per unit peripheral distance

triangular (Figure F30.3):	
- constant wall temperature:	Nu = 2.47
- constant heat flux and constant wall temperature in peripheral direction:	Nu = 3.11

Table F43.2: Turbulent Flow Nusselt Numbers[13]

cross section	Nussel number
circular (Figure F30.1):	$Nu = 0.023\ Re^{0.8}\ Pr^{0.33}$
rectangular (Figure F30.2):	
- uniform heat flux and peripheral wall temperature:	
- square:	$Nu = 0.0405\ Re^{0.75}$ for $10^4 < Re < 10^6$
- other rectangles: (properties at film temperature)	$Nu = 0.023\ Re^{0.8}\ Pr^{0.4}$
triangular (Figure F30.3):	
- uniform heat flux and peripheral wall temperature:	
- equilateral triangle:	$Nu = 0.0333\ Re^{0.743}$ for $10^4 < Re < 10^6$ and $Pr \cong 1$

G LINEARIZED SOFC PERFORMANCE ANALYSIS

G1 INTRODUCTION

Fuel cells convert chemical energy into electrical energy. However, the energy supplied as fuel gas per unit time or the chemical input power P_{in} is not completely converted into electric power P_e. The portion of P_{in} converted to P_e by electrochemistry at the electrolyte interfaces is given by the Gibbs efficiency η_G (or the Nernst efficiency η_N) and the fuel utilization u_f.

$$P_e = \eta_G u_f P_{in} \qquad \text{(G101)}$$

Fuel utilization is determined by system design and operation, while the Gibbs efficiciency depends on fuel gas and temperature.

If a current is drawn from a fuel cell, then internal losses occur which further reduce the useful output. Some loss mechanisms have been discussed in Chapters C and D. In addition, electric power dissipation in the peripheral system also contributes to the losses of system performance. Theses losses are assumed to obey Ohm's law.

Generally, the ohmic resistance of materials depends on the temperature T, but not on the electric current I. The performance of solid oxide fuel cells is dominated by this type of resistance R_0. In addition, there is a current-dependent resistance $R(I)$ (e.g. polarization, charge transfer etc.). The total internal resistance R_{int} of an SOFC system is thus composed of two parts

$$R_{int} = R_0 + R(I) \qquad \text{(G102)}$$

$$= R_0 \, (1 + R(I)/R_0)$$

$$= R_0 \, (1 + \varepsilon)$$

Fortunately, under normal operating conditions the current-dependent resistance $R(I)$ is much smaller than the ohmic resistance R_0.

$$0 < \varepsilon = R(I)/R_0 < 0.05 \qquad \text{(G103)}$$

The performance analysis[25] can thus be linearized by assuming that the internal resistance is independent of the current I (or the charge flux intensity = current density $i = I/A$), i.e.

$$R_{int} = R_0.$$

G2 ELECTRIC POWER OUTPUT

The electric power output P_e of a fuel cell system having an internal resistance of $R_{int} \cong R_0$ can then be experessed in terms of supplied chemical power P_{in}, a voltage efficiency η_V, the Gibbs efficiency η_G ane the fuel utilization u_f

$$P_e = \eta_V \, \eta_G \, u_f \, P_{in} \tag{G201}$$

For this linearized analysis it is assumed that the effective voltage is equal to the Gibbs voltage U_G at open circuit and that the voltage drop at current load I is governed by Ohm's law. The voltage efficiency is given by

$$\eta_V = \frac{U_G - R_0 \, I}{U_G} = 1 - \frac{R_0 \, I}{U_G} \tag{G202}$$

But at the electrolyte interface the Gibbs voltage U_G and current I are related to the chemical power input by

$$P_{in} = \frac{I \, U_G}{\eta_G \, u_f} \tag{G203}$$

or

$$I = \frac{\eta_G \, u_f \, P_{in}}{U_G} \tag{G204}$$

By substituting I in Equation G202 on obtains

$$\eta_V = 1 - \frac{\eta_G \, u_f \, R_0}{U_G^2} \, P_{in} = 1 - P_{in}/P_s \tag{G205}$$

The term

$$P_s = \frac{U_G^2}{\eta_G \, u_f \, R_0} \tag{G206}$$

is called the "shunt power" or "short circuit power" of the SOFC system. It signifies the electric power generated by the fuel cell and dissipated within the SOFC system itself when the two output terminal are connected with each other.

Equation G201 then reads

$$P_e = \eta_G \, u_f \, (1 - P_{in}/P_s) \, P_{in} \qquad (G207)$$

This is the equation of an inverted parabola passing through the origin ($P_e = P_{in} = 0$) and the shunt point ($P_{in} = P_s$), as shown in Figure G30.1.

The electric conversion efficiency $\eta_e = P_e/P_{in}$ then becomes

$$\eta_e = \eta_G \, u_f \, (1 - P_{in}/P_s) \qquad (G208)$$

In Figure G20.1 this efficiency is depicted for hydrogen, a fuel cell operating temperature of about 1000 K and a fuel utilization of about 90%.

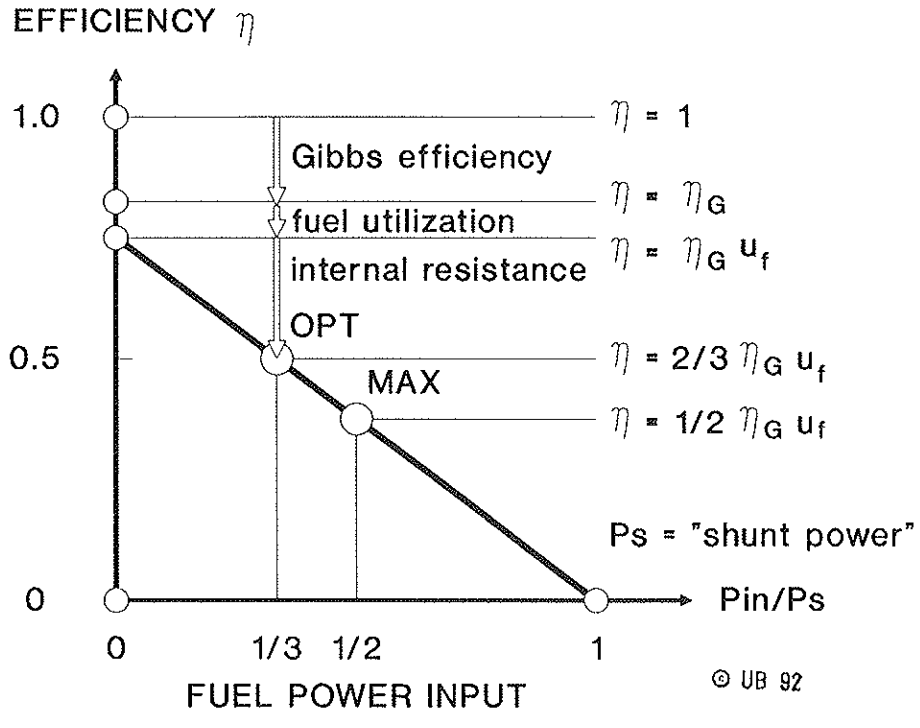

Figure G20.1: Electric conversion efficiency of an SOFC system

G3 MAXIMA AND OPTIMA

By differentiation of Equation G207 or by symmetry considerations one can find for the electric output maximum

$$P_{e,max} = 1/4\ \eta_G\ u_f\ P_s$$

at $P_{in}/P_s = 1/2$

and $\eta_{V,max} = 1/2$ (G301)

These results are depicted in Figure G30.1. According to this linearized theory, the system voltage efficiency at the maximum power point ("MPP") is exactly equal to 1/2. The electric conversion efficiency of an SOFC system can thus not exceed $\eta_{e,max} = 0.5\ \eta_G\ u_f$ ($\cong 0.38$ for hydrogen) at the point of maximum power output. For higher efficiencies the system must be operated at lower output levels.

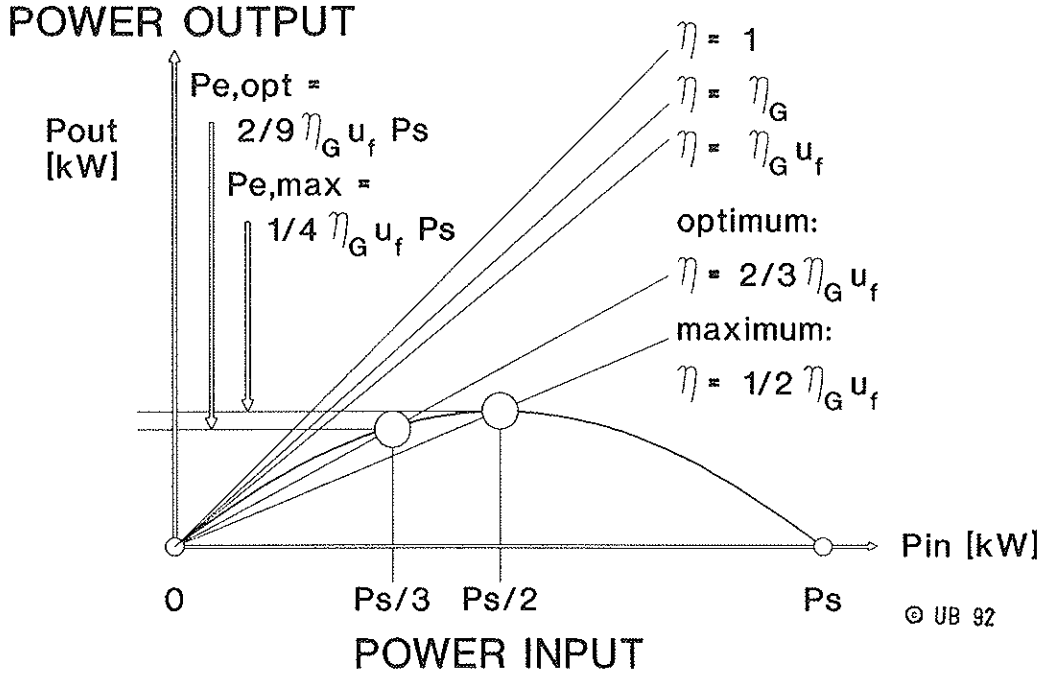

Figure G30.1: Power output parabola for fuel cells

Also of interest is the electric power output under conditions of optimum operation. At the optimum operation point ("OOP") a maximum of electric power it generated compared to the chemical power supplied. In electric power engineering this point is defined by the optimum of the product of electric conversion efficiency η_e and electricn power output P_e . OOP-conditions are found by differentiation of this product:

$$P_{e,opt} = 2/9\ \eta_G\ u_f\ P_s$$

at $$P_{in}/P_s = 1/3$$

and $$\eta_{v,opt} = 2/3 \qquad \text{(G302)}$$

These results are also depicted in Figure G30.1. The system voltage efficiency at the optimum opoerating point is exactly equal to 2/3. The OOP-system electric conversion efficiency can thus not exceed the value of $\eta_{e,opt} = 0.5\ \eta_G\ u_f$ ($\cong 0.50$ for hydrogen). For higher efficiencies the system must be operated at even lower output levels.

At the optimum operating point the conversion is optimized with regard to the fuel input, but not with regard to the system cost. For generating the cheapest electricity commercial parameters such as initial system cost, stack replacement or maintenance cost etc. must be included in the analysis. Then a third optimum is obtained for the commercial operation of an SOFC system. This then reflects the balance between various cost components including the expenditures for fuel gas and income from sales of electricity.

G4 REAL PERFORMANCE OF AN SOFC GENERATOR

So far, thermal losses have not been considered in the linearized analysis of an ideal SOFC generator. But even before electricity can be generated, the chemical power has to be supplied for heating up the system. Once the operational temperature has been reached, fuel gas is needed to balance heat losses. These may depend on the power level at which the SOFC system is operated, i.e. on P_{in} . As a consequence, the electric performance parabola no longer passes through the origin, but it is shifted towards higher levels of input power.

Also, the electric DC/AC conversion system generally perform poorly at low power levels. Thus, the first power generated may not reach the system terminals but is dissipated in the converter circuitry. This effect tends to shift the performance parabola downward.

In addition, the fuel utilization may depend on the load level and the total resistance may not remain constant at high currents. All in all, the power parabola will be distorted by such effects and curves like the one depicted in Figure G40.1 may be obtained.

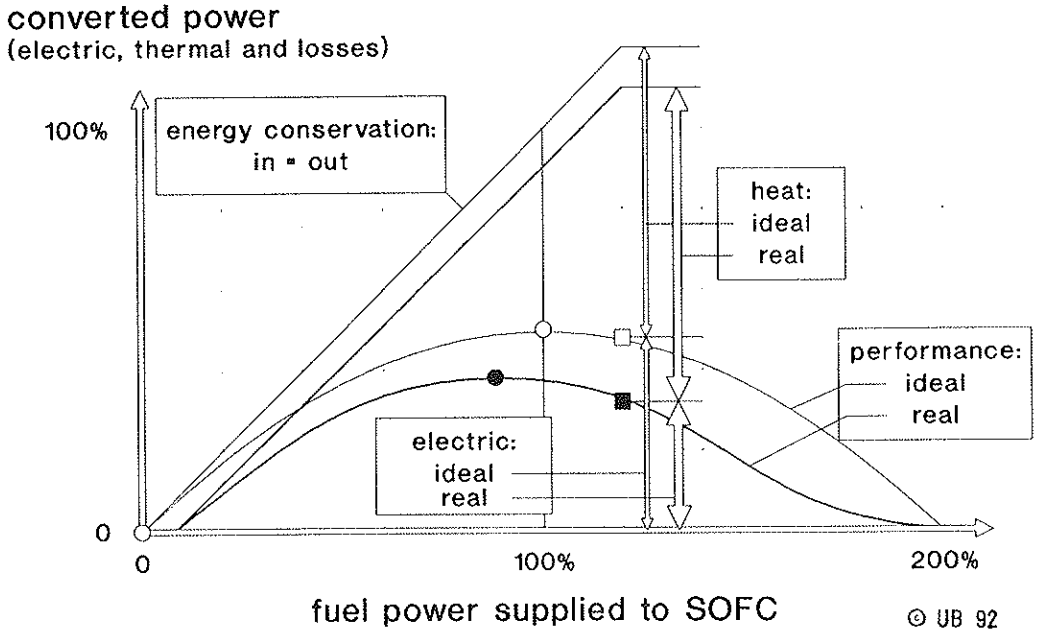

Figure G40.1: Ideal and real power parabolas of an SOFC generator

G5 OPPORTUNITIES FOR SOFC SYSTEM IMPROVEMENTS

These results indicate that the efficiency of an SOFC is an operating parameter rather than a quantity which can be improved by smart system design, advanced materials or fundamental research. But the losses of all system surrounding the fuel cell stack can be reduced by proper design and smart operation.

Research and development efforts can be spent on improving the system periphery to minimize thermal and electrical losses and, thereby, improving the overall system efficiency. But it is misleading to develop SOFC stacks of higher efficiency. Any stack can be operated at high efficiency, but not at arbitrary power levels.

What must be improved is the span of the power parabola. The shunt power P_S of the SOFC, Equation G207, system should be moved towards larger values of P_{in} basically by reducing the internal resistance R_0 of the fuel cell system. This can be accomplished by careful recognition of all aspects of the electric current flow in SOFS stacks and elements as sketched in Chapter D.

R REFERENCES

[1] **JANAF Thermochemical Tables**

[2] Weast, R.C., **CRC Handbook of Chemistry and Physics**, 63rd Edition, CRC Press, Boca Raton, Florida (1982-83)

[3] Reid, R.C., Prausnitz, J.M. and Poling, B.E., **The Properties of Gases and Liquids**, McGraw-Hill, New York, (1987)

[4] M. Chindemi, Eniricerche/INAR, I-20097 S. Donato Milanese, Milano, Italy (private communication)

[5] Denbigh, K., **The Principles of Chemical Equilibrium** 3rd Edition, Cambridge University Press (1971)

[6] Kinoshita, K., F.R. McLarnon and E.J. Cairns, **Fuel Cells, a Handbook**, Report No. DE88010252, U.S. Department of Energy, Morgantown, West Virginia (1988)

[7] Rortrup-Nielsen, J.R., Catalytic Steam Reforming in **Catalysis, Science and Technology**, Vol. 15, J.R. Anderson and M. Boudart, eds., Springer-Verlag, Berlin (1983)

[8] Bird, R.B., W.E. Steward and E.N. Lightfoot, **Transport Processes**, John Wiley & Sons, New York, N.Y. (1960)

[9] Vetter, K.J., **Electrochemical Kinetics, Theoretical and Experimental Aspects**, Academic Press, New York, N.Y. (1967)

[10] Dunbar, W.R., **Computer Simulation of a High Temperature Solid Electrolyte Fuel Cell**, M.S. Thesis, Marguette University, Wisconsin (1983)

[11] Nguyen, B.C., T.A. Lin and D.M. Mason, **Electrocatalytic Reactivity of Hydrocarbons on a Zirconia Electrolyte Surface**. J. Electrochem. Soc., Vol. 133, 9, pp. 1807 (1986)

[12] Streeter, V.L. and E.B. Wylie, **Fluid Mechanics**, McGraw-Hill, New York, N.Y. (1973)

[13] Rohsenow, W.M. and J.P. Hartnett, **Handbook of Heat Transfer**, McGraw-Hill, New York, N.Y. (1973)

[14] Eckert, E.G.R. and R.M. Drake, **Analysis of Heat and Mass Transfer**, McGraw-Hill, New York, N.Y. (1975)

[15] Gauckler, L., ETH Zurich/Switzerland, private communication

[16] Rohr, F.J., ABB Research Center Heidelberg/Germany, private communication

[17] van Herle, J., EPFL Lausanne/Switzerland, private communication

[18] Poulsen, F. W., RISO Roskilde/Denmark, private communication

[19] de Vries, K.J, Kuipers, R.A., de Haart, L.G.J., **Planar Solid Oxide Fuel Cells Based on Very Thin YSZ Electrolyte Layers.** Proceedings of the Second International Sympoisum on Solid Oxide Fuel Cells, Athens/Greece, July 2 to 5, 1991

[20] Bossel, U.G., **Characterization of Active SOFC Layers by Two Parameters.** Proceedings of the second International Symposium on Solid Oxide Fuel Cells. Athens/Greece, July 2 to 5, 1991.

[21] Sverdrup, E.F., Warde, C. J. and Eback, R. L., **Design of High-temperature Solid-electrolyte Fuel-cell Batteries for Maximum Power Output per Unit Volume.** Energy Conversion, Vol. 13, pp. 129-141, 1973

[22] Nisancioglu, K., Ohmic Losses. **Proceedings of the 1st IEA Workshop on Mathematical Modelling of SOFC Fuel Cells and Systems**, Charmey/Switzerland, July 2 to 6, 1989

[23] Vayenas, C.G., Debenedetti, P.G., Yentekakis, I. and Hegedus, L.L., Ind. Eng. Chem. Fundam., Vol. 24, p. 316, 1985

[24] Boehme, H.J., Zeitschrift für Raumfahrtforschung, Vol. 4, pp. 154-156, 1970

[25] Bossel, U.G., **Solid Oxide Fuel Cells**, Proceedings of the 1st IEA Workshop on Mathematical Modelling of SOFC Fuel Cells and Systems, Charmey/Switzerland, July 2 to 6, 1989

[26] Welty, J.R., Wicks, C.E. and Wilson, R.E., **Fundamentals of Momentum, Heat and Mass Transport**, 3rd ed., John Wiley & Sons, Inc. 1984

[27] **Perry's Chemical Engineers' Handbook**, D.W. Green (ed.), McGraw-Hill Book Company, 1984

Information taken from standard textbooks of physics, chemistry and engineering has not been referenced.